Horizon 2020
Programme

GENIORS

Research and Innovation Action (RIA)

This project has received funding from the European Union's Horizon 2020 research and innovation programme under grant agreement No 755171.

Start date : 2017-06-01 Duration : 48 Months
http://geniors.eu/

GENIORS

Stability and safety studies of hold extraction systems (1 for each CyMe4BTBP, HidroBTBP, TODGA& PTD)

Authors : Dr. Bohumir GRUNER (IIC), IIC: D. Bavol, B. Gruner, CTU: P. Distler, M. Mindova, J. Sebesta, J. John Juelich: A. Wilden, G. Modolo CEA: A. Kimberlin, L. Berthon, P. Guilbaud, D. Guillaumont, G. Saint-Louis. POLIMI: E. Macerata, E. Mossini, M. Mariani, F. Galluccio, G. Colombo Dugoni, M. Giola. CIEMAT: Hitos Galán, Iván Sánchez-García, Laura Jiménez, Ana Núñez, Lorena Serrano and Sofía Durán.

GENIORS - Contract Number: 755171

Project officer: Roger Garbil

Document title	Stability and safety studies of hold extraction systems (1 for each CyMe4BTBP, HidroBTBP, TODGA& PTD)
Author(s)	Dr. Bohumir GRUNER, IIC: D. Bavol, B. Gruner, CTU: P. Distler, M. Mindova, J. Sebesta, J. John Juelich: A. Wilden, G. Modolo CEA: A. Kimberlin, L. Berthon, P. Guilbaud, D. Guillaumont, G. Saint-Louis. POLIMI: E. Macerata, E. Mossini, M. Mariani, F. Galluccio, G. Colombo Dugoni, M. Giola. CIEMAT: Hitos Galán, Iván Sánchez-García, Laura Jiménez, Ana Núñez, Lorena Serrano and Sofía Durán.
Number of pages	87
Document type	Deliverable
Work Package	WP2
Document number	D2.1
Issued by	IIC
Date of completion	2021-04-06 14:52:56
Dissemination level	Public

Summary

? The Deliverable Report, D2.1, Stability and safety studies of hold extraction systems (1 for each TODGA, mTDDGA, CyMe4-BTBP/BTPhen, Hydrophilic diglycolamides, CDTA, PTD, & hydrophilic SO3-Ph-BTP/BTBP/BTPhen, AHA and SO3-Ph-BTP), compiles radiolysis and hydrolysis studies of different extractants and hydrophilic complexants for minor actinides studied in GENIORS: ? TODGA ? mTDDGA ? CyMe4-BTBP and CyMe4-BTPhen ? Hydrophilic diglycolamides ? CDTA ? PTD ? Hydrophilic SO3-Ph-BTP/BTBP/BTPhen ? AHA and SO3-Ph-BTP The stability of the organic extracting molecules, selective stripping agent, and diluent plays crucial role in the design and development of radionuclide separating process. This Deliverable covers advanced studies on radiation stability of previously selected panel of extractants into organic phase as well as hydrophilic stripping and masking agents. The studies herein comprise determinations of the radiation stability of the extraction systems as well as a deeper insight into degradation processes proceeding in molecular structures of the individual ligands during irradiation under various conditions. The knowledge on stability of the extraction and stripping systems and identification of degradation products plays essential role in the respect to safety of the process.

Approval

Date	By
2021-04-06 23:14:01	Dr. Hitos GALAN (CIEMAT)
2021-04-07 07:47:37	Mr. Andreas GEIST (KIT)
2021-04-14 15:39:17	Mr. Stéphane BOURG (CEA)

CONTENT

This project has received funding from the EURATOM research and training programme 2014-2018 under grant agreement No 755171. The content of this deliverable reflects only the author's view. The European Commission is not responsible for any use that may be made of the information it contains.

This project has received funding from the EURATOM research and training programme 2014-2018 under grant agreement No 755171. The content of this deliverable reflects only the author's view. The European Commission is not responsible for any use that may be made of the information it contains.

INTRODUCTION

- The Deliverable Report, *D2.1, Stability and safety studies of hold extraction systems (1 for each TODGA, mTDDGA, CyMe$_4$-BTBP/BTPhen, Hydrophilic diglycolamides, CDTA, PTD, & hydrophilic SO$_3$-Ph-BTP/BTBP/BTPhen, AHA and SO$_3$-Ph-BTP),* compiles radiolysis and hydrolysis studies of different extractants and hydrophilic complexants for minor actinides studied in GENIORS:
- TODGA
- mTDDGA
- CyMe$_4$-BTBP and CyMe$_4$-BTPhen
- Hydrophilic diglycolamides
- CDTA
- PTD
- Hydrophilic SO$_3$-Ph-BTP/BTBP/BTPhen
- AHA and SO$_3$-Ph-BTP

The stability of the organic extracting molecules, selective stripping agent, and diluent plays crucial role in the design and development of radionuclide separating process. This Deliverable covers advanced studies on radiation stability of previously selected panel of extractants into organic phase as well as hydrophilic stripping and masking agents. The studies herein comprise determinations of the radiation stability of the extraction systems as well as a deeper insight into degradation processes proceeding in molecular structures of the individual ligands during irradiation under various conditions. The knowledge on stability of the extraction and stripping systems and identification of degradation products plays essential role in the respect to safety of the process.

TODGA

The *N*,*N*,*N*',*N*'- tetraoctyl diglycolamide (TODGA) (Figure 1) has been extensively studied as efficient extractant for trivalent radionuclides, also regarding its radiolytic stability[1-7]. However, the role of phase modifiers on the radiolytic stability of TODGA has been less understood[5]. Therefore, the role of 1-octanol in the radiolysis mechanism of TODGA degradation was studied[8].

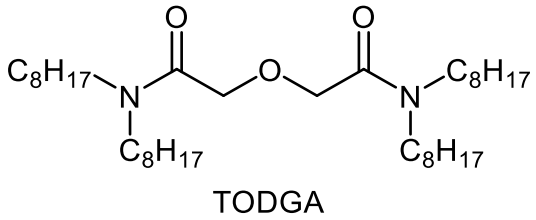

Figure 1: Chemical structure of TODGA.

Details are given in reference[8]. The summary on this paper is presented below:

"To mitigate third phase formation in next generation used nuclear fuel reprocessing technologies, the addition of 1-octanol has been tried. However, contradictory reports on the radiolytic effect of 1-octanol incorporation on separation ligand degradation need to be resolved. Here, 50 mM *N*,*N*,*N*',*N*'-tetraoctyldiglycolamide (TODGA) dissolved in n-dodecane was gamma irradiated in the presence and absence of 1-octanol (2.5-10 vol. %) and a 3.0 M HNO$_3$ aqueous phase. Radiation-induced TODGA degradation exhibited pseudo-first-order decay kinetics as a function of absorbed gamma dose for all investigated solution and solvent system formulations. The

This project has received funding from the EURATOM research and training programme 2014-2018 under grant agreement No 755171. The content of this deliverable reflects only the author's view. The European Commission is not responsible for any use that may be made of the information it contains.

addition of 1-octanol afforded diametrically different effects on the rate of TODGA degradation depending on solvent system formulation. For organic-only irradiations, 1-octanol promoted TODGA degradation (d = 0.0057 kGy^{-1} for zero 1-octanol present vs. ≈0.0073 kGy^{-1} for 7.5-10 vol. %) attributed to a favourable hydrogen atom abstraction reaction free energy (-0.31 eV) and the ability of 1-octanol to access a higher yield of n-dodecane radical cation ($RH^{\bullet+}$) at sub-nanosecond timescales. This was rationalized by determination of the rate coefficient (k) for the reaction of 1-octanol with $RH^{\bullet+}$, k = (1.23 ± 0.07) × 10^{10} M^{-1} s^{-1}. In contrast, irradiation in the presence of 1-octanol and a 3.0 M HNO_3 aqueous phase afforded significant radioprotection (d = 0.0054 kGy^{-1} for zero 1-octanol present vs. ≤ 0.0044 kGy^{-1} for > 2.5 vol. %) that increases with 1-octanol concentration, relative to the single phase, organic-only solutions. This effect was attributed to the extraction of sufficiently high concentrations of HNO_3 and H_2O into the organic phase by TODGA and 1-octanol as adducts which interfere with the hydrogen atom abstraction process between the 1-octanol radical and TODGA. Our findings suggest that the addition of 1-octanol as a phase modifier will enhance the radiation robustness of TODGA-based separation technologies under envisioned solvent system conditions in the presence of aqueous HNO_3."

Another aim of this work is to investigate the effect of several parameters on the stability of the organic solution based TODGA.

- The effect of the composition of the organic phase, including the metal loading, was investigated toward the determination of the radiolytic yield (G_0 value).
- In-situ alpha (provided by the decay of ^{241}Am) and external gamma radiolysis (by a ^{137}Cs source) of the TODGA solutions were compared.
- After identification of the main degradation products, metal speciation in organic solutions was investigated to determine how the degradation products formed affect metal complexation in the organic solvent.

The quantification of TODGA in solution after radiolysis was investigated using high performance liquid chromatography in tandem with electrospray ionization mass spectroscopy (HPLC-ESI-MS). Metal speciation in degraded TODGA solutions was also probed using UV-Visible spectroscopy, and ESI-MS. To support the experimental data, theoretical calculations were also carried out. Bond dissociation energy calculations of the molecule were performed to determine the weakest bond in the TODGA molecules, and radical Fukui function calculations were used to predict solvent radical attack site on TODGA under various solvation conditions and for various structural conformations.

ANALYSIS OF GAMMA IRRADIATED SOLUTION

QUANTITATIVE ANALYSIS OF TODGA AFTER DEGRADATION

Gamma irradiation of TODGA solutions using a ^{137}Cs external irradiation source was done under seven different solution conditions. The solutions irradiated are described in Table 1.

This project has received funding from the EURATOM research and training programme 2014-2018 under grant agreement No 755171. The content of this deliverable reflects only the author's view. The European Commission is not responsible for any use that may be made of the information it contains.

Table 1: Solutions irradiated by an external ^{60}Co source. C_{TODGA} corresponds to the TODGA concentration in the degraded solution determined by HPLC-ESI-MS.

Organic phase	Aqueous phase	Dose (kGy)	C_{TODGA} after irradiation * ($mol.L^{-1}$)
0.1 M TODGA in dodecane	1.0M HNO_3	0	-
0.1M TODGA in dodecane + 5%$_{v/v}$ octanol	2.5M HNO_3	0	-
0.1 M TODGA in dodecane	None	299	0.031
		571	0.012
0.1M TODGA in dodecane + 5%$_{v/v}$ octanol		303	0.024
		568	0.010
0.1 M TODGA in dodecane	1.0M HNO_3	341	0.031
		546	0.017
0.1M TODGA in dodecane + 5%$_{v/v}$ octanol		334	0.032
		533	0.012
0.1M TODGA in dodecane + 5%$_{v/v}$ octanol	2.5M HNO_3	332	0.032
		663	0.015
0.1 M TODGA in dodecane	1mM Nd in 1M HNO_3	249	0.038
		494	0.022
0.1M TODGA in dodecane + 5%$_{v/v}$ octanol	1mM Nd in 2.5M HNO_3	265	0.050
		505	0.024
	10mM Nd in 2.5M HNO_3	227	0.048
		451	0.029
	50mM Nd in 2.5M HNO_3	221	0.063
		448	0.040

In order to evaluate the impact of the radiolysis on the TODGA solutions, the concentration of TODGA remaining after irradiation was quantified using HPLC-ESI-MS (Table 1). Literature data indicate an exponential decrease of the concentration of TODGA with absorbed dose suggesting pseudo first order kinetics[2-3,6-7,9]. The dose constants and G_0 values were calculated using Eq 1 and 2 (from Mincher et al.[10-11]) where C_0 is the initial TODGA concentration in mmol/kg, d is the dose constant, ρ is the concentration of TODGA in millimolality, and D is the integrated dose by solvent in kGy.

$$C = C_0 e^{dD} \qquad \text{Eq. 1}$$

$$G_0 = d\rho C_0 \qquad \text{Eq. 2}$$

The results are shown in Table 2. The dose constants determined in absence of metallic solute in the organic phase are consistent with literature data[1,6,9,12,13,14]. Comparing the decay constants, several trends can be determined.

- Firstly, nitric acid seems to provide a slight protective effect, as there is a decrease in dose constant between solutions contacted with nitric acid and those without a pre-contact. Whether this is due to extracted water or nitric acid is undetermined because water is co-extracted in the organic phase with nitric acid. This is in agreement with some previous work[4].
- Secondly, the results show that octanol appears to have a slight sensitizing effect, which was determined by comparing the d value for the dodecane only and dodecane + 5%$_{Vol}$ octanol solvents. This is in agreement with previous paper[4]. This effect is observed for both solutions without aqueous phase contact or when the solutions are pre-contacted with 1.0M HNO_3.This sensitive effect could be

This project has received funding from the EURATOM research and training programme 2014-2018 under grant agreement No 755171. The content of this deliverable reflects only the author's view. The European Commission is not responsible for any use that may be made of the information it contains.

due either to the presence of octanol or to the increase of the water concentration in the organic phase.

- Then, the presence of neodymium nitrate in relatively high concentration (30mM) in the organic phase seems to have a protective effect whereas the presence of low concentration (up to 10 mM) has no significant effect. Literature reports a stoichiometry 1:3 or 1:4 for Nd:TODGA complexes[15], so, when Nd concentration is about 30 mM in the organic phase, the solution is closed to saturation, almost each TODGA molecule is involved in Nd complex. When Nd concentration is lower 10 mM, the concentration of TODGA involved complex is lower 30-40 mM, the free TODGA concentration remains major and the protector effect would not be observed. This explains the different behavior observed depending on the metal concentration in the organic phase. This means that when TODGA is involved in a complex, its stability increases.

Table 2: Dose constants (MGy^{-1}) and G_0 values ($\mu mol*J^{-1}$) for TODGA degradation.

Organic phase	Aqueous phase	*d* (MGy^{-1})	G_0 ($\mu mol\ J^{-1}$)
0.1 M TODGA in dodecane	-	-3.79	-0.50 ± 0.01
	1.0M HNO_3	-3.24	-0.43 ± 0.01
	1 mM Nd /1.0M HNO_3	-3.27	-0.44 ± 0.03
0.1M TODGA in dodecane + 5%$_{v/v}$ octanol	-	-4.13	-0.55 ± 0.02
	1.0M HNO_3	-3.95	-0.53 ± 0.02
	2.5M HNO_3	-2.86	-0.38 ± 0.02
	1 mM Nd /2.5M HNO_3	-2.78	-0.37 ± 0.01
	10 mM Nd /2.5M HNO_3	-2.88	-0.38 ± 0.02
	50 mM Nd /2.5M HNO_3	-2.08	-0.28 ± 0.02

ESI-MS CHARACTERIZATION OF SOLUTIONS AFTER GAMMA IRRADIATION

Each solution was characterized by ESI-MS before and after irradiation (some examples are presented Figure 2). Numerous degradation products have been identified after irradiation. Major and important peaks important for discussion are reported in Table 3 and complemented with corresponding hypothetical structures. All of the structures formed are theoretical, although some have additional supporting evidence from MS^2 spectra. Peak assignments for both, protonated form and sodium complexes were considered, as the solutions contacted with nitric acid contained primarily Na^+ peaks. The identified radiolysis products agree with those reported previously in literature for TODGA[2, 4].

A wider variety of degradation products was observed when the solutions were contacted with nitric acid. No degradation products could be assigned to be the result of nitrate addition, even though nitrate appears to facilitate the formation of many products. Additionally, several degradation products associated with the addition of the phase modifier *n*-octanol are observed in solutions with 5%$_{v/v}$ octanol. At higher doses, addition of degradation products onto TODGA occurs. With a high concentration of metal, no additional major

This project has received funding from the EURATOM research and training programme 2014-2018 under grant agreement No 755171. The content of this deliverable reflects only the author's view. The European Commission is not responsible for any use that may be made of the information it contains.

degradation products appear. From the identification of the degradation products, a degradation scheme is proposed, see Figure 3.

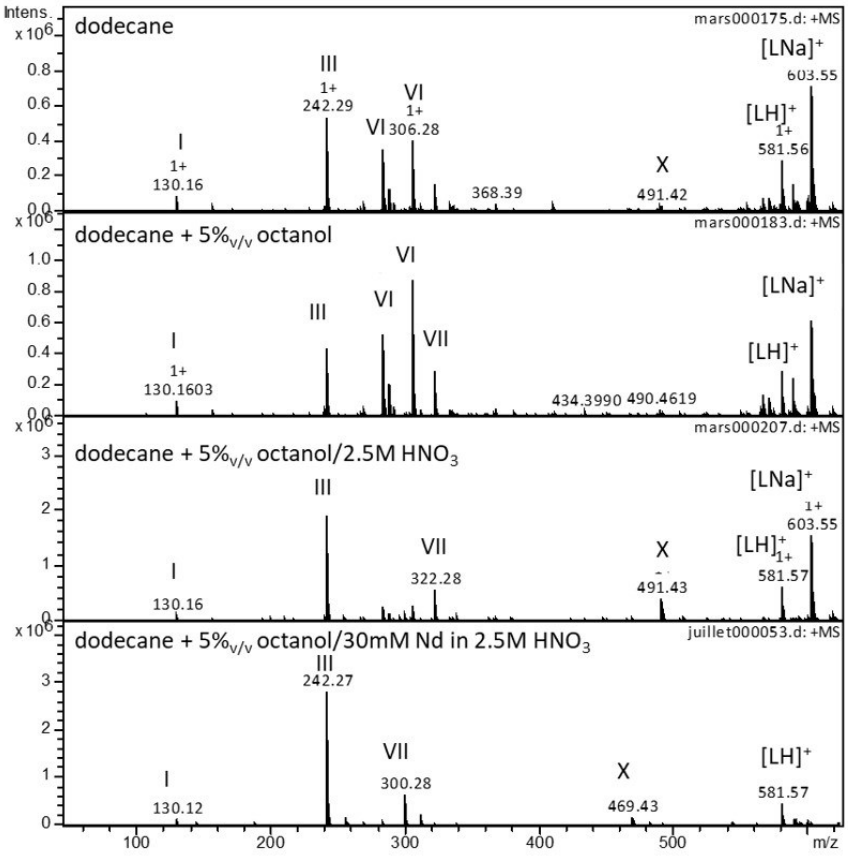

Figure 2: Example ESI-MS spectra of TODGA solutions irradiated to 500 kGy (gamma irradiation) showing the variety of degradation products as a function of the experimental conditions. The labels refer to degradation products in Table 3.
Conditions: organic phase: 0.1M TODGA in dodecane (a) or in dodecane +5%$_{v/v}$ *n*-octanol (b, c and d); Aqueous phase: without (a and b), 2.5M HNO_3(c) and 30mM Nd^{3+} (d) in 2.5M HNO_3 .

This project has received funding from the EURATOM research and training programme 2014-2018 under grant agreement No 755171. The content of this deliverable reflects only the author's view. The European Commission is not responsible for any use that may be made of the information it contains.

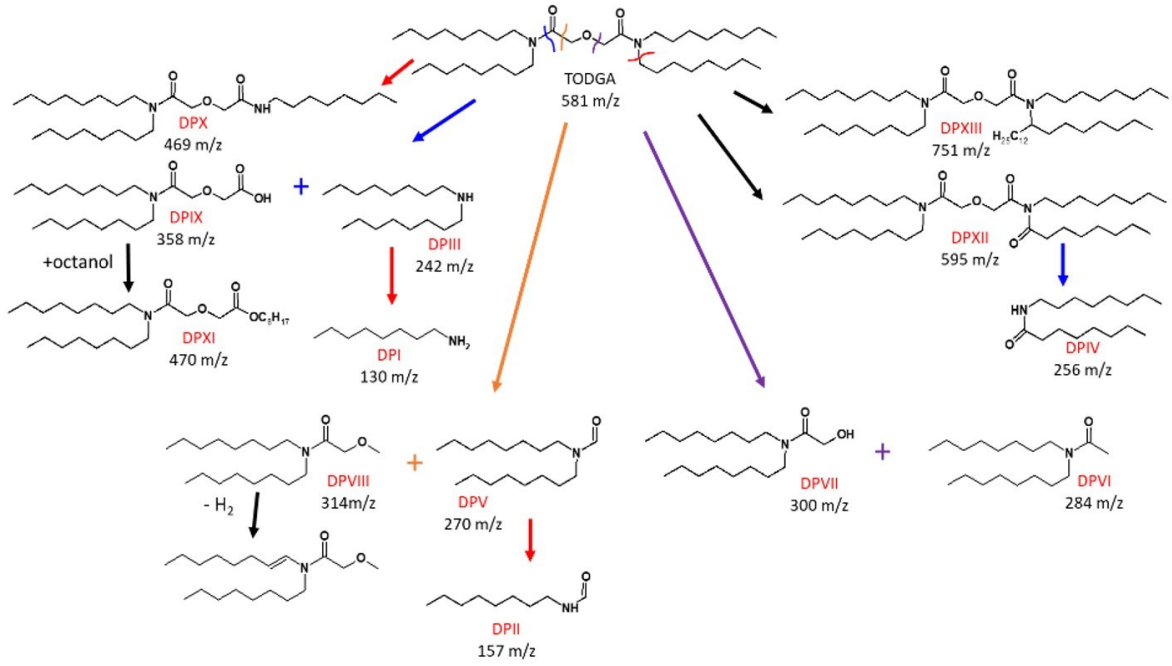

Figure 3: Degradation schema proposed for the formation of the main degradation products of TODGA and m/z of the protonated species MH^+.

Table 3: Major degradation products proposed form the ESI-MS spectra.

DP	Theoretical Structure	*m/z* of H^+ species	*m/z* of Na^+ adduct
I	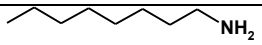	130	152
II	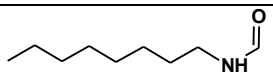	157	179
III	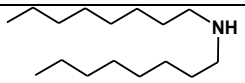	242	264
IV	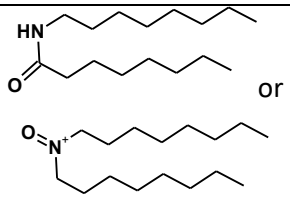	256	278
V	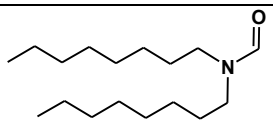	270	292
VI	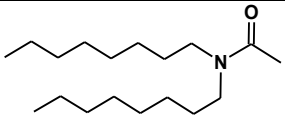	284	306

This project has received funding from the EURATOM research and training programme 2014-2018 under grant agreement No 755171. The content of this deliverable reflects only the author's view. The European Commission is not responsible for any use that may be made of the information it contains.

VII	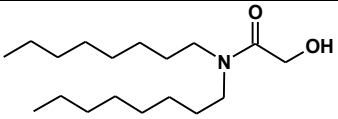	300	322
VIII	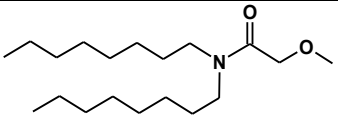	314	336
IX	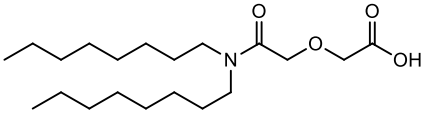	358	380
X	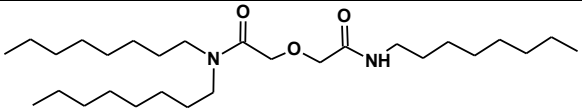	469	491
XI	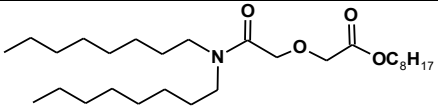	470	492
XII	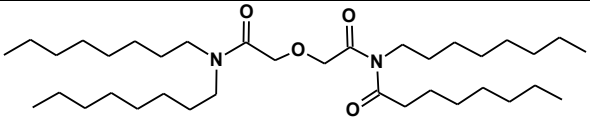	595	617
XIII	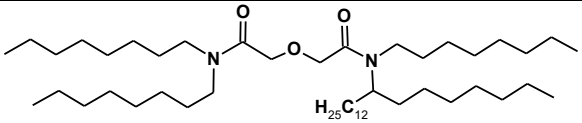	751	773

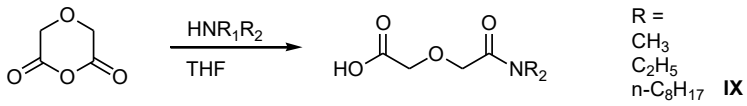

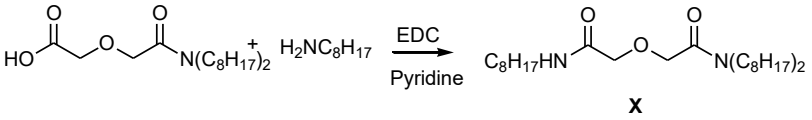

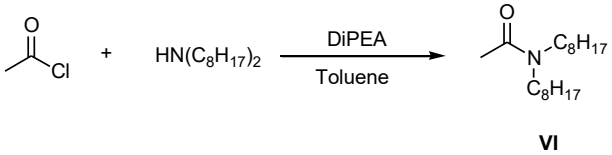

Figure 4: Synthesis of a series of degradation products and their structures.

A series of TODGA degradation products was synthesized by Twente. The numbering of the different degradation compounds differ from the original identification of compounds done by CIEMAT that can be find in other documents of GENIORS projects. In this document, the numbering has been assigned as function of mass. The preparation of a series of synthetically straightforward degradation products is summarized in in Figure 4 and Figure 5.

This project has received funding from the EURATOM research and training programme 2014-2018 under grant agreement No 755171. The content of this deliverable reflects only the author's view. The European Commission is not responsible for any use that may be made of the information it contains.

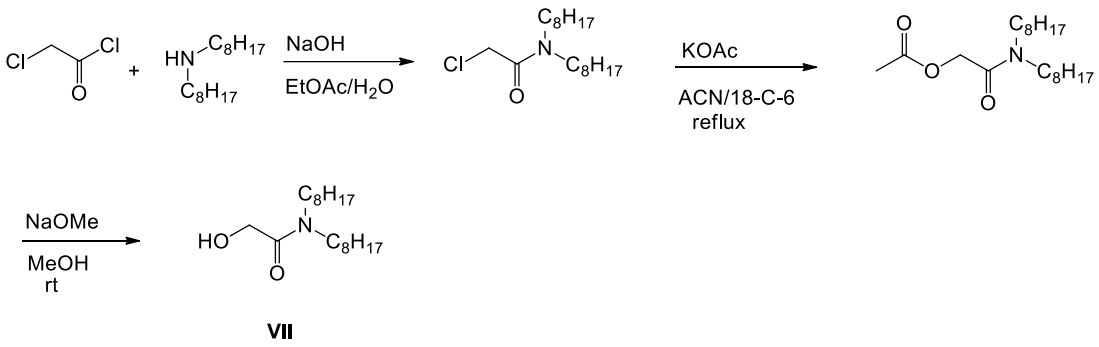

Figure 5: Multistep synthesis of degradation product VII.

CHARACTERIZATION OF METAL COMPLEXES IN SOLUTION AFTER IRRADIATION

To determine if any of the degradation products were directly complexing the metal, 15mM of neodymium nitrate was extracted by irradiated solution containing 1-octanol after contact with 2.5 M HNO_3. UV-VIS spectra were then recorded to observe any changes in Nd speciation (Figure 6). The largest change is the increase of the 582 nm peak with a relative decrease in the shoulder peaks at 575 nm and 588 nm. There is a change in the 740 nm transition as well. This indicates that at least one of the degradation products is altering the metal coordination environment.

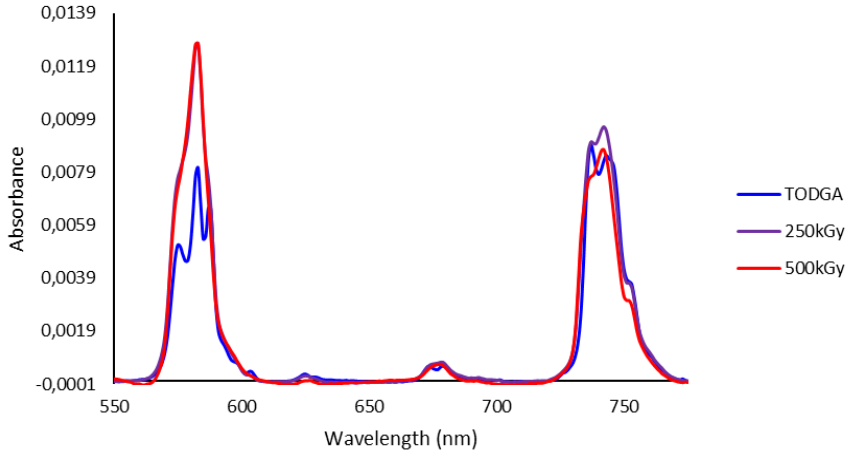

Figure 6: UV-Vis spectra of Nd extracted into irradiated TODGA solutions. Organic phase: TODGA 0.1M in dodecane with 5%$_{v/v}$ octanol aqueous phase: 2.5M HNO_3/ 15mM Nd. Blue: before irradiation, Purple, after 250 kGy dose; Red: after 500kGy dose. These spectra have been background corrected and concentration normalized.

ESI-MS analyses were done to determine which degradation products are likely to causing this coordination change. Several degradation products have been identified in Nd species. An example spectrum after Nd extraction is shown Figure 7. The species containing Nd in the mass spectra are listed in Table 4. Ions observed at m/z = 628.5; 973.8 and 1429.0 are assigned to $[Nd(TODGA)_3]^{3+}$, $[Nd(TODGA)_3(NO_3)]^{2+}$ and $[Nd(TODGA)_2(NO_3)_2]^{+}$ and correspond to complexes formed between TODGA and Nd. They are already present after extraction of Nd nitrate with a fresh solution (non-degraded). These ions are consistent with the Nd:TODGA stoichiometries reported in the literature indicating the presence of different complexes Nd:TODGA

This project has received funding from the EURATOM research and training programme 2014-2018 under grant agreement No 755171. The content of this deliverable reflects only the author's view. The European Commission is not responsible for any use that may be made of the information it contains.

from 1:2 to 1:4 depending on the polarity of the diluent[15]. Other peaks at *m/z* = 591.1; 633.5; 684.6; 784.7; 981.7 and 1153.9 are observed. They are assigned to ($[Nd(TODGA)_2(DPX)]^{3+}$), ($[Nd(TODGA)_2(DPXII)]^{3+}$), ($[Nd(TODGA)_2(DPXIII)]^{3+}$), ($[Nd(TODGA)_3(DPXI)]^{3+}$), $[Nd(TODGA)_2(DPXII)NO_3]^{2+}$) respectively and the peaks at 1153.9 m/z is currently unassigned. This suggests that several degradation products (compounds X, XI, XII, XIII, Table 3) are involved in the Nd complexes, this is consistent since all of these compounds kept a diglycolamide skeleton. These results are in agreement with the invariant D_{Am} and D_{Eu} values with the irradiation dose[16,17] and with the Eu and Am extraction or complexation properties of compound X[4,18].

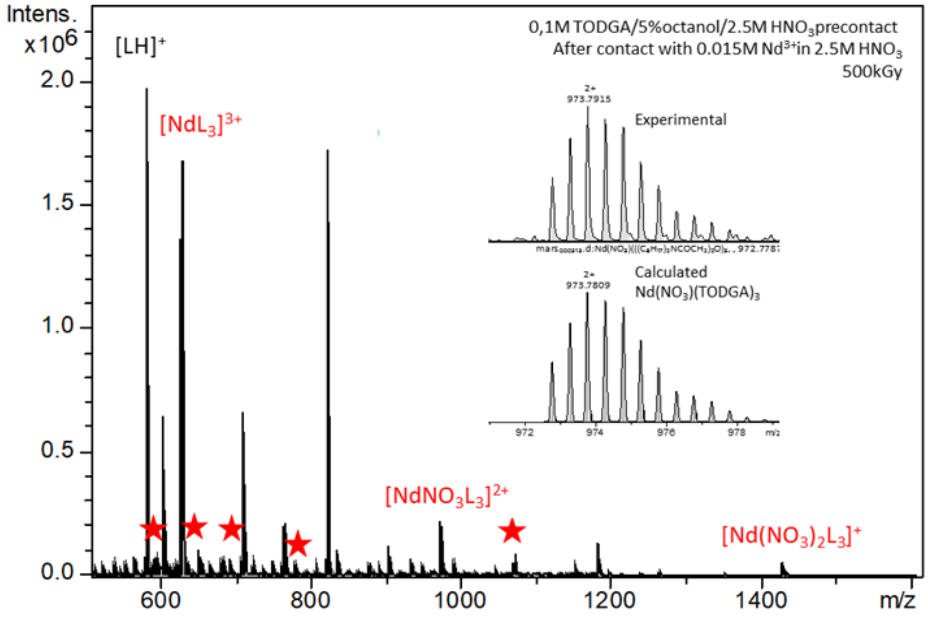

Figure 7: ESI-MS spectrum of irradiated TODGA solution after Nd^{3+} extraction. Labeled peaks corresponds to Nd complexes found in the spectrum. Unlabeled peaks are mostly Na^+ and Ca^{2+} adducts. Insert depicts the isotopic patterned used to identify Nd^{3+} peaks. Red stars indicate Nd ions in which degradation products are involved. L is TODGA.

Table 4: Nd species found via ESI-MS in samples degraded by radiolysis and in synthetic solutions. The complexes were formed after extraction of Nd into TODGA solutions post-irradiation. A * indicates that the peak indicated was found in that solution and a *ε indicates that the peak was found but had a low intensity. Red text indicates peaks found in fresh undegraded TODGA solutions.

		Irradiated solutions		
Proposed Stoichiometry	*m/z*	OctOH	octOH 1M HNO_3	Oct 2.5M HNO_3
$[Nd(TODGA)_2(DPX)]^{3+}$	591.1		*	*ε
$[Nd(TODGA)_3]^{3+}$	628.5	*	*	*
$[Nd(TODGA)_2(DPXII)]^{3+}$	633.5		*	*
$[Nd(TODGA)_2(DPXIII)]^{3+}$	684.6		*	* ε
$[Nd(TODGA)_3(DPVII)]^{3+}$	*728.3*			
$[Nd(TODGA)_3(DPXI)]^{3+}$	784.7		*	*
$[Nd(TODGA)_2(DPIX\ H_{-1})]^{2+}$	830.6		* ε	
$[Nd(NO_3)(TODGA)_2(DPX)]^{2+}$	917.7		ε	ε
$[Nd(TODGA)_3(NO_3)]^{2+}$	973.8	*	*	*
$[Nd(NO_3)(TODGA)_2(DPXII)]^{2+}$	981.7		ε	* ε
Nd species non identified	1153.9		*	*
$[Nd(TODGA)_2(NO_3)_2]^+$	1429.0		*	*

This project has received funding from the EURATOM research and training programme 2014-2018 under grant agreement No 755171. The content of this deliverable reflects only the author's view. The European Commission is not responsible for any use that may be made of the information it contains.

It should also be noted that a colour change was observed when contacting the 500kGy solutions with the 15mM Nd in 2.5M HNO_3 for the aforementioned UV-VIS spectra. The solution that had not been precontacted with nitric acid turned a slight pink colour, the solution that had been precontacted with 2.5M HNO_3 turned a burnt orange colour, and the solution that had 1mM Nd present before irradiation turned a dark yellow colour. There was no colour change in the solution that had been precontacted with 1M HNO_3. These colour changes are shown in Figure 8. After sitting on the benchtop for a couple of days, the colour changed from pink to colourless and from orange to a dark yellow color. This is most likely due to a reaction between the nitrate and degradation products having created unstable products that decomposed over time.

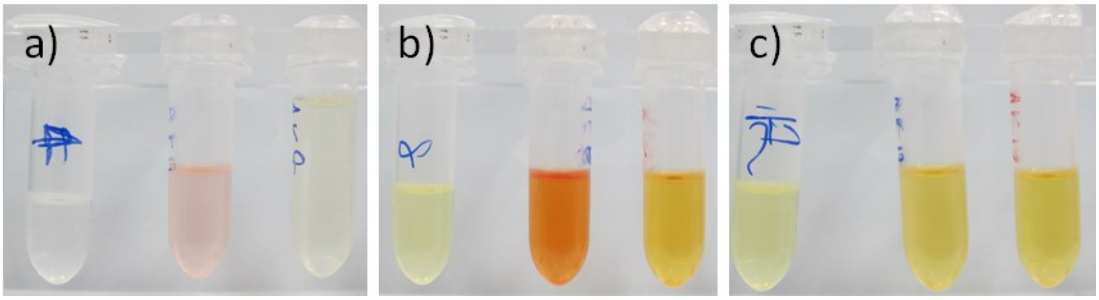

Figure 8: Colour change of the irradiated 0.1M TODGA in dodecane 5% v/v octanol solutions (500kGy) upon contact with 2.5M nitric acid. The first vial is before contact, the second is freshly contacted solution and the third is after the contacted solution had been left for a couple of days. a) not precontacted b) 2.5M HNO_3 contact before irradiation c) 1mM Nd/ 2.5M HNO_3 contact before irradiation.

ANALYSIS OF ALPHA IRRADIATED TODGA SOLUTIONS

To gain further understanding of degradation, solutions of 0.1M TODGA in dodecane + 5%$_{v/v}$ octanol were internally alpha irradiated using ^{241}Am decay. ESI-Mass spectra were recorded at certain time intervals corresponding to selected doses applied to the solution. Two different dose rates were used. Additionally, solutions were left to irradiate both in isolation and in contact with 2.5M HNO_3 (≈2:1 aq:org ratio) without stirring. Both the degradation products of TODGA and the Am complexes were investigated.

The low dose rate solution (1mM Am, 0.16 kGy/hr) was irradiated up to 400 kGy. The only degradation products formed are dioctyl amine (DP III at 242 *m/z*) and octyl amine (DP I at 130 *m/z*), the removal of one octyl chain from TODGA (DP X at 469 *m/z*), and the addition of octanol onto TODGA to form the ester (DP XI at 470 *m/z*). All of these products seem to be hydrolysis products, as blank solutions run under similar conditions without Am also formed these products, albeit at a lower rate. There seems to be no difference between the solution left in contact with nitric acid and the solution irradiated in isolation.

The high dose rate solution (10 mM Am, 1.6 kGy/hr) was irradiated to 1500 kGy in order to determine when the TODGA starts degrading from direct irradiation damage, as opposed to hydrolysis. Selected ESI-MS spectra for the alpha irradiation of TODGA are shown in Figure 9. All of the products in the low dose rate solutions are also present in the high dose solution. TODGA starts to split at the C-O ether bond at about 500 kGy of alpha irradiation, forming products DP VI and DP VII. DP IV (256 *m/z*) also forms, but most likely due to a reaction of dioctylamine with the acetonitrile dilution solvent. Overall, these products are identical to the ones formed when irradiating with gamma rays as opposed to alpha particles. The only difference is that a peak at 270 *m/z* consistently appears in the Am solutions left in contact with nitric acid, which corresponds to DP V. The only other change present when solutions are irradiated in contact with nitric acid is that lower molecular weight products (<242 *m/z*) are not present. This is most likely due to their increased water solubility, as most of these products only contain one octyl chain.

This project has received funding from the EURATOM research and training programme 2014-2018 under grant agreement No 755171. The content of this deliverable reflects only the author's view. The European Commission is not responsible for any use that may be made of the information it contains.

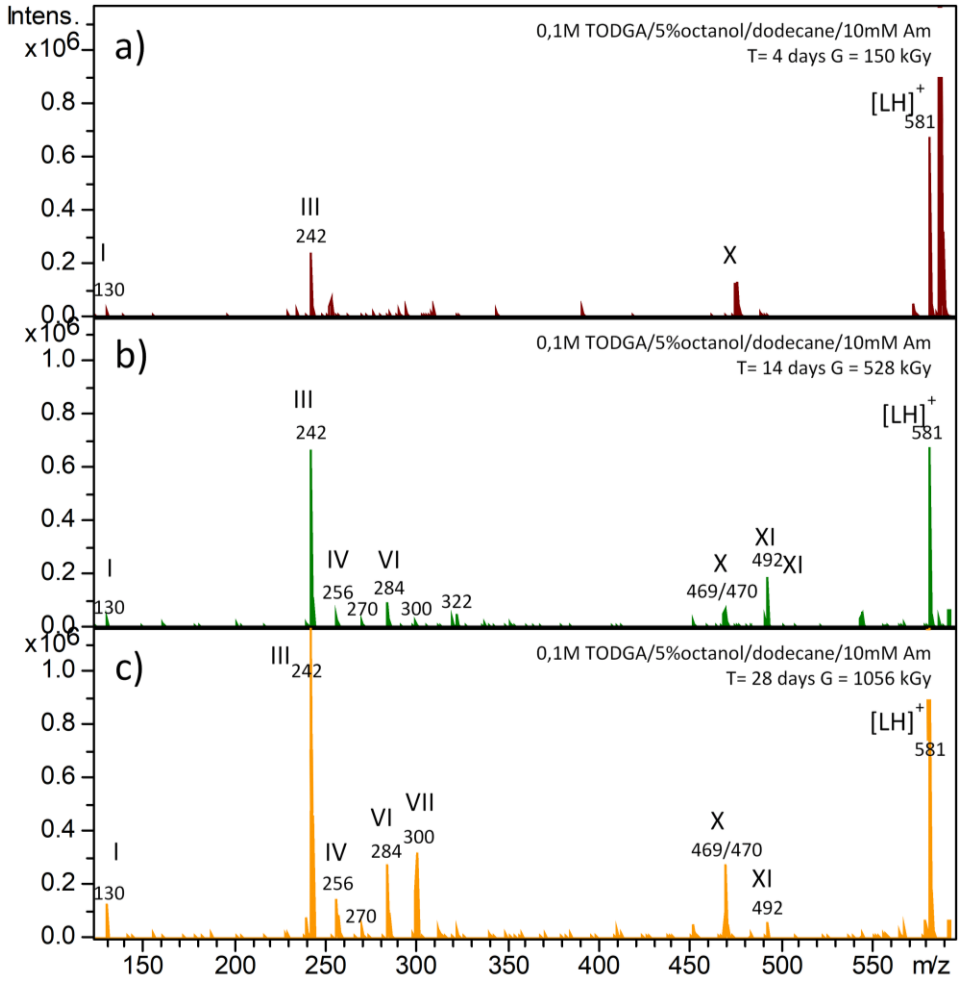

Figure 9: ESI-MS spectra of TODGA degraded using in-situ alpha irradiation from ^{241}Am. Extraction Conditions: Org Phase: 0.1M TODGA in dodecane with 5% octanol; Aq Phase: 10mM Am^{3+} in 2.5M HNO_3. Solutions left in contact with HNO_3 during irradiation. Dose rate determined from the gamma activity. a) 150kGy, b) 500kGy and c) 1000kGy.

Regarding the Am^{3+} complexes (shown in Figure 10), the most of the Am was distributed between the TODGA species $Am(TODGA)_3^{3+}$ at 661 *m/z*, $Am(TODGA)_3(NO_3)^{2+}$ at 1022 *m/z*, and $Am(NO_3)_2(TODGA)_2^{+}$ at 1526 *m/z*. After about 1000kGy, species with degradation products are appearing. The complexes are roughly the same in the solution irradiated without aqueous phase and in the solution irradiated in the presence of nitric acid. The most common degradation product forming a complex with Am corresponds to the product X (see Table 5), which is TODGA minus one octyl chain. This matches what was observed when irradiating with gamma rays. In addition to this product, the carboxylic acid derivative of TODGA (product IX – see Table 5) appears in an Am species at 879 *m/z* $[Am(TODGA)_2(DP\ IX)]^{2+}$ with a deprotonated formed of DP IX suggesting that the carboxylic acid is deprotonated when complexed to Am. The two other degradation products that form complex with Am in the mass spectrum are products with a TODGA skeleton: compound XII which has a ketone group located on sites of the alkyl chain and compound XIII which has a dodecyl group covalently bound to an alkyl chain. These products appear in the following ions: $Am(TODGA)_2(DPXII)^{3+}$ at 666 *m/z*, $Am(NO_3)(TODGA)(DPXII)^{2+}$ at 1030 *m/z* and $Am(NO_3)(TODGA)_2(DPXII)^{2+}$ at 1540 *m/z* for compound XII and $Am(TODGA)_2(DPXIII)^{3+}$ at 717 *m/z*, $Am(NO_3)(TODGA)(DPXIII)^{2+}$ at 817 *m/z*, and $Am(NO_3)(TODGA)_2(DPXIII)^{2+}$ at 1107 *m/z* for compound XIII.

This project has received funding from the EURATOM research and training programme 2014-2018 under grant agreement No 755171. The content of this deliverable reflects only the author's view. The European Commission is not responsible for any use that may be made of the information it contains.

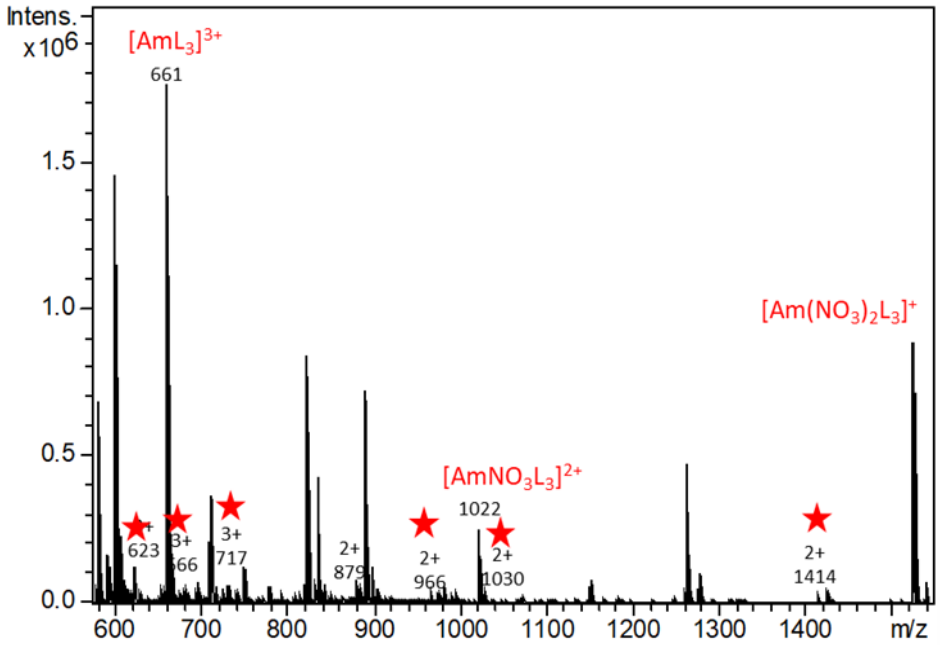

Figure 10: ESI-MS of high mass range of TODGA irradiated by in-situ alpha particles delivered via the decay of Am-241. Labelled peaks contain Am^{3+}. Other peaks are H^+, Na^+, and Ca^{2+} adducts of TODGA and its degradation products. Red stars indicate Nd complexes in which degradation products are involved. L is TODGA. Extraction Conditions: Org Phase: 0.1M TODGA in dodecane with 5% octanol; Aq Phase: 10mM Am^{3+} in 2.5M HNO_3. Irradiated in isolation, i.e. not in contact with aqueous phase.

Table 5: Am^{3+} complexes identified in ESI-MS.

Degradation Product	Complex	*m/z*	Comments
none	$Am(TODGA)_3^{3+}$	661	In all solutions
	$Am(NO_3)(TODGA)_3^{2+}$	1022	In all solutions
	$Am(NO_3)_2(TODGA)_2^{+}$	1526	In all solutions
DP X	$Am(TODGA)_2(DP\ VII)^{3+}$	623	1000kGy
	$Am(NO_3)(TODGA)(DP\ VII)^{2+}$	966	1000kGy
	$Am(NO_3)_2(TODGA)(DP\ VIII)^{2+}$	1414	1000kGy
DP IX	$Am(TODGA)_2(DP\ XII)^{2+}$	879	1000kGy, DPIX is deprotonated
DP XII	$Am(TODGA)_2(DP\ XII)^{3+}$	666	500kGy
	$Am(NO_3)(TODGA)(DP\ XII)^{2+}$	1030	1000kGy
	$Am(NO_3)_2(TODGA)(DP\ XII)^{+}$	1540	1000kGy
DP XIII	$Am(TODGA)_2(DP\ XIII)^{3+}$	717	In all degraded solutions
	$Am(NO_3)(TODGA)(DP\ XIII)^{2+}$	817	1500kGy
	$Am(NO_3)(TODGA)_2(DP\ XIII)^{2+}$	1107	1500kGy

The main difference in Am(III) speciation observed between gamma and alpha irradiation is the formation of a complex with compound XIII in the case of alpha irradiation. It is likely that alpha irradiation increased the formation of DP XIII compared to gamma irradiation. Metal complexes containing this product are present in alpha irradiated solutions even at low dose (100kGy). Even more of this product is formed and multiple Am-TODGA-DPXIII complexes are observed at higher doses. With gamma irradiation, however, DPXIII only appears in the presence of low concentrations of Nd (1mM). One explanation for this could be that the dodecane radical has a higher kinetic energy when formed from alpha radiation. This could provide enough activation

This project has received funding from the EURATOM research and training programme 2014-2018 under grant agreement No 755171. The content of this deliverable reflects only the author's view. The European Commission is not responsible for any use that may be made of the information it contains.

energy for the radical to combine with TODGA to form compound XIII rather than pass the radical onto the extractant. Another explanation is that TODGA radicals are directly formed in the alpha particle track and these react with the dodecane radical.

THEORITICAL CALCULATIONS

To complement the experimental work, the bond dissociation energies (BDE) of the molecule were calculated to determine the weakest bond in the TODGA molecules. As radical Fukui function were already proven to act as a good indicator to estimate the probability of radical reaction[19,20], they were used to predict likely solvent radical attack sites on TODGA under various solvation conditions and structural conformations.

BOND DISSOCIATION ENERGIES

Bond dissociation energies of TODGA were calculated from quantum chemistry calculations on a model molecules using Gaussian 16 and are shown in Table 6. The energies of the two fragments formed by the homolytic cleavage of bonds were calculated using the G3MP2 method. The difference in total energy of the fragments and the whole molecule is the bond dissociation energy. To reduce computation time, the bond dissociation energies for TEDGA were calculated for the center of the molecule, three of the octyl chains in TODGA were replaced with ethyl chains when calculating the alkyl C-C bond dissociation energies, and the "half" of TODGA corresponding to alpha-hydroxyamide was used for the calculation of C-H bonds in the alkyl chains (see Figure 11).

The weakest bond in the molecule is between the etheric C and O. The amide C-N bond is the strongest, therefore least likely to be broken by direct excitation, i.e. being attacked by a dodecane radical. The alkyl chains, for the most part, have the same high energy, making fragmentation of the alkyl chain more unlikely than fragmentation closer to the polar centre of the molecule.

The bond between the first (C_1) and second (C_2) carbons on the alkyl chain seems unusually weak, considering that the adjacent amide would strengthen the C_1-N bond, but not weaken the next bond. This result is due to the computational method used, as each fragment made by the homolytic cleavage of the bond is calculated separately. The fragment containing the amide is stabilized due to the presence of a partial double bond (●CH_2≈N-C=O), which causes the overall energy of that fragment to decrease.

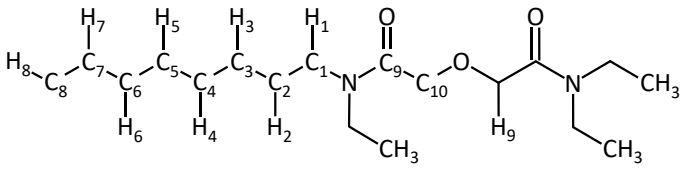

Figure 11: Schematic representation of the molecule used in TODGA bond dissociation energy calculations.

This project has received funding from the EURATOM research and training programme 2014-2018 under grant agreement No 755171. The content of this deliverable reflects only the author's view. The European Commission is not responsible for any use that may be made of the information it contains.

Table 6: Bond Dissociation Energies, see Figure 11 for atom labels.

Bond	Dissociation Energy (eV)
N_{amide}-C_1	3.81
C_1-C_2	3.61
C_2C_3	3.89
C_3-C_4	3.82
C_4-C_5	3.82
C-$_5$-C_6	3.86
N_{amide}-C_9	3.96
C_9-C_{10}	3.34
C_{10}-O_{ether}	3.31
C_{10}-H_9	3.64
C_5-H_5	4.29
C_4-H_4	4.25
C_3-H_3	4.28
C_2-H_2	4.30
C_1-H_1	4.00

RADICAL FUKUI FUNCTIONS

Fukui functions were recently used to compute the likely radical attack site on TODGA by Koubský et al.[19]. They can be used to determine likely sites for electrophilic, nucleophilic, or radical attack on a molecule. The Fukui function used is comprised to 3 separate equations, listed as follows:

$$E(A) = P(A)_{n+1} - P(A)$$

$$N(A) = P(A) - P(A)_{n-1}$$

$$R(A) = \frac{1}{2}(P(A)_{n+1} - P(A)_{n-1}) = \frac{1}{2}(E(A) + N(A))$$

Where P(A) is the electron population of atom A, $P(A)_{n+1}$ and $P(A)_{n-1}$ are the population around atom A with one electron added or removed from the overall structure, respectively, and E(A), N(A), and R(A) are the electrophilic, nucleophilic, and radical Fukui functions, respectively.

All calculations were performed using Gaussian 16[21]. Geometry was first optimized for the neutral TODGA molecule in the gas phase using the 6-311G basis set[22,23]. Then, using the same basis set for TODGA, a further optimization was done using a CPCM model for a heptane solvent[24,25]. A final optimization using the 6-311G++(d,p) basis set with the heptane solvent modelled with CPCM was then performed. A single point energy calculation was completed for the N+1 and N-1 ions of the molecular system, utilizing the optimized geometry of the neutral molecule.

Radical Fukui functions were calculated for TODGA in both a cis and trans configuration. In addition to this, a geometrically constrained TODGA molecule was tested with the alkyl chains covering the etheric protons and exposing the etheric protons to determine if the configuration of the chains has an effect. To be representative of the configuration of TODGA in organic solution of the processes, calculations also were performed on TODGA that had been hydrogen bonded to a single water, nitric acid, and octanol. To get a better idea about

This project has received funding from the EURATOM research and training programme 2014-2018 under grant agreement No 755171. The content of this deliverable reflects only the author's view. The European Commission is not responsible for any use that may be made of the information it contains.

how the Fukui function would behave under conditions more akin to real solutions, molecular dynamic simulations were performed on a system of 106 molecules of TODGA, 30 molecules of H_2O, and 3000 molecules of heptane (see GENIORS deliverable D3.3 "Status on TODGA organic phase loading"). The molecular dynamics calculation created several small (2-6 TODGAs) reverse micellar structures[26]. A few of the TODGAs from these structures were used as the starting point for DFT Fukui function calculations. The same colour scheme is used on all images on Figure 12, with a red colour indicating the most likely region for radical attack.

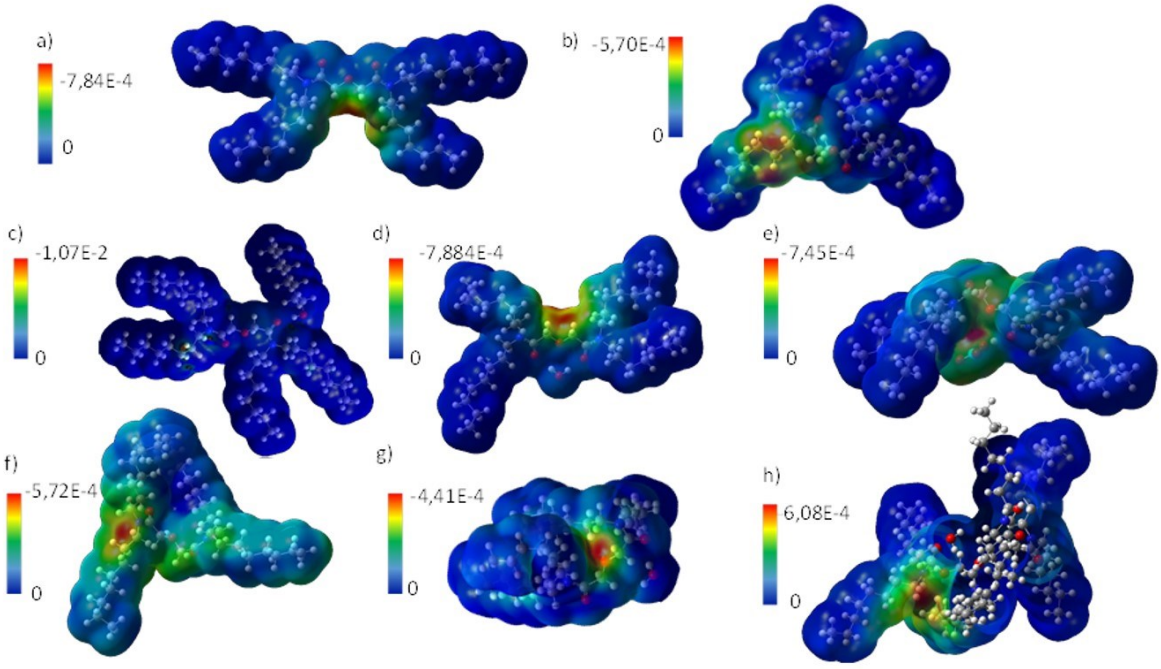

Figure 12: Results of the Fukui Function Calculations performed on TODGA. Color scales depict the values of the Fukui function calculated in $e^-/Å^3$. a) *cis*-TODGA b) *trans*-TODGA c) TODGA+octanol d) TODGA+H_2O e) TODGA+HNO_3 f) Molecular dynamics TODGA (partial heptamer) g) Molecular dynamics TODGA (partial tetramer) h) Molecular dynamics TODGA dimer.

First, a lone TODGA molecule was calculated. Because it is known from molecular dynamic simulations and NMR spectroscopy that free TODGA molecule (non-complexed) rapidly rotates along the ether moiety[27], making both the cis and trans configurations likely, both configurations were modelled. As shown in Figure 12, there is a difference between the two configurations. In the cis configuration (structure a), the etheric protons are the most likely places for radical attack. This matches the results obtained by Kobsky et al.[19]. Because the alkyl chains are highly mobile in solution compared to the thermodynamic minimum calculated, the chains were frozen in a couple different configurations to determine if they may provide a protective effect for the ether protons in actual solutions. In both the exposed and protected positions, the etheric protons are still the most likely site for radical attack. In the protected version, the site itself is smaller, due to the alkyl chains covering the vulnerable protons. In the trans configuration (structure b,) the alkyl carbons closest to the amide become the most likely place for radical attack.

In addition to modelling TODGA alone, which is probably not representative of TODGA conformation in processes organic solutions, Fukui functions for TODGA hydrogen bound octanol, nitric acid, and water were calculated. Several different starting configurations (hydrogen bonded to different oxygens, *cis* vs. *trans* TODGA) were used, but all converged to roughly the same structure. For the nitric acid, it was assumed that the nitric acid remains associated in the organic phase based off of Singh's recent article[28]. The most protective

This project has received funding from the EURATOM research and training programme 2014-2018 under grant agreement No 755171. The content of this deliverable reflects only the author's view. The European Commission is not responsible for any use that may be made of the information it contains.

group was octanol (structure c), which eliminated the radical attack site from the side of TODGA it was bonded to and shifted it over to the amide and first two methylenes of the alkyl chain. The radical attack sites are much smaller and lower in value than the other Fukui functions calculated. Water (structure d) locked TODGA into the cis position and thus the etheric protons were the most likely sites for radical attack again. Nitric acid (structure e) became the likely site for radical attack when hydrogen bonded to TODGA. It cannot be determined solely from the computations if this effect is an overall protective or sensitizing effect, however, as it is unknown if the energy from the radical transfer is stabilized on the nitrate or if it passes onto the TODGA molecule.

It has been shown that TODGA molecules in solution are self-organized in reverse micelle type structures, particularly after contact with an aqueous medium[28-30]. Molecular dynamic simulations were used to predict TODGA configurations that may be present in solution[26]. Three different structures were pulled from the simulations: TODGA from a reverse micelle comprised of 7 TODGAs and 6 waters, TODGA from a tetramer that is hydrogen bonded to one water molecule, and a TODGA dimer with one water molecule in the centre. For the heptamer and tetramer (structure f and g respectively), only one TODGA molecule was pulled from the structure for analysis. For the dimer (structure h), the entire structure was used. The calculation for the largest micelle shows that the radical attack site is most likely on the carbons on the alkyl chain closest to the amide. The most likely radical attack site for the small micelle is different however, as the etheric protons become the most likely site for radical attack. Finally, for the dimer of TODGA the attack site again shifts back to the alkyl chains close to the amide. These results indicate that the environment of the TODGA molecule (concentration, water and nitric acid extraction, presence of octanol) alter the site for radical attack and lead to distribution of degradation products depending on the experimental conditions.

LINK BETWEEN CALCULATION AND TODGA DEGRADATION

When looking at the differences between the different conditions studied, the addition of nitric acid appears to have the largest effect on degradation. When no nitric acid is present, the only degradation products to appear are the ones from the radiolytic cleavage of TODGA. The presence of these compounds is also consistent with the relative strength of the bonds. The bond dissociation energies (BDE) calculation of the molecule indicates the weakest bond in the molecule is between the etheric C and O. The amide C-N bond is the strongest, therefore least likely to be broken by indirect radiolysis, i.e. being attacked by a dodecane radical. In general, the alkyl chains have the same high energy, making fragmentation of the alkyl chain more unlikely than fragmentation closer to the polar centre of the molecule. As nitric acid is added, however, many more products are introduced via hydrolysis.

Additionally, from the Fukui functions, it appears that nitric acid may protect the TODGA from direct radiolysis, as it becomes the most likely radical attack site when directly bonded to TODGA, and octanol would protect TODGA from radical attacks. The experimental effect observed in presence of nitric acid is consistent with calculation. In contrast to the expected results from calculation, the octanol present in the solution sensitized the TODGA degradation. In presence of octanol in solution, TODGA-octanol adducts are formed but several other parameters have to be considered. More water molecules are extracted in the organic phase and then more •OH radicals are formed. So, an increase of the TODGA degradation is expected either by electron transfer or by H-atom abstraction[9]. In presence of octanol, the stability of the TODGA molecule is an outcome of several competitive effects.

This project has received funding from the EURATOM research and training programme 2014-2018 under grant agreement No 755171. The content of this deliverable reflects only the author's view. The European Commission is not responsible for any use that may be made of the information it contains.

mTDDGA

The radiolytic stability of mTDDGA was studied in detail. mTDDGA has been under investigation for application in a new EURO-GANEX process[31]. It is an analogue of TODGA with longer alkyl side chains and additional methyl substituents in the backbone. The radiolytic stability of the double methylated TODGA, Me_2-TODGA, was studied before[13]. mTDDGA can form different diastereomers (Figure 13), of which the *cis* diastereomer is preferably used in process applications, as it is the better extractant. The same improved extraction of the *cis* diastereomer was observed for Me_2-TODGA[32]. In the radiolysis studied, a mixture of diastereomers was used, as well as the pure *cis* diastereomer.

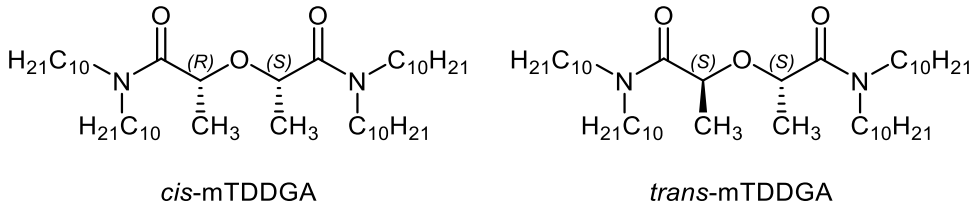

Figure 13: Chemical structure of *cis* and *trans*-mTDDGA.

Solutions of mTDDGA in alkane diluents were irradiated in the BRIGITTE facility at SCK CEN, Mol, Belgium with ^{60}Co γ radiation with and without contact to an aqueous phase. The dose constant (*d*) was derived as the slope of the resulting linear equation from the linear fitting of the natural logarithm of the concentration as a function of the absorbed dose. Values of $-3.0 \pm 0.4 \times 10^{-6}$ Gy^{-1} and $-2.7 \pm 0.6 \times 10^{-6}$ Gy^{-1} were determined for the irradiation without contact and in contact with 2.5 mol L^{-1} HNO_3, respectively. Compared to TODGA, mTDDGA shows a slightly lower dose constant. This observation is in line with what could be expected from the results of previous work of Galán *et al*[13]. in which double methylated TODGA derivates showed a lower dose constant.

The degradation products of mTDDGA were identified using high resolution mass spectrometry, of which the seven most important ones are shown in Figure 14 and 15. These degradation products agree very well with the degradation products identified previously for related diglycolamides[1-9,13]. The degradation compounds were synthesized by TWENTE and used for a quantitative analysis of irradiated samples. A series of degradation products of mTDDGA (samples of 0.5 – 1 g) was synthesized as outlined in Figure 154 to be studied in Juelich. The first product, didecyl lactamide, was prepared by amidation of lactic acid. The second reaction is a simple amidation between propionyl chloride and didecylamine in the presence of base. The other ones are reactions of a (di)carboxylic acid with (di)decylamine under peptide coupling conditions.

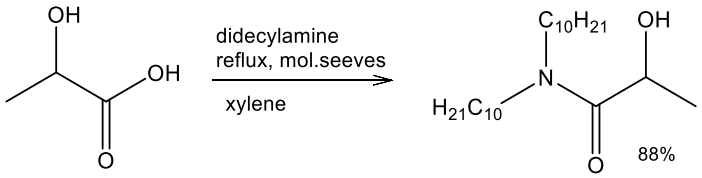

This project has received funding from the EURATOM research and training programme 2014-2018 under grant agreement No 755171. The content of this deliverable reflects only the author's view. The European Commission is not responsible for any use that may be made of the information it contains.

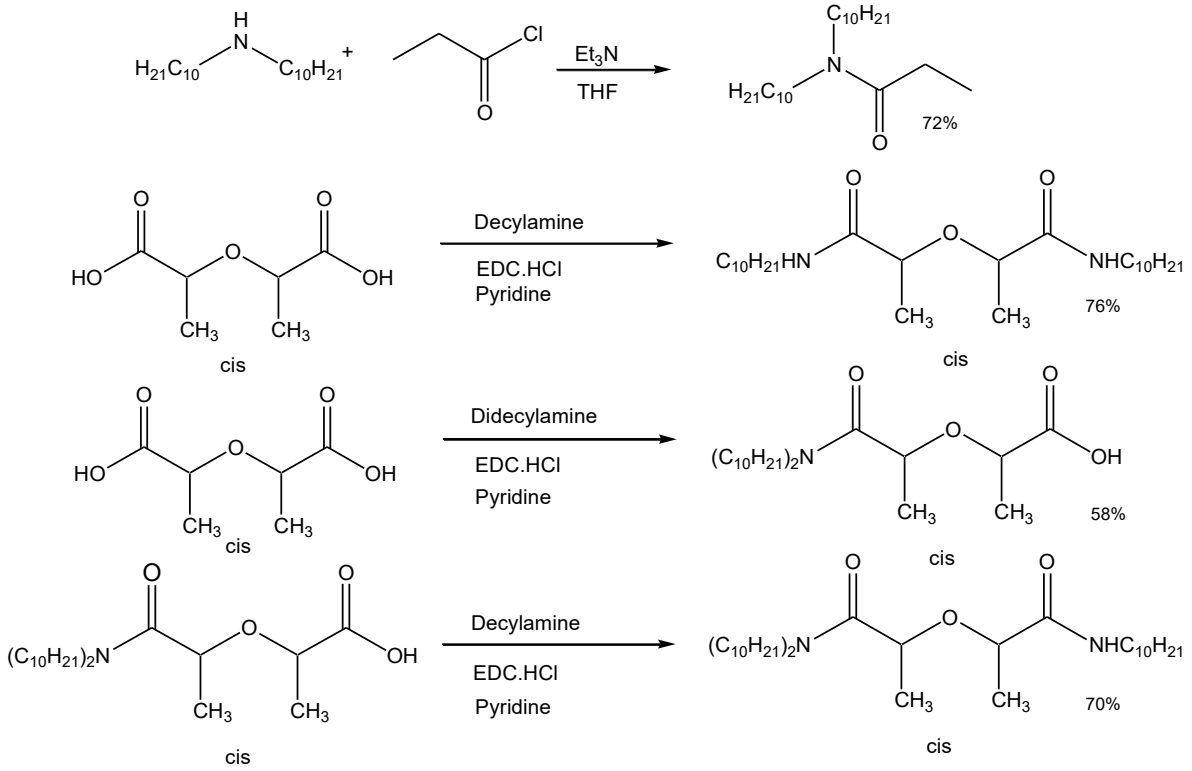

Figure 14: Synthesis of degradation products of mTDDGA

The results show that the C_{ether}-O_{ether} bond breaking product (DC III, with the alcohol group) is the most abundant degradation product, independent of the chemical conditions during irradiation. The presence of an aqueous nitric acid phase suppressed the formation of the other C_{ether}-O_{ether} bond breaking product (DC II) or causes it to be practically absent in the organic phase (e.g. by protonation and precipitation). The carboxylic acid degradation product (DC VII) does not appear in significant concentrations in the samples. For the irradiation of the neat organic phase, the concentration of didodecylamine was found to increase as a function of the absorbed dose. This was not the case when an acidic aqueous phase was present, as the amine was protonated and formed an insoluble precipitate. For the irradiation in contact with 2.5 mol L^{-1} HNO_3, the degradation products with the second highest concentration is DC I, the single de-alkylation product of mTDDGA. Evaluation of solvent extraction properties will be most interesting for DC I and DC III, because they dissolve easily in *n*-dodecane and were found in high concentrations in irradiated solvents. For TODGA and other related molecules, it was also previously shown that ether bond breaking compounds are mainly present in irradiated solvents[1,11,32].

Solvent extraction experiments with irradiated *cis*-mTDDGA of realistic concentrations (0.5 mol L^{-1}) showed only slightly decreasing distribution ratios for the actinides up to an absorbed dose of 450 kGy, proving the good radiolytic stability of the extractant. The degradation products were found to be only weak extractants, which should not interfere too much in a process application.

This project has received funding from the EURATOM research and training programme 2014-2018 under grant agreement No 755171. The content of this deliverable reflects only the author's view. The European Commission is not responsible for any use that may be made of the information it contains.

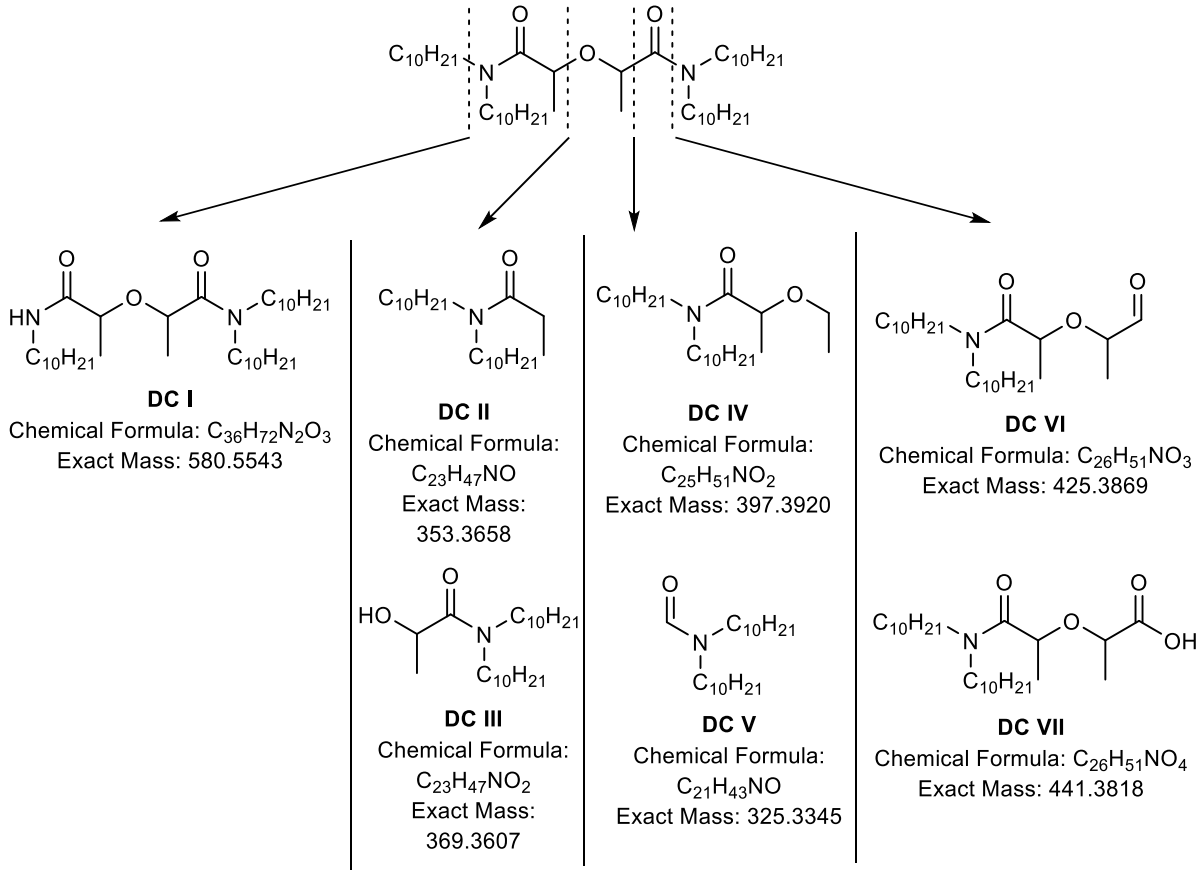

Figure 15: Identified degradation compounds of mTDDGA with their chemical formulas and monoisotopic molecular weights.

CyMe$_4$-BTBP and CyMe$_4$-BTPhen

RADIOLYTIC STABILITY STUDIES OF CyMe$_4$-BTBP AND CYME$_4$-BTPHEN IN 70% FS-13/30% TBP

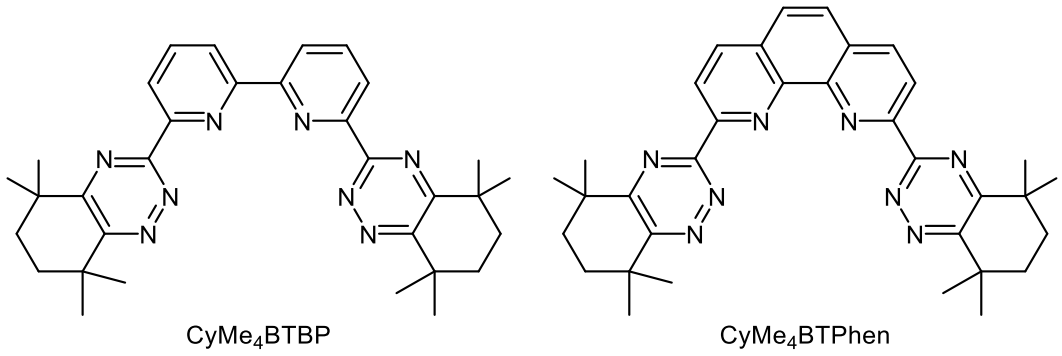

Figure 16. Chemical structure of CyMe$_4$BTBP and CyMe$_4$BTPhen.

As described in the recent paper, the GANEX (CHALMEX) system based on the use of phenyl trifluoromethyl sulfone (FS-13), CyMe$_4$-BTBP and TBP has shown promising results for extraction of actinides from spent

This project has received funding from the EURATOM research and training programme 2014-2018 under grant agreement No 755171. The content of this deliverable reflects only the author's view. The European Commission is not responsible for any use that may be made of the information it contains.

nuclear fuel[34-36]. During the project, the radiolytic stability of $CyMe_4$-BTBP and $CyMe_4$-BTPhen (Figure 16) in fluorinated diluent FS-13 used in CHALMEX process (0.01 M $CyMe_4$-BTBP in 70% FS-13/30% TBP; 4 M HNO_3) was studied in detail. More specifically, the behaviour of this system at different temperatures was investigated. Negative values of ΔH and ΔS were found for the extraction quantities in the tested system. In agreement with the earlier reports on the Chalmex process[36] the systems showed high stability. With increasing absorbed dose, both D_{Am} and D_{Eu} decreased. This decrease was slower when the organic phase was in contact with the aqueous phase during the irradiation. Comparison of the data with FS-13/TBP diluent compared to earlier data on octanol or another recently tested fluorinated solvent BK1 is presented in more detail in a manuscript in final stages of preparation[37].

Below, the most recent data are presented on the behaviour of the CHALMEX system (10 mM $CyMe_4$-BTBP in 70% FS-13 and 30% TBP) after irradiation by accelerated electrons at different temperatures. The aims of this study addressed the kinetics of extraction of Am(III) and Eu(III) in the given system and the influence of temperature on the values of extraction quantities. To get closer to reality during the reprocessing, the work focused on examining the properties of the systems after irradiation at different doses up to 500 kGy at four different temperatures in combination with different concentrations of nitric acid. For irradiated systems, the residual concentration of $CyMe_4$-BTBP was studied as a function of the absorbed dose (in cooperation with IIC).

NON-IRRADIATED SYSTEMS

KINETICS AT 1,500 RPM AT AMBIENT TEMPERATURE

Firstly, the kinetics of extraction of Am(III), Eu(III), and Cm(III) was studied at 21 ± 2 °C. The dependence of Percentage of extraction (%E) on time is shown in Figure 17. As it can be seen, the equilibrium for Am(III) was achieved approximately after 20 minutes of shaking at 1,500 rpm, while for Eu(III) and Cm(III) 30 minutes were needed. These results are in good agreement with published data[38]. The equilibrium values of %E were the following: $\%E_{Am}$ = 96, $\%E_{Cm}$ = 92, and $\%E_{Eu}$ = 21.

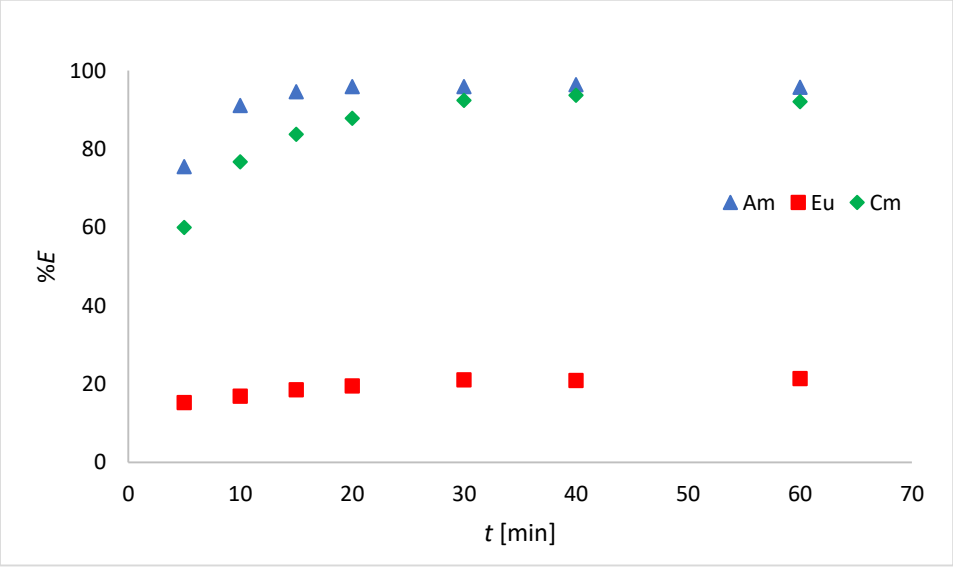

Figure 17: Kinetics of radionuclides extraction in CHALMES process at 1,500 rpm. 10 mM $CyMe_4$-BTBP in 70 % FS-13 and 30 % TBP, 4 M HNO_3 (%E = percentage of extraction).

This project has received funding from the EURATOM research and training programme 2014-2018 under grant agreement No 755171. The content of this deliverable reflects only the author's view. The European Commission is not responsible for any use that may be made of the information it contains.

DEPENDENCE OF THE KINETICS OF EXTRACTION ON TEMPERATURE

Next, the kinetics of extraction was studied at different temperatures. Lower shaking rate (250 rpm) and a linear shaker was used. At 250 rpm, the equilibration time was app. 40 minutes for Eu(III), 60 minutes for Am(III), and app. 120 min for Cm(III). The equilibrium values of %E are similar as for shaking rate of 1,500 rpm. The difference in equilibrium times can be explained by different mixing of phases during the shaking. At the lower rate, the moving is linear, while the higher mixing speed was achieved by vortexing. The values measured are shown in Table 7.

Table 7: Percentage of extraction (%*E*) for Am(III), Eu(III), and Cm(III) in the CHALMEX system (10 mM $CyMe_4$-BTBP in 70% FS-13 and 30% TBP, 4 M HNO_3) at 25 °C.

t [min]	%*E* (Am)	+/-	%*E* (Eu)	+/-	%*E* (Cm)	+/-
20	81.0	0.7	17.7	0.6	72.7	1.8
40	90.3	0.5	20.6	0.7	84.8	1.6
60	93.1	0.5	20.3	0.7	88.3	1.5
120	95.5	0.4	21.1	0.7	92.2	1.2
180	95.6	0.4	21.0	0.7	93.3	1.1

THE OVERALL MASS-TRANSFER COEFFICIENTS

To elucidate the rate-controlling process of extraction in this system, six kinetic models were tested. The methodology is described in[39] and the values of goodness-of-fit criteria, *WSOS/DF*, and the corresponding overall mass-transfer coefficients, *k*, are summarised in Table 8.

Table 8: Overall mass-transfer coefficients, *k,* and the corresponding goodness-of-fit criteria, *WSOS/DF,* values for six kinetic models describing vortexing at ambient (22°C) and shaking at thermostatted linear shaket (25°C) for the CHALMEX system (10 mM $CyMe_4$-BTBP in 70% FS-13 and 30% TBP, 4 M HNO_3).

Model	22 °C - Am		25 °C - Am		22 °C – Eu		25 °C - Eu	
	k [1/min]	*WSOS/DF*	*k* [1/min]	*WSOS/DF*	*k* [1/min]	*WSOS/DF*	*k* [1/min]	*WSOS/DF*
DM	1.18E-02	0.187	3.25E-03	2.61	8.46E-02	0.0362	2.27E-02	0.0641
FD	2.69E-01	0.188	5.92E-02	10.4	1.98E-02	0.0796	6.58E-03	0.0772
ID	6.54E-02	13	1.00E-02	11.6	5.20E-03	0.0128	1.55E-03	0.0179
CR	4.66E-01	38.8	8.19E-02	0.834	3.26E-02	0.0187	1.07E-02	0.579
GD	2.16E-03	7.04	4.31E-04	2.63	2.15E-02	0.0178	6.99E-03	0.0418
RLD	2.84E-03	13	4.57E-04	11.6	1.63E-02	000541	6.32E-03	0.0266

The values of *WSOS/DF* for Eu(III) extraction are very small and cannot be considered reliable, the best kinetic model should therefore be selected based on the Am-data. Similarly to the previous studies[39], the model based on the mass transfer (DM) was found to describe the best the kinetic data. This model is based on the so-called two-film theory of interphase diffusion.

This project has received funding from the EURATOM research and training programme 2014-2018 under grant agreement No 755171. The content of this deliverable reflects only the author's view. The European Commission is not responsible for any use that may be made of the information it contains.

The overall mass-transfer coefficients are app. 3-5 times higher for the faster speed of shaking. The values of overall mass-transfer coefficients for the mass transfer model are: k_{Am1} = 0.0118 min^{-1} (22 °C, 1500 RPM), k_{Am2} = 0.00325 min^{-1} (25 °C, 250 RPM), k_{Eu1} = 0.0846 min^{-1} (22 °C, 1500 RPM), k_{Eu2} = 0.0227 min^{-1} (25 °C, 250 RPM). Most probably, this should be ascribed to increase of the interphase area with increasing shaking rate (higher degree of dispergation and decrease of the thickness of the "liquid film").

THERMODYNAMICS OF THE CHALMEX SYSTEM

Firstly, equilibrium *D*-values were calculated at 15, 25, 35 and 45 °C. As an example, dependence of ln D_{Eu} on 1/*T* is shown in Figure 18. From the obtain values, changes in enthalpy and changes in entropy were calculated according to procedure in[40] and are shown in Table 9.

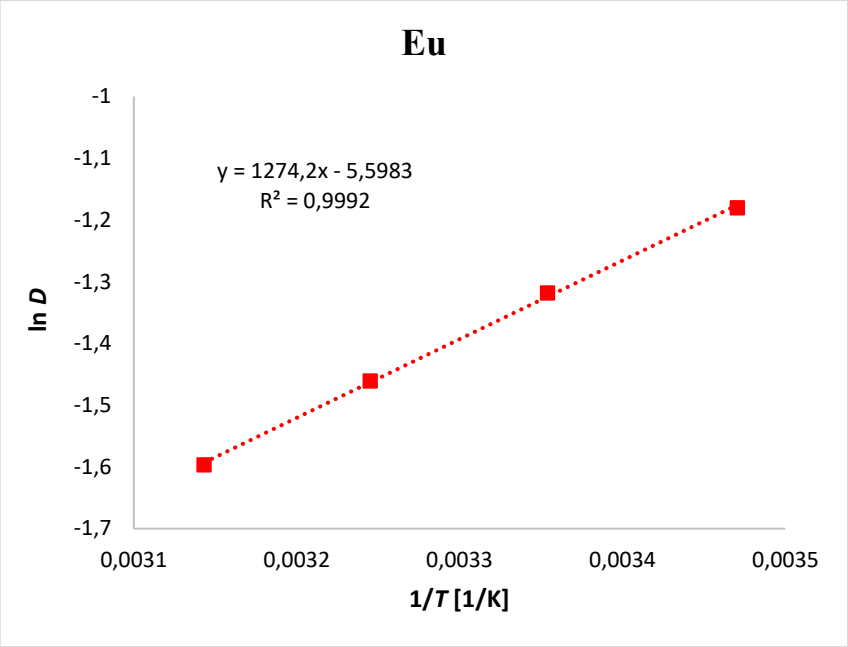

Figure 18: Dependence of ln D_{Eu} on 1/*T* for Eu(III) extraction in CHALMEX process (10 mM CyMe$_4$-BTBP in 70% FS-13 and 30% TBP, 4 M HNO_3).

Table 9: The thermodynamic quantities for the CHALMEX system (10 mM CyMe$_4$-BTBP in 70% FS-13 and 30% TBP, 4 M HNO_3).

	***ΔH* [kJ/mol]**			***ΔS* [J/mol·K]**		
Am	-16.7	+/-	2.2	-30.9	+/-	7.4
Eu	-10.6	+/-	0.2	-46.5	+/-	0.7

For a comparison, *ΔH* and *ΔS* values for the extraction of Eu, Am, and Cm by CyMe$_4$-BTBP or CyMe$_4$-BTPhen in different diluents are shown in Table 10. It should be noted that the CHALMEX system contains not only CyMe$_4$-BTBP, but also TBP, that functions as a diluent but also as an extracting compound.

The obtained value (Table 10) for the change in enthalpy for Am(III) is similar to CyMe$_4$-BTBP in cyclohexanone or hexan-1-ol. The value for Eu(III) is similar to CyMe$_4$-BTPhen in cyclohexanone. The change in entropy of Am(III) extraction was also negative and close to that measured for the extraction of Am(III) by CyMe$_4$-BTBP in nitrobenzene. In the case of the change in entropy of Eu(III) extraction, the system behaves similarly to CyMe$_4$-BTPhen in cyclohexanone. In general, difference in the values listed in Table 10 can be caused by two

This project has received funding from the EURATOM research and training programme 2014-2018 under grant agreement No 755171. The content of this deliverable reflects only the author's view. The European Commission is not responsible for any use that may be made of the information it contains.

different extracting compounds and their concentrations, different diluents, and various concentration of HNO_3 solutions.

Table 10: The thermodynamic quantities for different extracting systems.

	ΔH [kJ/mol]			*ΔS* [J/mol·K]		
CyMe$_4$-BTBP in cyclohexanone[41]						
Am	-21.0	+/-	1.8	29.0	+/-	6.0
CyMe$_4$-BTBP in hexan-1-ol[41]						
Am	-19.0	+/-	1.1	37.0	+/-	3.6
CyMe$_4$-BTBP in nitrobenzene[41]						
Am	-44	+/-	6.2	-23	+/-	21
Eu	-26.2	+/-	3.8	0.60	+/-	13
CyMe$_4$-BTPhen in acetonitrile[42]						
Eu	-113	+/-	6	-224	+/-	23
CyMe$_4$-BTPhen in cyclohexanone[40]						
Am	-25.4	+/-	2	-57	+/-	7
Cm	-23.3	+/-	4.7	-56	+/-	15
Eu	-7.7	+/-	2.6	-41	+/-	8

IRRADIATED SYSTEMS

The extraction systems were irradiated by pulse linear electron accelerator LINAC 4-1200 (Tesla v.t. Mikroel). The mean electron energy was 4.5 MeV, pulse width 3 μs and repeating frequency 500 Hz. The total doses were up to 500 kGy. Ampules were shaked and termostated during the irradiation.

IRRADIATION OF THE NEAT SOLVENT

The obtained values for D_{Am} and D_{Eu} and their dependences on the absorbed dose are shown in Table 11 and Table 12. When compared with other previously tested systems, the CHALMEX process seems to be quite stable against radiation. In the case of CyMe4-BTBP in 1-octanol, the extraction system was able to extract Am(III) up to 200 kGy and Eu(III) up to 100 kGy[44]. When using fluorinated BK-1, the system was able to extract only up to 50 kGy[44]. However, in another fluorinated diluent, FS-13, D_{Am} and D_{Eu} values increased with increasing doses[45]. From the *D*-values, $SF_{Am/Eu}$ were calculated. It can be seen that $SF_{Am/Eu}$ decreases with increasing doses (Table 13). From the HPLC-ESI-MS analysis, done at the IIC CAS, the residual concentrations of CyMe4-BTBP were determined. These values are shown in Table 14. The values for different temperatures are very similar and match well with the similar values of distribution ratios (Table 11 and Table 12).

This project has received funding from the EURATOM research and training programme 2014-2018 under grant agreement No 755171. The content of this deliverable reflects only the author's view. The European Commission is not responsible for any use that may be made of the information it contains.

Table 11: The dependence of D_{Am} values on absorbed dose at different temperatures for the CHALMEX system (10 mM $CyMe_4$-BTBP in 70% FS-13 and 30% TBP, 4 M HNO_3).

		***D*(Am)**											
		15 °C			**25 °C**			**35 °C**			**45 °C**		
***D*[kGy]**	**0**	24.1	+/-	3.2	21.4	+/-	2.1	16.5	+/-	1.7	12.6	+/-	1.1
	50	17.6	+/-	2.2	16.1	+/-	1.8	13.0	+/-	1.4	11.0	+/-	1.2
	100	12.6	+/-	1.3	11.8	+/-	1.1	10.1	+/-	1.0	8.8	+/-	0.9
	200	7.7	+/-	0.6	7.3	+/-	0.5	7.8	+/-	0.6	5.8	+/-	0.4
	350	3.5	+/-	0.2	3.9	+/-	0.2	4.7	+/-	0.3	4.0	+/-	0.3
	500	2.1	+/-	0.1	2.3	+/-	0.1	2.6	+/-	0.1	2.7	+/-	0.2

Table 12: The dependence of D_{Eu} values on absorbed dose at different temperatures for the CHALMEX system (10 mM $CyMe_4$-BTBP in 70% FS-13 and 30% TBP, 4 M HNO_3).

		***D*(Eu)**											
		15 °C			**25 °C**			**35 °C**			**45 °C**		
***D*[kGy]**	**0**	0.31	+/-	0.02	0.27	+/-	0.01	0.23	+/-	0.01	0.20	+/-	0.01
	50	0.29	+/-	0.02	0.23	+/-	0.01	0.21	+/-	0.01	0.20	+/-	0.01
	100	0.22	+/-	0.01	0.22	+/-	0.01	0.19	+/-	0.01	0.18	+/-	0.01
	200	0.17	+/-	0.01	0.17	+/-	0.01	0.18	+/-	0.01	0.17	+/-	0.01
	350	0.12	+/-	0.01	0.11	+/-	0.01	0.15	+/-	0.01	0.13	+/-	0.01
	500	0.10	+/-	0.01	0.10	+/-	0.01	0.11	+/-	0.01	0.10	+/-	0.01

Table 13: The dependence of $SF_{Am/Eu}$ values on absorbed dose at different temperatures for the CHALMEX system (10 mM $CyMe_4$-BTBP in 70% FS-13 and 30% TBP, 4 M HNO_3).

		***SF*(Am/Eu)**											
		15 °C			**25 °C**			**35 °C**			**45 °C**		
***D*[kGy]**	**0**	78	+/-	11	80	+/-	6	71	+/-	8	62	+/-	7
	50	62	+/-	9	71	+/-	9	61	+/-	8	55	+/-	7
	100	56	+/-	7	53	+/-	6	54	+/-	7	50	+/-	6
	200	45	+/-	5	42	+/-	4	43	+/-	5	35	+/-	4
	350	29	+/-	3	34	+/-	3	31	+/-	3	30	+/-	3
	500	21	+/-	2	22	+/-	2	25	+/-	3	28	+/-	3

Table 14: The dependence of residual concentrations of $CyMe_4$-BTBP on absorbed dose at different temperatures for the CHALMEX system (10 mM $CyMe_4$-BTBP in 70% FS-13 and 30% TBP, 4 M HNO_3).

		***c* [mmol/l]**			
		15 °C	**25 °C**	**35 °C**	**45 °C**
***D*[kGy]**	**0**	10.0	10.0	10.0	10.0
	50	5.9	7.2	7.7	7.2
	100	6.3	6.3	6.2	6.7
	200	4.7	4.8	5.0	5.1
	350	3.7	3.7	3.6	3.6
	500	2.8	2.7	2.7	2.8

This project has received funding from the EURATOM research and training programme 2014-2018 under grant agreement No 755171. The content of this deliverable reflects only the author's view. The European Commission is not responsible for any use that may be made of the information it contains.

From the values of residual concentrations, radiation-chemical yield G was calculated according to formula:

$$G = \frac{c_0 - c_r}{D \cdot \rho} \quad ,$$

where c_0 is an initial concentration of CyMe$_4$-BTBP (10 mM), c_r is a residual concentration of CyMe$_4$-BTBP, D is an absorbed dose, and ρ is a density of solvent (calculated from the percentage of each diluent; ρ = 1.274 kg/l). Calculated G-values are shown in Table 15. The G-values decrease with increasing doses. This trend is logical since the concentration of CyMe$_4$-BTBP decreases in course of the irradiation. For the dose of 50 kGy, the G-value is the highest since the concentration of extracting ligand is the highest.

Table 15: The dependence of radiation-chemical yield, *G*, on absorbed dose, *D*, at different temperatures for the CHALMEX system (10 mM CyMe$_4$-BTBP in 70% FS-13 and 30% TBP, 4 M HNO$_3$).

		***G* [µmol/J]**			
		15 °C	**25 °C**	**35 °C**	**45 °C**
***D*[kGy]**	**50**	0.0641	0.0434	0.0367	0.0437
	100	0.0292	0.0289	0.0299	0.0258
	200	0.0206	0.0203	0.0196	0.0192
	350	0.0142	0.0141	0.0143	0.0143
	500	0.0112	0.0114	0.0115	0.0114

The theoretical D-values (Table 16 and Table 17) were calculated from the values of residual CyMe$_4$-BTBP concentrations and compared with the experimental D-values. Based on the stoichiometry of the reaction, TBP is not a part of formed complexes. The formula used for the calculation was:

$$D_{theo} = \frac{D_0(M)}{c_0^2} \cdot c_r^2 \quad ,$$

where D_0(M)is a distribution ratio for a non-irradiated sample. When compared with the experimental D-values (Table 11 and Table 12, the theoretical values are lower. It means that some of the CyMe$_4$-BTBP degradation products or adducts of CyMe$_4$-BTBP or TBP are probably able to extract the studied metals, too, or positively influence their extraction in another way.

Table 16: The theoretical values of D_{Am} as a function of absorbed dose, *D*, for the CHALMEX system.

		***D*$_{theo}$(Am)**			
		15 °C	**25 °C**	**35 °C**	**45 °C**
***D*[kGy]**	**50**	8.4	11.2	9.7	6.6
	100	9.5	8.5	6.3	5.7
	200	5.4	5.0	4.1	3.3
	350	3.2	3.0	2.2	1.6
	500	1.9	1.6	1.2	1.0

This project has received funding from the EURATOM research and training programme 2014-2018 under grant agreement No 755171. The content of this deliverable reflects only the author's view. The European Commission is not responsible for any use that may be made of the information it contains.

Table 17: The theoretical values of D_{Eu} as a function of absorbed dose, *D*, for the CHALMEX system.

		D_{theo}(Eu)			
		15 °C	**25 °C**	**35 °C**	**45 °C**
***D*[kGy]**	**50**	0.108	0.141	0.135	0.104
	100	0.122	0.108	0.088	0.090
	200	0.070	0.063	0.058	0.052
	350	0.042	0.038	0.030	0.026
	500	0.025	0.020	0.017	0.015

IRRADIATION OF THE SOLVENT IN CONTACT WITH HNO_3

The obtained values for D_{Am} and D_{Eu} are shown in Table 18 and Table 19. As under the irradiation without the aqueous phase, the D_{Am} values decrease with increasing dose. In the case of Eu(III) the *D*-values decrease much less (they are almost constant). In this case, decrease in *D*-values is lower compared to irradiation of only organic phase.

Table 18: The dependence of D_{Am} values on absorbed dose, *D*, at different temperatures for the CHALMEX system (10 mM $CyMe_4$-BTBP in 70% FS-13 and 30% TBP) irradiated in the presence of aqueous phase (4 M HNO_3).

		***D*(Am)**											
		15 °C			**25 °C**			**35 °C**			**45 °C**		
***D*[kGy]**	**0**	24.1	+/-	3.2	21.4	+/-	2.1	16.5	+/-	1.7	12.6	+/-	1.1
	50	16.0	+/-	1.8	15.6	+/-	1.8	11.4	+/-	1.3	10.6	+/-	1.1
	100	17.8	+/-	2.4	15.7	+/-	1.8	10.9	+/-	1.2	8.8	+/-	0.9
	200	16.1	+/-	1.8	13.3	+/-	1.5	9.2	+/-	0.8	7.2	+/-	0.7
	350	12.9	+/-	1.4	9.5	+/-	0.9	7.5	+/-	0.7	5.6	+/-	0.4
	500	9.5	+/-	0.8	8.1	+/-	0.7	N/A			4.8	+/-	0.3

Table 19: The dependence of D_{Eu} values on absorbed dose, *D*, at different temperatures for the CHALMEX system (10 mM $CyMe_4$-BTBP in 70% FS-13 and 30% TBP) irradiated in the presence of aqueous phase (4 M HNO_3).

		***D*(Eu)**											
		15 °C			**25 °C**			**35 °C**			**45 °C**		
***D*[kGy]**	**0**	0.31	+/-	0.02	0.27	+/-	0.01	0.23	+/-	0.01	0.20	+/-	0.01
	50	0.25	+/-	0.02	0.24	+/-	0.01	0.20	+/-	0.02	0.17	+/-	0.01
	100	0.26	+/-	0.02	0.23	+/-	0.01	0.21	+/-	0.02	0.16	+/-	0.01
	200	0.26	+/-	0.02	0.24	+/-	0.02	0.19	+/-	0.01	0.15	+/-	0.01
	350	0.26	+/-	0.01	0.21	+/-	0.01	0.18	+/-	0.01	0.14	+/-	0.01
	500	0.26	+/-	0.02	0.21	+/-	0.01	N/A			0.15	+/-	0.01

For a better comparison of the influence of the presence of aqueous phase during irradiation, Table 20 shows D_{Am} values for 15 °C. It is obvious that the presence of HNO_3 decrease the drop in D_{Am} values. This effect is caused by the higher residual concentration of $CyMe_4$-BTBP at the higher doses (see Table Table 22). This stabilization effect may be also ascribed to scavenging of free radicals created during the radiolysis by HNO_3[43].

This project has received funding from the EURATOM research and training programme 2014-2018 under grant agreement No 755171. The content of this deliverable reflects only the author's view. The European Commission is not responsible for any use that may be made of the information it contains.

Table 20: Comparision of the influence of the presence of 4 M HNO_3 during the irradioation of the CHALMEX system (10 mM $CyMe_4$-BTBP in 70% FS-13 and 30% TBP, 4 M HNO_3).

		***D*(Am)**					
		only solvent			**solvent + HNO_3**		
***D*[kGy]**	**0**	24.1	+/-	3.2			
	50	17.6	+/-	2.2	16.0	+/-	1.8
	100	12.6	+/-	1.3	17.8	+/-	2.4
	200	7.7	+/-	0.6	16.1	+/-	1.8
	350	3.5	+/-	0.2	12.9	+/-	1.4
	500	2.1	+/-	0.1	9.5	+/-	0.8

Again, the CHALMEX system irradiated in contact with HNO_3 is more stable than most of the other tested systems where the solvent was in contact with aqueous phase during the irradiation. In the case of $CyMe_4$-BTBP in 1-octanol, the extraction system was able to extract Am(III) and Eu(III) up to 300 kGy with very small decrease in *D*-values[43]. When using $CyMe_4$-BTBP in BK-1, the system was able to extract Am(III) and Eu(III) up to 150 kGy only[44]. The values of Am/Eu separation factors, $SF_{Am/Eu}$, are shown in Table 21. It can be seen that the $SF_{Am/Eu}$ values decrease and are approx. two times lower at 500 kGy dose. The decrease in SF is slower than under the previous irradiation conditions (without the presence of aqueous phase with HNO_3 during the irradiation).

Residual concentrations of $CyMe_4$-BTBP were also determined and are shown in Table 22 together with presence of degradation products (their measured masses) in the samples by tandem LC-MS (Figure 19). It can be seen that they are higher than in the case of irradiation in absence of aqueous phase which clearly explains the measured much higher *D*-values for extraction of Am(III) and Eu(III).

Table 21: The dependence of Am/Eu separation factor, $SF_{Am/Eu}$, on absorbed dose, *D*, at different temperatures for the CHALMEX system (10 mM $CyMe_4$-BTBP in 70% FS-13 and 30% TBP) irradiated in the presence of aqueous phase (4 M HNO_3).

		***SF*(Am/Eu)**											
		15 °C			**25 °C**			**35 °C**			**45 °C**		
***D*[kGy]**	**0**	78	+/-	11	80	+/-	6	71	+/-	8	62	+/-	7
	50	65	+/-	8	65	+/-	9	58	+/-	8	65	+/-	8
	100	67	+/-	10	69	+/-	9	53	+/-	7	54	+/-	7
	200	62	+/-	8	57	+/-	7	49	+/-	6	49	+/-	6
	350	50	+/-	6	45	+/-	5	42	+/-	5	39	+/-	4
	500	37	+/-	4	39	+/-	4	N/A			33	+/-	4

Table 22: The dependence of residual concentrations of $CyMe_4$-BTBP on absorbed dose, *D*, at different temperatures for the CHALMEX system (10 mM $CyMe_4$-BTBP in 70% FS-13 and 30% TBP) irradiated in the presence of aqueous phase (4 M HNO_3).

		***c* [mmol/l]**			
		15 °C	**25 °C**	**35 °C**	**45 °C**
***D*[kGy]**	**0**	10.0	10.0	10.0	10.0
	50	7.9	7.9	8.0	7.0
	100	7.3	7.5	7.6	7.9
	200	6.7	6.7	6.8	7.3
	350	6.1	5.9	6.4	6.1
	500	5.6	5.4	N/A	5.3

This project has received funding from the EURATOM research and training programme 2014-2018 under grant agreement No 755171. The content of this deliverable reflects only the author's view. The European Commission is not responsible for any use that may be made of the information it contains.

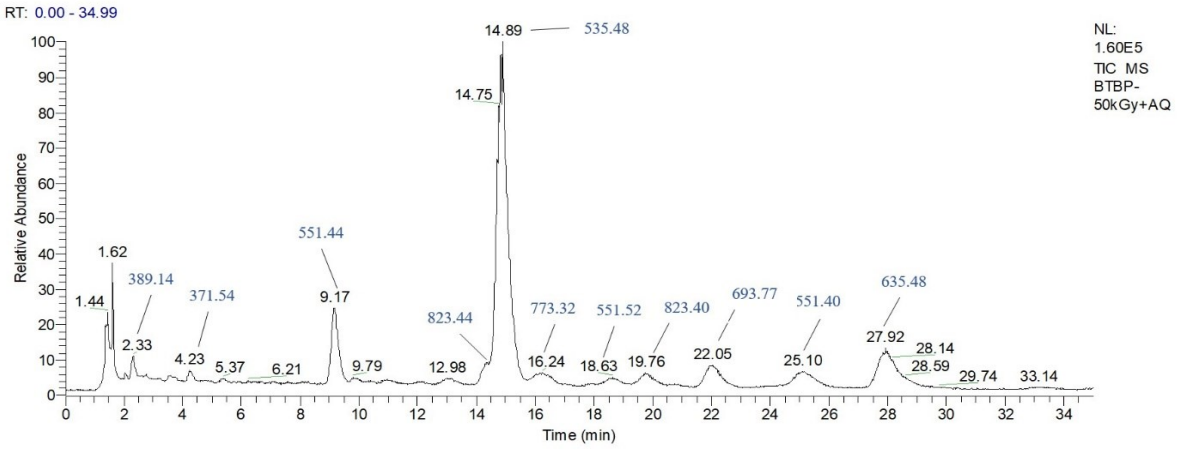

Figure 19: Example of HPLC chromatograms with isocratic elution of CyMe$_4$-BTBP (70% FS-13 and 30% TBP) irradiated with a 50 kGy dose in presence of aqueous phase (4 M HNO_3); measured with MS detection; flow rate 0.3 mL/min; column: Gemini-NX C18 110 Å (3 µm, 150 x 2.00 mm *I.D.*); mobile phase: 10 mM DEAO pH 8.2 with 78% ACN.

From the values of the residual concentrations, radiation-chemical yield was calculated (Table 23). When compared with the data in Table 15, the *G*-values are lower. *D*-values, residual concentration and *G*-values proved that system with irradiation of both phases is much more stable.

Table 23: The dependence of radiation-chemical yield, *G*, on absorbed dose, *D*, at different temperatures for the CHALMEX system (10 mM CyMe$_4$-BTBP in 70% FS-13 and 30% TBP) irradiated in the presence of aqueous phase (4 M HNO_3).

		***G* [µmol/J]**			
		15 °C	**25 °C**	**35 °C**	**45 °C**
***D*[kGy]**	**50**	0.0327	0.0327	0.0318	0.0470
	100	0.0209	0.0194	0.0192	0.0168
	200	0.0128	0.0128	0.0125	0.0104
	350	0.0088	0.0092	0.0081	0.0087
	500	0.0069	0.0072	N/A	0.0074

The theoretical D-values (Table 24 and Table 25) were calculated from the values of residual CyMe$_4$-BTBP concentrations and compared with experimental *D*-values. When compared with the experimental *D*-values (Table 18 and Table 19), the theoretical values are slightly lower, but higher than in the previous case. Again, this confirms positive influence of the presence of HNO_3 on suppressing the degradation of CyMe$_4$-BTBP.

Table 24: The theoretical values of D_{Am} as a function of absorbed dose, *D*, for the CHALMEX system irradiated in the presence of aqueous phase (4 M HNO_3).

		***D*$_{teo}$(Am)**			
		15 °C	**25 °C**	**35 °C**	**45 °C**
***D*[kGy]**	**50**	15.1	13.4	10.5	6.2
	100	13.0	12.1	9.4	7.8
	200	11.0	9.7	7.6	6.8
	350	8.9	7.5	6.8	4.7
	500	7.6	6.2	N/A	3.5

This project has received funding from the EURATOM research and training programme 2014-2018 under grant agreement No 755171. The content of this deliverable reflects only the author's view. The European Commission is not responsible for any use that may be made of the information it contains.

Table 25: The theoretical values of D_{Eu} as a function of absorbed dose, *D*, for the CHALMEX system irradiated in the presence of aqueous phase (4 M HNO_3).

		D_{teo}(Eu)			
		15 °C	**25 °C**	**35 °C**	**45 °C**
***D*[kGy]**	**50**	0.194	0.169	0.146	0.098
	100	0.167	0.153	0.131	0.124
	200	0.141	0.123	0.107	0.108
	350	0.115	0.094	0.094	0.075
	500	0.098	0.079	N/A	0.056

INFLUENCE OF THE CONCENTRATION OF HNO_3 PRESENT DURING THE IRRADIATION

Next, the influence of HNO_3 concentration (2, 4 and 8 M) present during the irradiation on the properties of the irradiated solvent was tested. As expected, for the non-irradiated systems, with increasing *c*(HNO_3) the *D*-values for tested ions decrease (Table 26 and Table 27). For the irradiated systems, the dependence of *D*-values on the absorbed dose depends on the HNO_3 concentration. As observed before and demonstrated above, in 4 M HNO_3 the *D*-values decrease with the increasing dose; when irradiated with 8 M HNO_3 this decrease is much faster. However, when the solvent was irradiated with 2 M HNO_3, *D*-values for Am(III) and Eu(III) increase with the increasing dose. The most probable explanation of this behaviour is that upon the radiolysis products/adducts are formed that are efficient extractants but, contrary to the original ligands that extract by solvation mechanism, those extract by ion exchange mechanism. The extraction efficiency of such ligands is known to depend strongly on the concentration of H^+-ions, increasing with increasing *p*H / decreasing acidity.

The values of $SF_{Am/Eu}$ decrease with increasing HNO_3 concentration as well as with the increasing absorbed dose (Table 28). This means that the new radiolytically formed extractants don´t exhibit significant An/Ln selectivity. The residual concentrations of $CyMe_4$-BTBP for these systems determined by HPLC methods at IIC are shown in Table 29. The concentrations of extracting compound decrease independently on the HNO_3 concentration. It supports the previously stated explanation that on the nature of extraction properties of the new radiolysis degradation products/adducts. As before, the radiation-chemical yields were calculated (Table 30), their values are independent, again, on HNO_3 concentration and are the highest for the lowest absorbed doses when the $CyMe_4$-BTBP residual concentration is the highest.

Table 26: The dependence of D_{Am} values on absorbed dose, *D*, for the CHALMEX system (10 mM $CyMe_4$-BTBP in 70% FS-13 and 30% TBP) irradiated in the presence of aqueous phase (2, 4 or 8 M HNO_3).

		D(Am)								
		2 M			**4 M**			**8 M**		
***D*[kGy]**	**0**	25	+/-	8	21.4	+/-	2.1	0.53	+/-	0.04
	50	59	+/-	17	15.6	+/-	1.8	0.13	+/-	0.01
	100	67	+/-	22	15.7	+/-	1.8	0.12	+/-	0.01
	200	75	+/-	24	13.3	+/-	1.5	0.09	+/-	0.01
	350	79	+/-	24	9.5	+/-	0.9	0.08	+/-	0.01
	500	71	+/-	22	8.1	+/-	0.7	0.08	+/-	0.01

This project has received funding from the EURATOM research and training programme 2014-2018 under grant agreement No 755171. The content of this deliverable reflects only the author's view. The European Commission is not responsible for any use that may be made of the information it contains.

Table 27: The dependence of D_{Eu} values on absorbed dose, *D*, for the CHALMEX system (10 mM CyMe$_4$-BTBP in 70% FS-13 and 30% TBP) irradiated in the presence of aqueous phase (2, 4 or 8 M HNO_3).

		D(Eu)								
		2 M			4 M			8 M		
D[kGy]	0	0.20	+/-	0.03	0.27	+/-	0.01	0.060	+/-	0.010
	50	0.55	+/-	0.05	0.24	+/-	0.01	0.054	+/-	0.006
	100	0.87	+/-	0.07	0.23	+/-	0.01	0.053	+/-	0.007
	200	1.20	+/-	0.11	0.24	+/-	0.02	0.055	+/-	0.007
	350	1.63	+/-	0.15	0.21	+/-	0.01	0.057	+/-	0.007
	500	2.28	+/-	0.24	0.21	+/-	0.01	0.053	+/-	0.007

Table 28: The dependence of $SF_{Am/Eu}$ values on absorbed dose, *D*, for the CHALMEX system (10 mM CyMe$_4$-BTBP in 70% FS-13 and 30% TBP) irradiated in the presence of aqueous phase (2, 4 or 8 M HNO_3).

		SF(Am/Eu)								
		2 M			4 M			8 M		
D[kGy]	0	130	+/-	43	80	+/-	6	8.9	+/-	1.7
	50	108	+/-	33	65	+/-	9	2.3	+/-	0.3
	100	77	+/-	26	69	+/-	9	2.3	+/-	0.3
	200	63	+/-	21	57	+/-	7	1.7	+/-	0.3
	350	48	+/-	15	45	+/-	5	1.4	+/-	0.2
	500	31	+/-	10	39	+/-	4	1.4	+/-	0.2

Table 29: The HPLC determined residual concentrations of CyMe$_4$-BTBP on absorbed dose, *D*, for the CHALMEX system (10 mM CyMe$_4$-BTBP in 70% FS-13 and 30% TBP) irradiated in the presence of aqueous phase (2, 4 or 8 M HNO_3).

		c [mmol/l]		
		2 M	4 M	8 M
D[kGy]	0	10.0	10.0	10.0
	50	8.4	7.9	8.0
	100	7.7	7.5	7.5
	200	6.8	6.7	6.8
	350	6.0	5.9	6.0
	500	5.0	5.4	5.3

Table 30: The dependence of radiation-chemical yield, *G*, on absorbed dose, *D*, for the CHALMEX system (10 mM CyMe$_4$-BTBP in 70% FS-13 and 30% TBP) irradiated in the presence of aqueous phase (2, 4 or 8 M HNO_3).

		G [µmol/J]		
		2 M	4 M	8 M
D[kGy]	50	0.0252	0.0327	0.0314
	100	0.0181	0.0194	0.0199
	200	0.0125	0.0128	0.0127
	350	0.0089	0.0092	0.0090
	500	0.0078	0.0072	0.0074

This project has received funding from the EURATOM research and training programme 2014-2018 under grant agreement No 755171. The content of this deliverable reflects only the author's view. The European Commission is not responsible for any use that may be made of the information it contains.

Theoretical *D*-values were calculated (Table 31 and Table 32) from the values of residual $CyMe_4$-BTBP concentrations and compared with the experimental *D*-values (Table 26 and Table 27). As can be seen from the data in Table 31 and Table 32, the theoretical *D*-values decrease with the increasing absorbed dose for all HNO_3 concentrations. However, in experiment, this behaviour was observed only for 4 and 8 M HNO_3. In the case of 2 M HNO_3, the trend is opposite and the experimental *D*-values for both Am(III) and Eu(III) increase even though the concentrations of $CyMe_4$-BTBP decrease. One of the several possible explanations was proposed above the mechanism of the new radiolytical products/adducts reverted to the ion-exchange extraction. From the fundamental science level, this system with 2 M HNO_3 would deserve more detailed studies.

Table 31: The theoretical values of D_{Am} for the CHALMEX system irradiated in the presence of aqueous phase (2, 4 or 8 M HNO_3).

		D_{theo}(Am)		
		2 M	**4 M**	**8 M**
***D*[kGy]**	**50**	17.9	13.4	0.34
	100	15.0	12.1	0.30
	200	11.7	9.7	0.24
	350	9.2	7.5	0.19
	500	6.4	6.2	0.15

Table 32: The theoretical values of D_{Eu} for the CHALMEX system irradiated in the presence of aqueous phase (2, 4 or 8 M HNO_3).

		D_{theo}(Eu)		
		2 M	**4 M**	**8 M**
***D*[kGy]**	**50**	0.137	0.169	0.038
	100	0.115	0.153	0.034
	200	0.090	0.123	0.028
	350	0.071	0.094	0.022
	500	0.049	0.079	0.017

DEGRADATION CHEMISTRY OF $CyMe_4$-BTBP UNDER DIFFERENT CONDITIONS

PRE-SURVEY OF $CyMe_4$-BTBP DEGRADATION

During this project, pre-survey was focused on deeper analyses of the irradiated sample together with influence of irradiation conditions on the presence of degradation products. Firstly, the main attention was paid on deeper analyses of the previous samples (series F, J, G, for irradiation conditions see Table 33) supplied during the extension of the SACSESS Project, identification of the peaks of degradation products on chromatograms, their better separation and determining their relative abundance in the samples. The whole series of samples irradiated previously by CTU in collaboration with Chalmers have been used through this first study performed at IIC CAS and compared. Differences in composition of degradation products were found by HPLC and using detailed mass spectrometry measurements. The composition of degradation products in the samples was in significantly altered, provided that samples were irradiated in neat solvent, in contact with HNO_3, or in Ganex solvent containing TBP.

Surprisingly enough, the series G (in FS-13 with 30% TBP) gave the clearest image. Though there was a large solvent peak on HPLC, retention behavior of most of degradation products could be adjusted to allow for their better integration. Combining the small scale isolations of the components by semi-preparative HPLC with mass

This project has received funding from the EURATOM research and training programme 2014-2018 under grant agreement No 755171. The content of this deliverable reflects only the author's view. The European Commission is not responsible for any use that may be made of the information it contains.

spectrometry, two main peaks of degradation products could be isolated in essentially pure form by HPLC and have been identified by MS to correspond most probably to mono- and dihydroxy derivatives of $CyMe_4$-BTBP. However, there could be still several other isomeric species of dihydroxy derivative in the samples as suggest MS of other isolated HPLC fractions, which correspond to small, less resolved peaks (mixed) on the chromatograms. No strongly retained species, which would correspond to high molecular mass peaks in MS spectrum (arising from addition of solvent molecule, as observed previously for cyclohexanones) could be observed using HPLC method with gradient elution. The relative abundances of the two main peaks could be determined by analytical HPLC and are shown in Table 33. It can be seen, the mono derivative interconverts gradually to dihydroxy derivative as the dose increases and then to some other products. Apparently, these species have lower molecular mass and could not be resolved yet from solvent peak on chromatograms. According to MS analysis, the samples contain small amounts of other components with correspond m/z values 346, 371, 523, 532, 557, 573 and 603.

Table 33: Relative abundance of two main degradation products determined in samples from Series G ($CyMe_4$-BTBP in FS-13 with 30% TBP) in contact with 1.0, 2.0 and 4.0 M HNO_3. The calibrations were performed using $CyMe_4$-BTBP standard G, 239 nm.

Sample	Dose [kGy]	BTBP *c* [mmol]*	BTBP-OH [%]	σ_r	BTBP-$(OH)_2$ [%]	σ_r
BTBP+FS13+TBP (Chalmex solvent), 1M HNO_3						
G1M20	20	1.18	19.0	3.71	1.6	4.87
G1M50	50	0.56	31.0	3.93	5.3	2.11
G1M100	100	0.04	16.8	2.98	23.8	3.10
G1M200	200	0.02	4.3	4.44	34.2	3.00
G1M500	500	0.01	10.7	3.23	9.3	2.22
BTBP+FS13+TBP (Chalmex solvent), 2M HNO_3						
G2M20	20	2.85	34.6	4.01	1.4	1.82
G2M50	50	0.61	61.8	5.47	7.7	6.15
G2M100	100	0	36.5	1.77	23.2	1.57
G2M200	200	0	22.1	1.01	24.4	0.99
G2M500	500	0	12.1	0.72	21.4	1.13
BTBP+FS13+TBP (Chalmex solvent), 4M HNO_3						
G4M20	20	2.33	37.8	2.54	1.0	1.75
G4M50	50	0.42	68.2	0.91	4.9	1.36
G4M100	100	0.28	73.8	3.14	11.2	5.14
G4M200	200	0.02	25.1	0.64	37.3	0.57
G4M500	500	0.01	30.4	1.53	15.9	1.02

Next, series of 8 samples of volume 5.0 mL each had been irradiated at Chalmers facility by uniform dose 500 kGy either in presence or absence of aqueous phase (4 M HNO_3). These conditions were selected after discussion with Chalmers to reflect adequately:

a) Rich variety of approved solvents.

b) Conditions with and without of contact with acid.

c) Doses, which were assumed to degrade larger part of the ligand and generate appreciable quantities of degradation products in the samples. It was assumed, the amount of the samples would allow for isolation of the main degradation products in a sufficient quantity for performing their characterization by NMR methods (>0.5 mg of pure compound is necessary).

This project has received funding from the EURATOM research and training programme 2014-2018 under grant agreement No 755171. The content of this deliverable reflects only the author's view. The European Commission is not responsible for any use that may be made of the information it contains.

As could be seen in Table 34, contact with acid plays again positive role on stability of the systems in cases, when Chalmex diluent or octanol were used. Complete degradation was observed in both octanol samples without contact with acid. Furthermore, the degradation products in this case are different than in other samples in FS-13, and apparently corresponded to adducts with octanol. The degradation products in other samples mainly corresponded to peaks that are less retained than $CyMe_4$-BTBP. Presence of hydroxy derivative was observed by HPLC in white and orange samples in octanol and in lower concentration in green sample. Surprisingly enough, no hydroxy derivative was observed in yellow sample in FS-13 in contact with 4M HNO_3. The composition differs depending on the solvent, conditions used during irradiation (*i.e.* in neat solvent or in contact with HNO_3), or in presence of TBP (Ganex-type solvents).

Nevertheless, the amounts of products isolated using semi-preparative HPLC from these samples were not sufficient enough for performing NMR characterizations (ca. 2 mg of pure compound is necessary to collect). Therefore, for this, a larger-volume samples containing higher initial concentration of the ligand were prepared and irradiate at Chalmers Univ. and supplied to IIC. Also the irradiation doses were set up in such manner that the concentrations of individual degradation products in the irradiated samples Green, Blue and Red (described in the section below) would higher, although the last condition was fulfilled in part.

Table 34: Concentrations of BTBP found in the irradiated samples; the initial concentration of the ligand 10 mM.

Sample	Diluent	Contact	Dose [kGy]	Residual conc. [%][a]	BTBP *c* [mmol][a]	σ_r
Red Big	70% FS-13, 30% TBP	4M HNO_3	500	70.1	7.06	4.98
Green Big	70% FS-13, 30% TBP	No	500	35.2	3.52	1.81
Yellow Big	FS-13	4M HNO_3	500	53.8	5.38	1.05
Blue Big	FS-13	No	500	56.3	5.63	7.02
Orange Big	70% Oct, 30% TBP	4M HNO_3	200	62.9	6.29	1.81
Pink Big	70% Oct, 30% TBP	No	200	0.0	0.00	-
White Big	Octanol	4M HNO_3	200	63.7	6.37	1.65
Grey Big	Octanol	No	200	0.0	0.00	-

a) Calculated based on Standards small samples supplied.

HPLC-APCI-MS ANALYSIS OF IRRADIATED LARGE-VOLUME SAMPLES

In this section, the main attention is paid on deeper analyses of the sample together with formed degradation products, their identification and relative abundance in the sample. The various $CyMe_4$-BTBP samples in large-volume of solvent (up to 50 mL) and larger initial concentration (10, 50 and 50 mM) Green, Blue, and Red were prepared and irradiated by doses 700, 1200 and 300 kGy, respectively (Table 35). These conditions were chosen to be the most suitable based on results obtained from previous results, which obtained on smaller volumes of the samples under different conditions of irradiation in various solvent combinations. The concentrations, volumes and doses resulted from discussions between partners. All mentioned samples were irradiated by Chalmers Univ. and CTU to cover adequately:

a) All approved solvents.
b) Clearer degradation pathways observed previously in presence of aqueous phase - all samples were irradiated in the presence of 4M HNO_3.
c) Doses were designed according to previous results and were further tuned in course of irradiation determining residual concentration by HPLC and presence of degradation products by MS.
d) The irradiation was stopped at the stages, when a larger part of the ligand was degraded (according to HPLC analyses) and appreciable quantities of degradation products formed in the samples.

This project has received funding from the EURATOM research and training programme 2014-2018 under grant agreement No 755171. The content of this deliverable reflects only the author's view. The European Commission is not responsible for any use that may be made of the information it contains.

For these purposes a new tandem LC-MS method was developed for more detailed analysis of the samples. This allowed for on-line monitoring molecular peaks of individual peaks on chromatograms. The analytical method is based on the use of volatile buffer, which is compatible with components of mass spectrometer. This method was used for analyses of all three samples and individual fractions from *semi*-preparative chromatographic separations. Illustration of its use for analysis of all three samples are depicted in Figure 20, Figure 22, Figure 24. Selected spectra of individual peaks are shown below and are all set of data is available on request from IIC CAS (see Figure 21, Figure 23, Figure 25). Retention times relating to each measured MS in chromatogram are shown in each image. Based on obtained results can be seen differences in composition of degradation products by using HPLC and by more detailed mass spectrometry measurements of each individual peaks performed across the various samples. The composition difference depending on the solvent (sample irradiated in 30% TBP with 1-octanol or FS-13; or just in FS-13), conditions used during the irradiation (second phase present or absent in the system), last but not least on initial concentration of $CyMe_4$-BTBP (10 or 50 mM) and total volume during irradiation plays its part.

Isolation of individual degradation products from the series containing three concentrated samples: Green (FS-13), Blue (Ganex, FS-13, 30% TBP), and Red (octanol, 30% TBP) of concentrations 10, 50 and 50 mM in large-volume of solvent (up to 50 mL) were carried out. Conditions and results from analytical determination of $CyMe_4$-BTBP residual content are summarized in Table 35.

Table 35: Residual concentrations of $CyMe_4$-BTBP found in the irradiated samples. Irradiated at Chalmers or CTU.

Sample	Diluent	Initial conc. [mM]	Dose [kGy]	Residual conc. [%][a]	BTBP c [mM][a]	σ_r
Green Big	FS-13	10	700	36.3	3.63	3.15
Blue Big	70% FS-13, 30% TBP	50	1200	63.6	31.83	4.60
Red Big	70% Oct, 30% TBP	50	300	44.3	22.1	1.41
Green Big (CTU)	FS-13	10	700	23.3	2.33	1.30
Blue Big (CTU)	70% FS-13, 30% TBP	50	1200	42.6	21.3	1.72

a) Calculated based on content of Yellow Standard supplied with the series.

This project has received funding from the EURATOM research and training programme 2014-2018 under grant agreement No 755171. The content of this deliverable reflects only the author's view. The European Commission is not responsible for any use that may be made of the information it contains.

SAMPLE BLUE

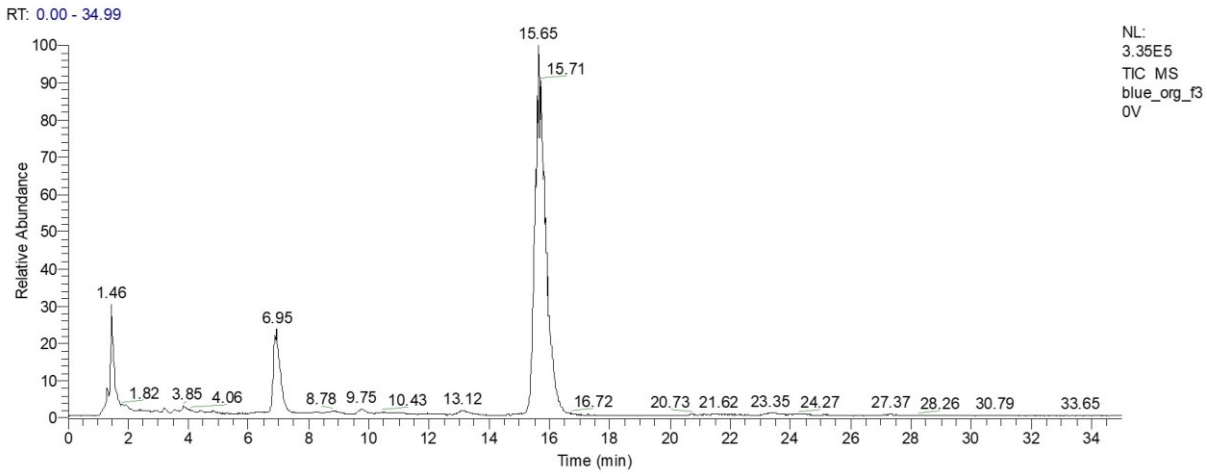

Figure 20: HPLC chromatograms with isocratic elution of sample (blue) in organic phase; measured with PDA and MS detection; flow rate 0.3 ml/min; column: Gemini-NX C18 110 Å (3 µm, 150 x 2.00 mm *I.D.*); mobile phase: 10 mM DEAO pH 8.2 with 78% ACN.

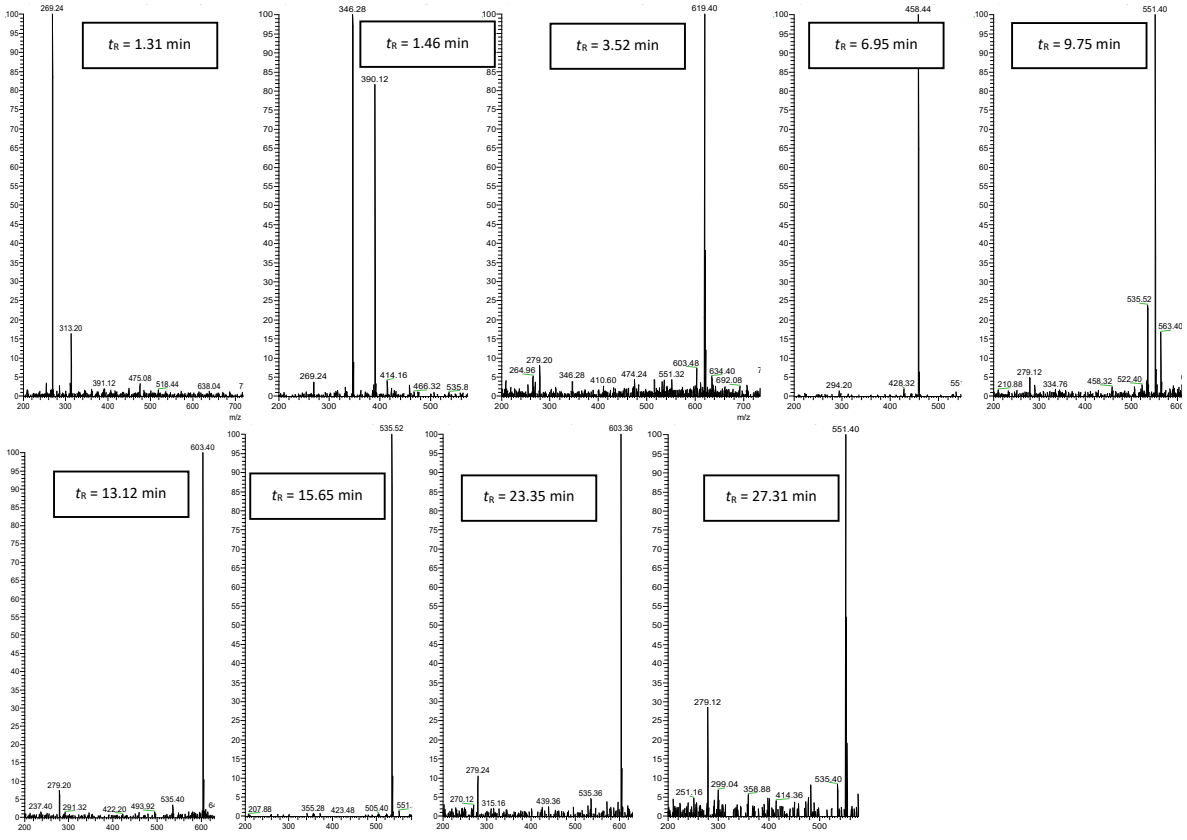

Figure 21: MS analyses of the collected fractions of the column effluent corresponding to the peaks on chromatogram depicted in Figure 20.

This project has received funding from the EURATOM research and training programme 2014-2018 under grant agreement No 755171. The content of this deliverable reflects only the author's view. The European Commission is not responsible for any use that may be made of the information it contains.

SAMPLE GREEN

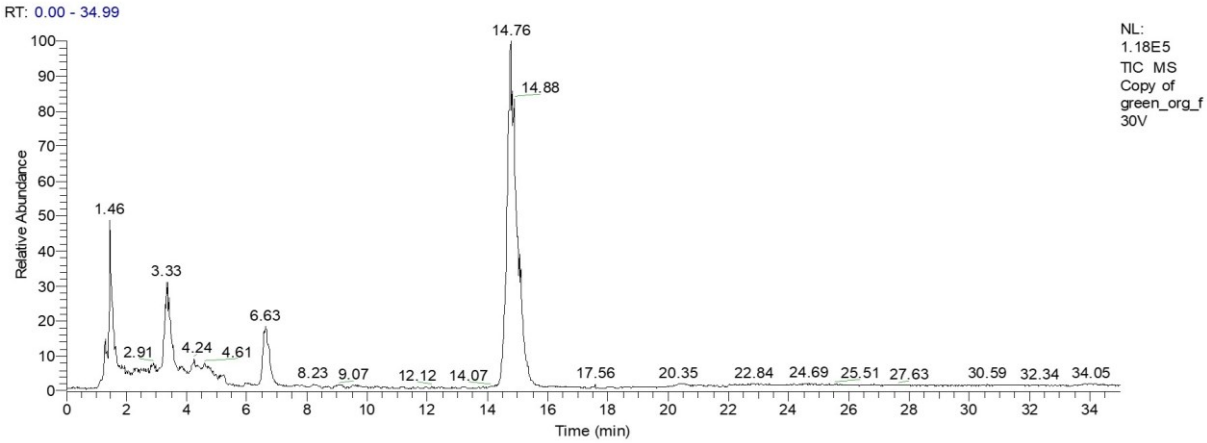

Figure 22: HPLC chromatograms with isocratic elution of sample (green) in organic phase; measured with PDA and MS detection; flow rate 0.3 ml/min; column: Gemini-NX C18 110 Å (3 µm, 150 x 2.00 mm *I.D.*); mobile phase: 10 mM DEAO pH 8.2 with 78% ACN.

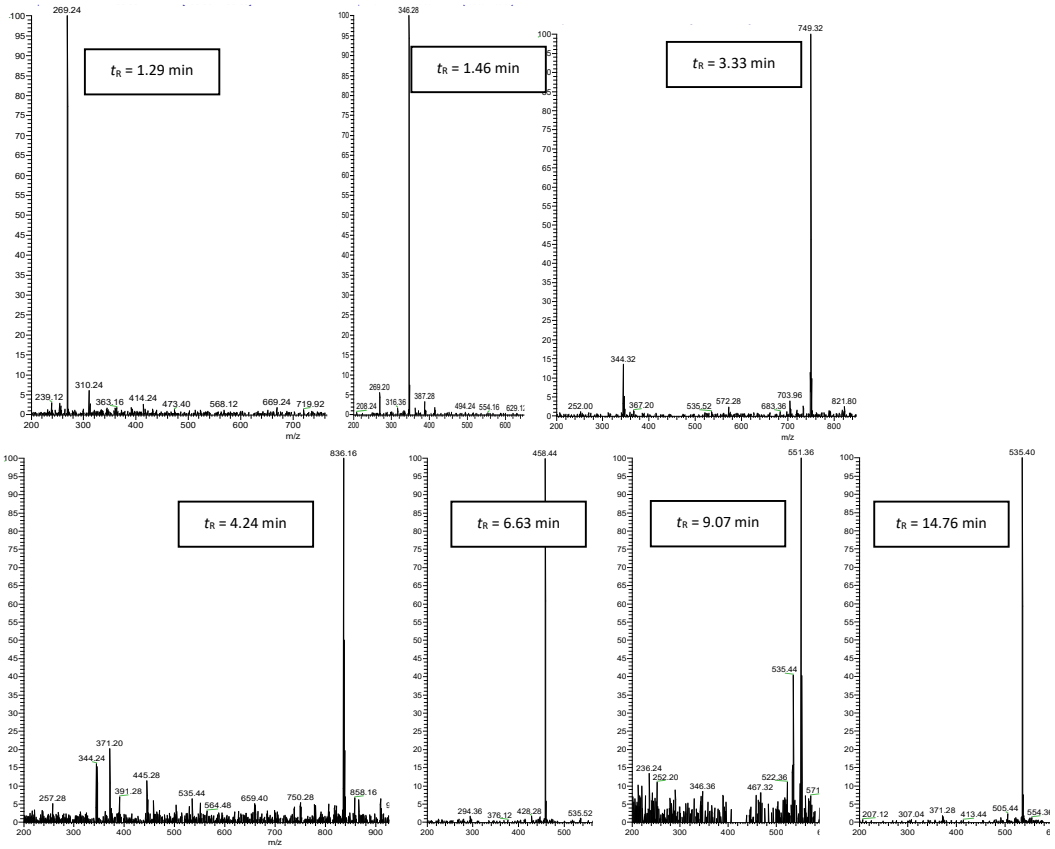

Figure 23: Examples of MS analyses of the collected fractions of the column effluent corresponding to the peaks on chromatogram depicted in Figure 22.

This project has received funding from the EURATOM research and training programme 2014-2018 under grant agreement No 755171. The content of this deliverable reflects only the author's view. The European Commission is not responsible for any use that may be made of the information it contains.

SAMPLE RED

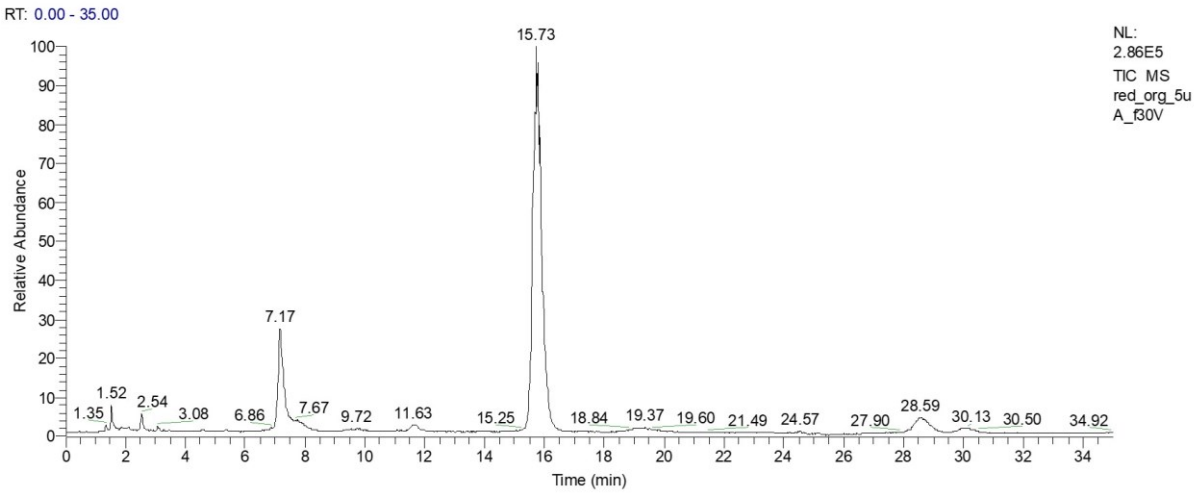

Figure 24: HPLC chromatograms with isocratic elution of sample (red) in organic phase; measured with PDA and MS detection; flow rate 0.5 mL/min; column: Gemini-NX C18 110 Å (3 µm, 150 x 3.00 mm *I.D.*); mobile phase: 10 mM DEAO pH 8.2 with 78% ACN.

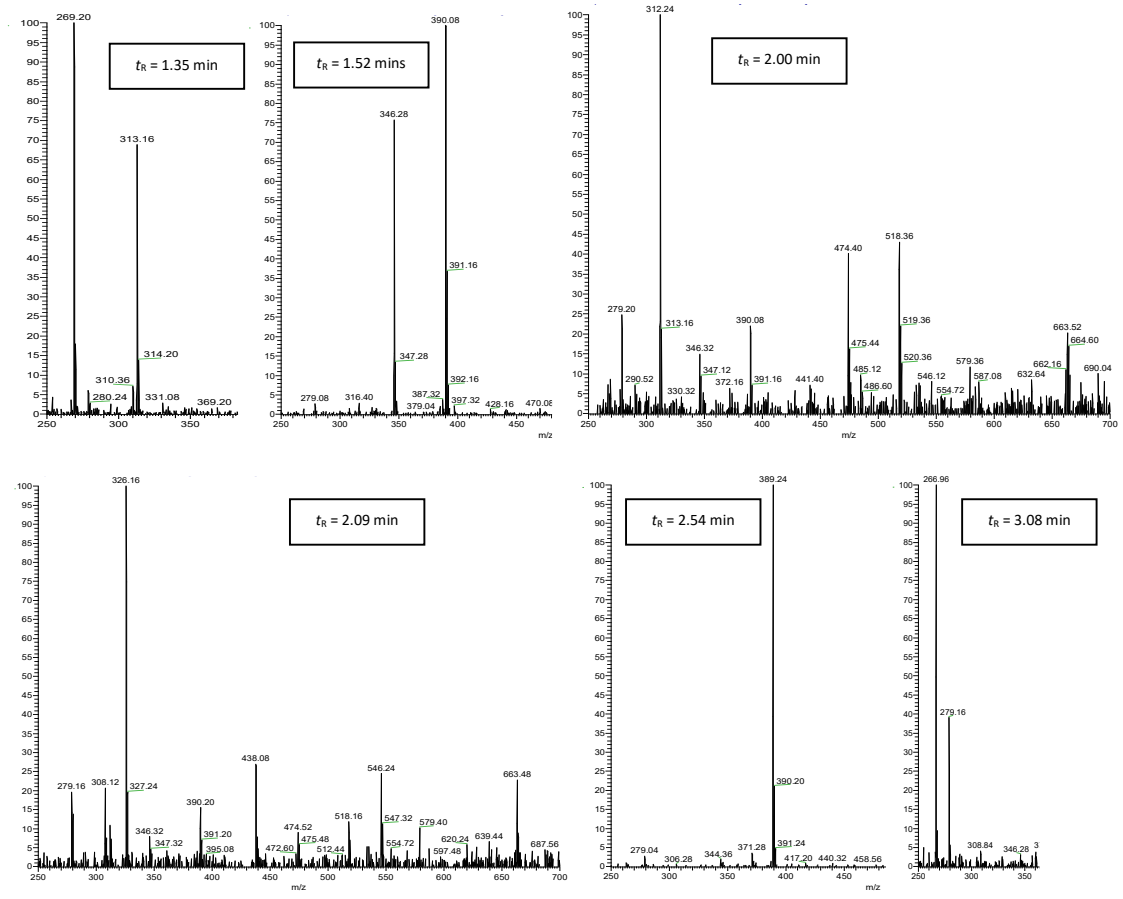

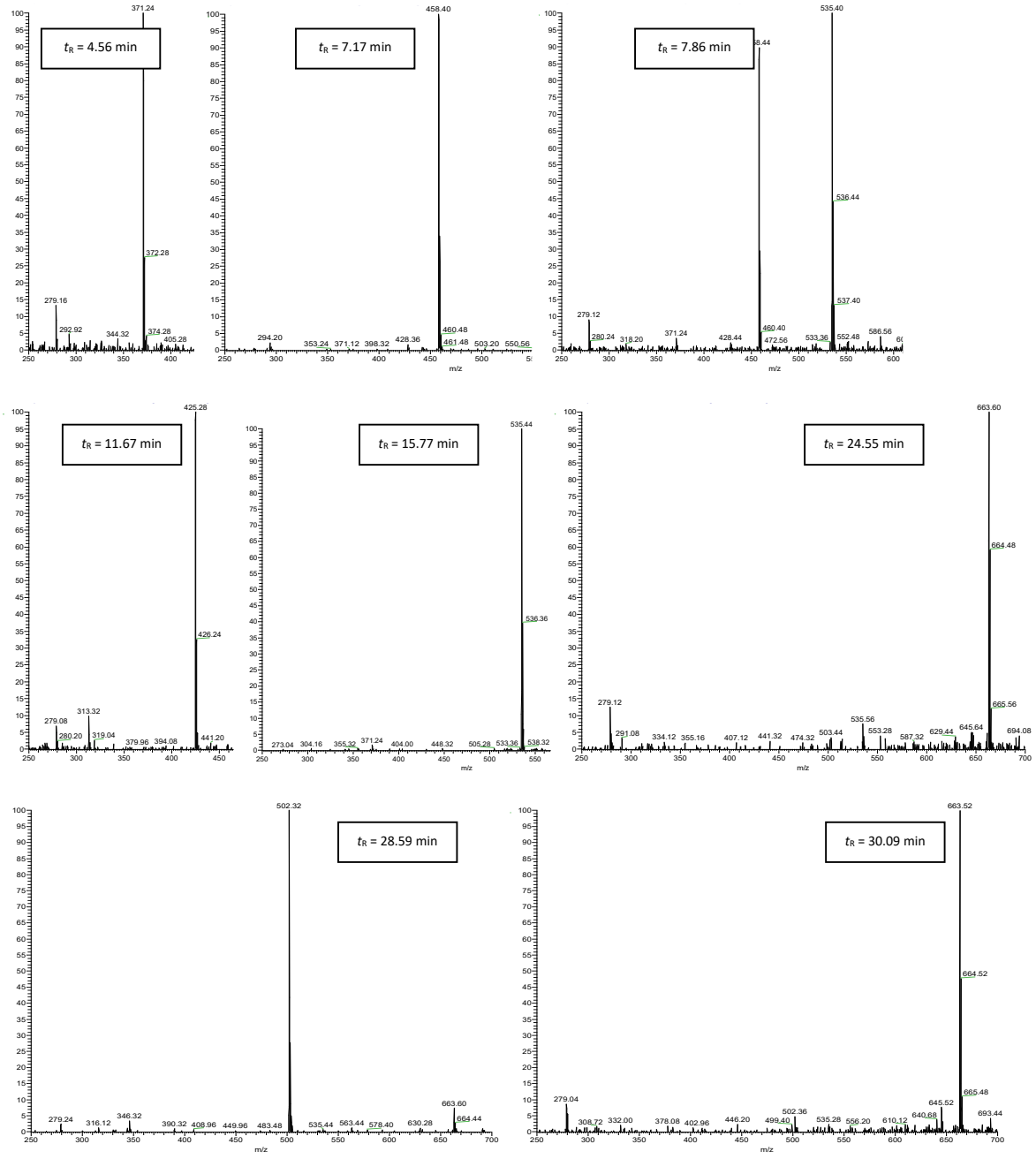

Figure 25: MS analyses of the collected fractions of the column effluent corresponding to the peaks on chromatogram depicted in Figure 24.

DIFFERENCES OBSERVED DUE TO DIFFERENT IRRADIATION CONDITIONS

Since the samples (volume up to 50 mL) supplied by Chalmers were already spend before completing the isolation of degradation products, CTU irradiated new large samples (volume up to 20 mL) from Green and Blue series of the same initial concentration (50 mM) and with the identical doses as in the original series. These newly prepared samples were used for continued isolations of degradation products and refinement of their ^{1}H NMR data. What is worth mentioning is that more pronounced degradation and slight differences in degradation products distribution were observed. This is exemplified by the Blue sample which MS analysis is

This project has received funding from the EURATOM research and training programme 2014-2018 under grant agreement No 755171. The content of this deliverable reflects only the author's view. The European Commission is not responsible for any use that may be made of the information it contains.

shown in Figure 26. The samples differed mainly in concentrations of degradation products with lower mass that correspond to degradation of lateral rings. The samples from CTU were further used for continuations of *semi*-preparative separations of the degradation products by HPLC.

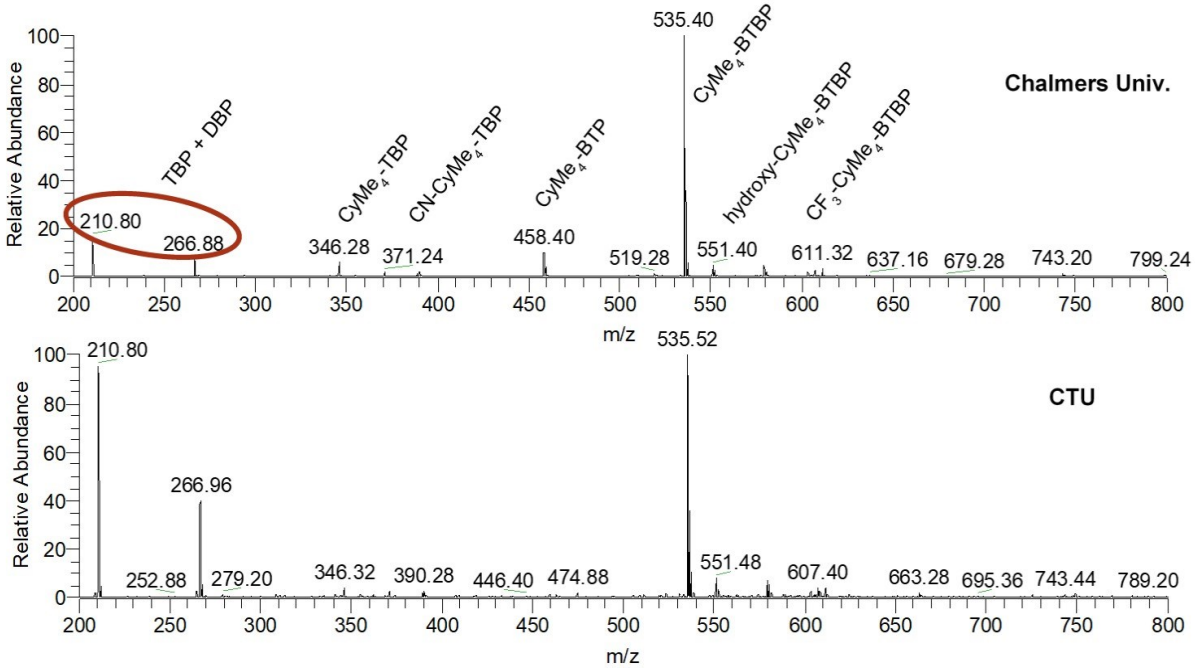

Figure 26: Comparison of MS spectra of Blue sample (50 mM, Ganex, FS-13, 30% TBP) irradiated by 1200 kGy, supplied from Chalmers Univ. and CTU.

SEMI-PREPARATIVE CHROMATOGRAPHIC SEPARATION

Based on previous LC-MS measurements, it is noticeable that the degradation of $CyMe_4$-BTBP in blue (and red) samples from Chalmers or CTU was, despite high doses, comparatively lower than in the samples with lower concentration of the ligand. Due to small concentrations of the degradation products and their number in the samples, it was not possible to separate the products during single HPLC run. Also, whereas higher mass degradation products could be separated from the solvent peaks by selected procedure, lower mass or higher polarity degradation products remained close to the solvent peaks or in overlay, what complicated their isolation and NMR characterization. All these complications resulted in the use of method that was based on several separation steps, from pre-concentration to isolation of almost pure individual degradation products.

Firstly, the main attention was focused on better separation of the solvent peaks from the rest of degradation products present in the sample. The first separation was successfully done on *semi*-preparative Flash RP column Merck LOBAR packed with LiChroprep RP-18 (40-63 um) (310 x 25 mm *I.D.*); mobile phase: from 30% via 100% aqueous CH_3CN to 100% THF. In order to obtain higher amounts of the products of decomposition in final fractions, a large scale sample volume of 10 mL was used.

The second separation of isolated fractions were carried out on *semi*-preparative HPLC RP columns MERCK Purospher Star C8, containing RP C8-silica (250 x 10 mm *I.D.*); mobile phase: 10 mM diethylamine in oxalic buffer, 55-78% aqueous CH_3CN, pH 8.2. This approach allowed for removal of mostly rest of the solvent from individual lower masses or higher polarity components and an initial separation of

This project has received funding from the EURATOM research and training programme 2014-2018 under grant agreement No 755171. The content of this deliverable reflects only the author's view. The European Commission is not responsible for any use that may be made of the information it contains.

degradation products into fractions, which contained one, but typically still several compounds. Conditions for both of *semi*-preparative HPLC chromatography were adjusted and optimized for each collected LC fraction from the first run to achieve optimal separation of degradation products. But even so, first eluted fractions were still loaded with some residual content of TBP or/and FS-13. Advantage is that the diagnostics peaks for CyMe4-BTBP and similar compounds are found in the range of aromatic (between ca. 9.5 - 7.5) and aliphatic (between ca.1.9 - 1.3 ppm) protons and thus, do not interfere with those for TBP and FS-13 shifted upfield.

Finally, the recovery was performed by removal of CH_3CN (or THF) at rotary evaporator, adjusting pH to 7.5 and extraction of the resulting aqueous solution with CH_2Cl_2 and evaporation of the solvent. The aqueous phase was checked by MS and in case of some persisting salt components the extraction with Et_2O was performed. This process led to recovery of the degradation products from water phase and almost no peaks of Et_2NH or oxalic acid were observed in NMR spectra.

Fractions separated by two-step *semi*-preparative procedure were analyzed by LC-MS and NMR spectroscopy. ^1H and ^{13}C NMR signals of the collected fractions were, in most cases, sufficiently strong and allowed for assignments of chemical shifts of individual degradation products. As expected, some of the products were identical in all irradiated samples, but some degradation products observed in individual samples (Blue, Green and Red) differ. This is caused by different solvent used, different irradiation doses, and different initial concentration of $CyMe_4$-BTBP in the used series. The structure of one of the main assumed degradation product occurring in all three sample series with retention time close to 7.00 min and corresponding *m/z* = 458 showed clear symmetric NMR spectrum that could be unambiguously assigned. Surprisingly enough, NMR and MS spectra correspond to $CyMe_4$-BTP, i.e. compound that probably persisted in the sample as impurity from synthesis (Figure 27). Another mass with *m/z* = 532 observed in Red and Blue samples was initially suspected also to be degradation product was then finally explained in terms of a TBP dimer, based on NMR and MS-MS fragmentation experiments (Figure 28). Based on performed fragmentation, was found that *m/z* = 210 not corresponding to degradation product, but to a DBP which probably arises upon sample irradiation from the TBP.

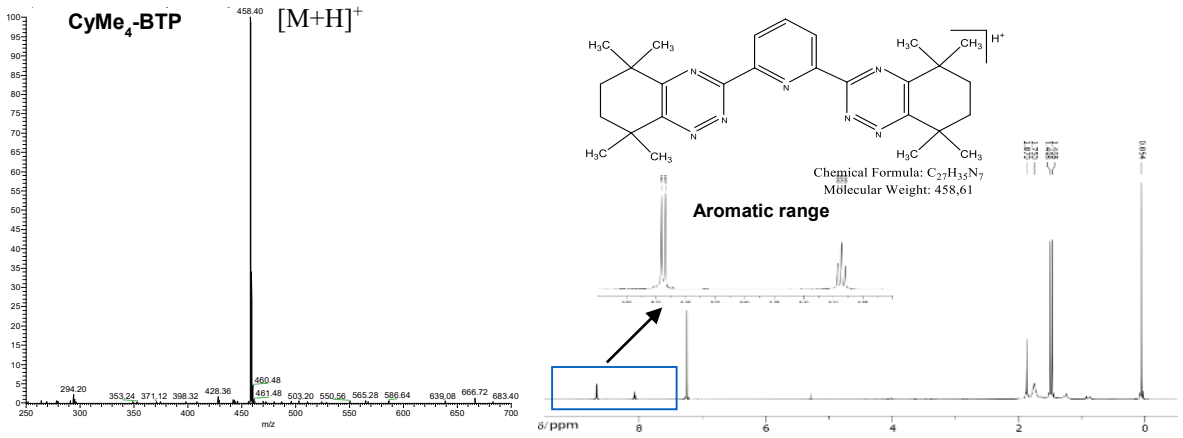

Figure 27: Mass and ^1H NMR spectra of $CyMe_4$-BTP.

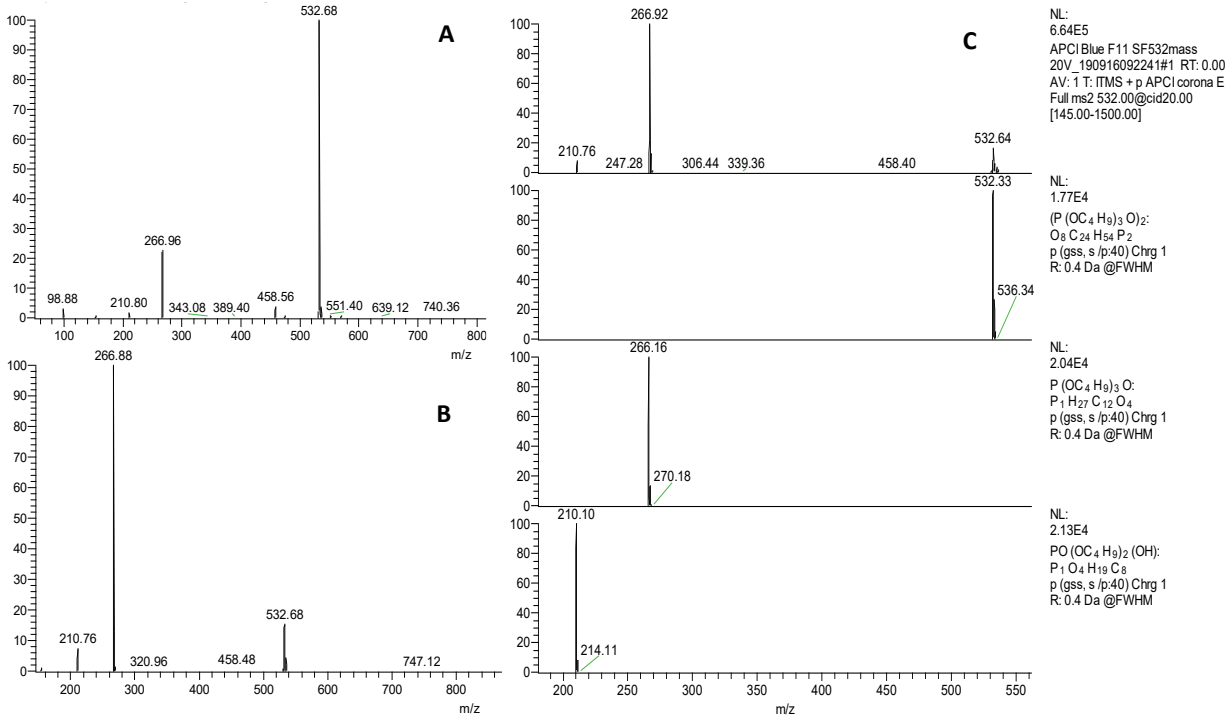

Figure 28: Plot of the mass spectra of the selected fraction containing TBP not fragmented (A), with source fragmentation (B), and description assignments (C).

BLUE SERIES

Blue series irradiated in FS-13 and TBP along with quite high amount of undestroyed CyMe$_4$-BTBP ligand with *m/z* = 535, that could be isolated back, hydroxy-CyMe$_4$-BTBP with *m/z* = 551, was observed and successfully separated and measured by both LC-MS and ^{1}H NMR (see Figure 29). According to NMR, the hydroxy group is most probably sitting at the central bipyridine unit at one of the two pyridine rings in the apical *para*-position to the nitrogen atom.

Another main degradation product with *m/z* = 603 that however could be identified only by MS and LC, corresponds probably to transfer of CF_3 moiety from FS-13 solvent to CyMe$_4$-BTBP molecule (Figure 30). No clear NMR spectra could be obtained for this compound, possibly due to presence of this compound in different isomeric forms. Therefore, the position of CF_3 fragment on the CyMe$_4$-BTBP scaffold remains unclear. Next, another two compounds could be separated that have lower mass than the parent ligand, corresponding to *m/z* = 371 and 346 (Figure 30). The compound with *m/z* = 346 can be, according to NMR and MS analysis, possibly assigned to CyMe$_4$-BTBP molecule, from which one cyclohexane ring was completely lost together with all methyl groups on this side. The last compound with *m/z* = 371 corresponds, according to ^{1}H NMR and MS, to a molecule that lost symmetry of parent ligand. This compound has unaffected central bipyridyl unit together with CyMe$_4$ part on one side, but on the other side lateral cyclohexane ring attached to triazinyl are most probably cleaved, with formation of CN-CyMe$_4$-TBP as a result. The ^{1}H NMR data for fractions that contained degradation products of CyMe$_4$-BTBP are summarized in Figure 30.

This project has received funding from the EURATOM research and training programme 2014-2018 under grant agreement No 755171. The content of this deliverable reflects only the author's view. The European Commission is not responsible for any use that may be made of the information it contains.

Figure 29: Obtained mass spectra and ^{1}H NMR of CyMe$_4$-BTBP and hydroxy-CyMe$_4$-BTBP.

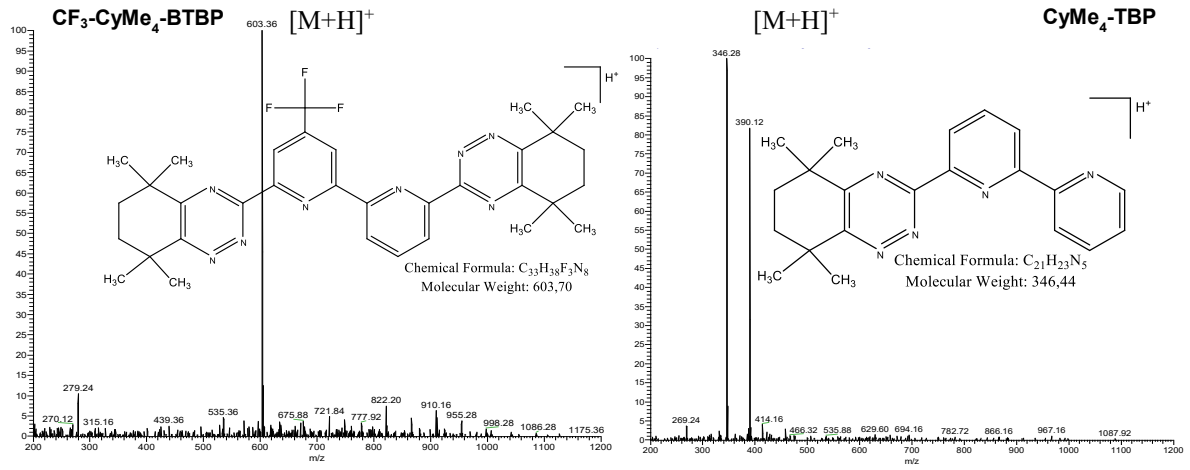

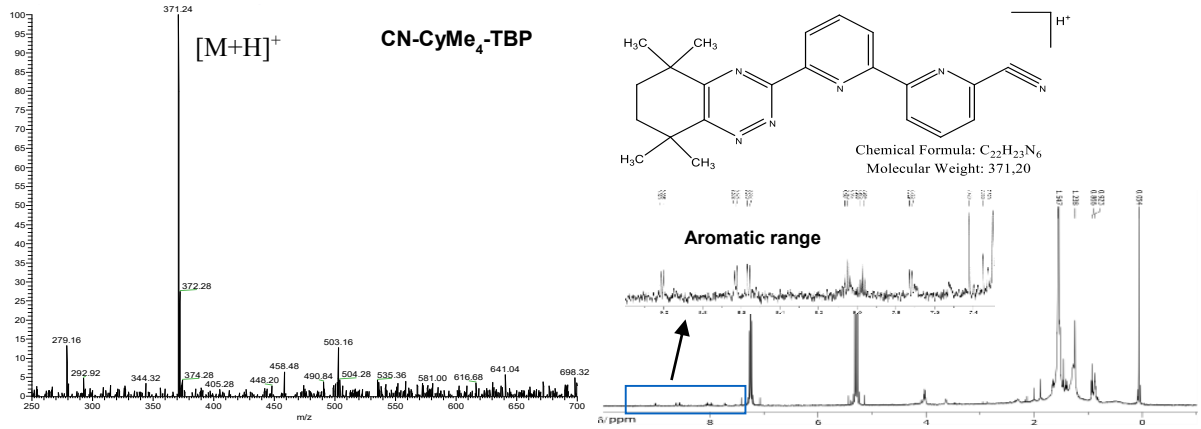

Figure 30: Plot of the mass spectra of the selected individual separated fractions (Blue) and possible structure of CyMe$_4$-BTBP degradation products, based on consideration from ^{1}H NMR, MS and LC-MS results.

GREEN SERIES

Both compounds mentioned above were identified also in green series (FS-13) together with previously mentioned *m/z* = 535 and 458. In the case of the Green sample, the products corresponding to *m/z* = 346 and 371 were also separated, although only in comparatively small amounts that provided less strong signals in NMR spectra.

RED SERIES

Degradation products that could be separated from red series (70% octanol, 30% TBP) correspond to *m/z* = 371 and *m/z* = 663 along with some previously mentioned compounds. The former compound corresponds according to ^{1}H NMR to a symmetrical molecule with cleaved cyclohexane rings at both sides of the CyMe$_4$-BTBP under formation of Me$_4$-BTBP; this was identified also in the Blue series. The second compound corresponds to adduct with octanol that was used as solvent (1-octanol, *m/z* = 130) (Figure 31). The site of substitution seems to correspond to bipyridine (BiPy) central unit of CyMe$_4$-BTBP, probably substituted in *para*-position to nitrogen atom with octanol attached by *α*-methylene carbon, although some evidence may also suggest for presence of other isomer with one of the rings of BiPy unit substituted in meta-position.

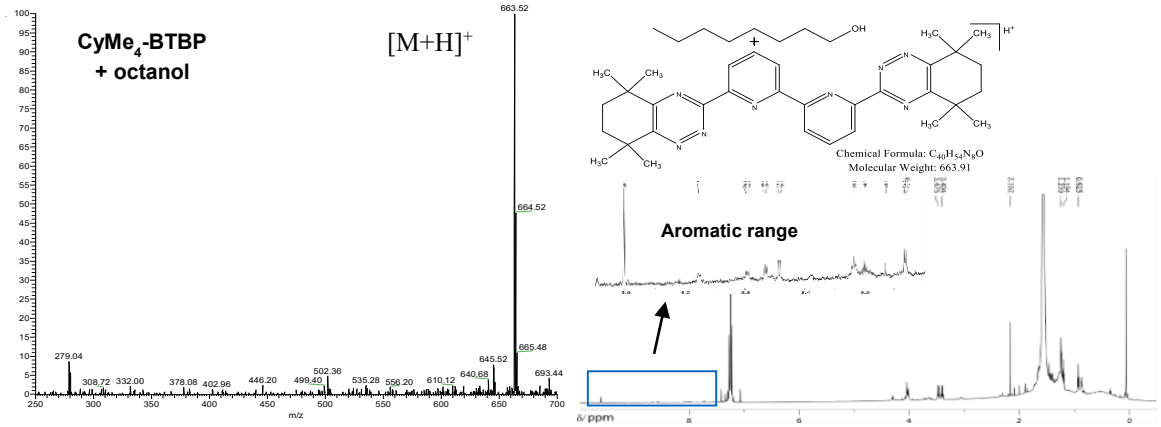

Figure 31: Mass spectrum of the selected individual separated fraction (Red) and possible structure of CyMe$_4$-BTBP degradation product, based on consideration from ^{1}H NMR, MS and LC-MS results.

This project has received funding from the EURATOM research and training programme 2014-2018 under grant agreement No 755171. The content of this deliverable reflects only the author's view. The European Commission is not responsible for any use that may be made of the information it contains.

In addition, the radiolysis of $CyMe_4BTBP$ and $CyMe_4BTPhen$ in octanol was studied comparatively by gamma and pulsed electron irradiation in 1-octanol solution with or without contact with nitric acid[46]. Solvent extraction studies showed a remarkable protective effect of nitric acid, yielding much higher metal distribution ratios for solvents irradiated in contact with nitric acid against solvents irradiated without contact or in contact with low concentrated nitric acid. The radiolysis products were identified and shown to be mostly addition products of the α-hydroxyoctyl radical, which is formed through direct radiolysis of the diluent 1-octanol. Quantification showed that the parent molecule's concentrations decreased, also when irradiated in contact with nitric acid. However, the formed radiolysis products seemingly are good extractants for trivalent metal ions with high selectivity towards trivalent actinides, themselves. The radiolysis mechanism was studied, and steady state pulsed electron experiments showed solvated electrons to be main reactive species in the radiolysis of $CyMe_4BTBP$ and $CyMe_4BTPhen$. When solvents were irradiated in contact with nitric acid, solvated electrons were preferentially captured by nitric acid instead of reacting with the ligands or the 1-octanol diluent, resulting in a partial protection of the ligand molecules. Details are given in reference[46]. The summary on this paper is presented below:

"The radiolytic stability of the highly selective ligands $CyMe_4BTBP$ and $CyMe_4BTPhen$ was studied in 1-octanol solution. $CyMe_4BTBP$ and $CyMe_4BTPhen$ were studied under identical experimental conditions to directly compare the effects of gamma and pulsed electron radiolysis on the ligands and systematically study the influence of the structural changes in the ligand backbone. Distribution ratios of Am^{3+}, Cm^{3+} and Eu^{3+}, the residual concentration of $CyMe_4BTBP$ and $CyMe_4BTPhen$ in solution, and the formation of radiolysis products were studied as a function of absorbed gamma dose and presence of an acidic aqueous phase during irradiation. Quantitative and semi-quantitative analyses were used to elucidate the radiolysis mechanism for both ligands. Addition products of alpha-hydroxyoctyl radicals formed through radiolysis of the 1-octanol diluent to the ligand molecules were identified as the predominant radiolysis products. These addition products are apparently also able to extract trivalent metal ions, as distribution ratios remained high although the parent molecule concentrations decreased considerably. Therefore, the utilization time of a solvent using these extractants could be longer than expected from only the reduction in their concentrations. Understanding the radiolysis mechanism helps in designing more radiation resistant extractants."

$CyMe_4$-BTBP in BK-1

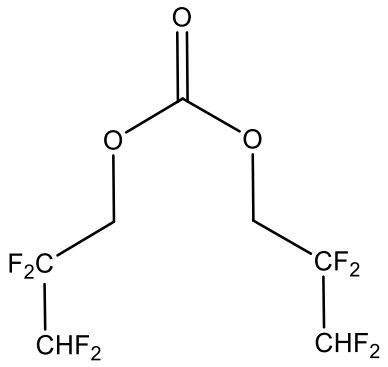

Figure 32. Chemical structure of BK-1.

Extraction systems containing $CyMe_4$-BTBP or $CyMe_4$-BTPhen dissolved in BK-1 (bis(2,2,3,3-tetrafluoropropyl) carbonate) (Figure 32) as a diluent were studied during the second half of the GENIORS project. The solubility of the ligands in BK-1 is not very high (app. 4 mM), and is even lower than the solubility in octanol or

This project has received funding from the EURATOM research and training programme 2014-2018 under grant agreement No 755171. The content of this deliverable reflects only the author's view. The European Commission is not responsible for any use that may be made of the information it contains.

cyclohexanone. However, the extraction properties of the BK-1-based solvents seemed promising. The highest values of separation factor were achieved in 1 – 4 mol/L HNO_3. ($SF_{Am/Eu} \approx 160$). Also all values of D_{Eu} were lower than 1 while all values of D_{Am} remained far above 1. The highest $SF_{Am/Cm}$ was observed in 1 M HNO_3 for CyMe4-BTBP ($SF_{Am/Cm} = 4.1 \pm 1.1$) and in 4 M HNO_3 for CyMe4-BTPhen ($SF_{Am/Cm} = 6.0 \pm 1.1$). The extraction rate was much faster with $CyMe_4$-BTPhen, the equilibrium was achieved within 15 minutes for Am(III) and Cm(III), the extraction of Eu(III) was much slower. The tested metals were not extracted by the neat diluent BK-1 (without any extracting compound). Radiation stability of CyMe4-BTBP and $CyMe_4$-BTPhen in fluorinated diluent BK-1 was also tested under irradiation by gamma radiation up to 300 kGy. $CyMe_4$-BTPhen was found to be significantly more stable than $CyMe_4$-BTBP in this diluent. In both cases, the presence of 1 M HNO_3 during the irradiation increased the stability of the extraction systems and suppressed the changes in the organic phase. For both systems, the presence of HNO_3 during irradiation improved their radiation stability. The results obtained indicated that the degradation products (or more exactly the adducts formed) act as extractants for Am(III) and Cm(III), to a certain extent, too. In general, the trends observed for Am/Cm separation factors were similar to those observed earlier for the Am(III) and Eu(III) extraction. The results of this study have been published in a paper[47].

CONCLUSIONS

Properties and radiation stability of two systems with hydrophobic ligands/extractants ($CyMe_4$-BTBP or $CyMe_4$-BTPhen) were studied throughout the project. The results obtained and the conclusions drawn can be summarized as follows:

- The studies on irradiation of $CyMe_4$-BTBP performed in fluorinated diluents FS-13, FS-13-BTP and octanol-TBP further confirmed that these system shows exceptionally high stability, in particular when the samples were irradiated in contact with aqueous HNO_3. The rate of degradation and the composition of the degradation products are dependent on the diluent used.
- A systematic study was performed using HPLC, LC-MS and semi-preparative HPLC methods combined with NMR techniques for identification of the degradation products. Main products originating after irradiation in FS-13 correspond to substitution of the BiPy central unit by hydroxyl group or also, in lower extend to transfer of CF_3 moiety to BiPy. In octanol, the solvent apparently binds on the BiPy central unit. In both cases, deeper degradation pathways proceed affecting the lateral rings of the molecule. No products were detected or isolated that would correspond to reactions with TBP or its degradations products.
- Another systematic study performed in 1-octanol has shown that under gamma irradiation addition products of alpha-hydroxyoctyl radicals formed through radiolysis of the $CyMe_4$-BTBP as the predominant radiolysis products. These addition products are apparently also able to extract trivalent metal ions, as distribution ratios remained high although the parent molecule concentrations decreased considerably[46].
- In the last part of the project, behaviour of the CHALMEX system (10 mM $CyMe_4$-BTBP in 70% FS-13 and 30% TBP) after irradiation by accelerated electrons up to 500 kGy at different temperatures was studied. The model based on mass transfer (DM model, based on the so-called two-film theory of interphase diffusion) as the rate-controlling process was found to best describe the kinetic behaviour of the system. Overall mass-transfer coefficients were evaluated using this model. The study of the irradiation of the solvent in the presence of aqueous phase containing nitric acid confirmed its earlier observed radioprotective effect. A comparison of the theoretical values of distribution ratios after irradiating the system with accelerated electrons, calculated from the residual concentrations of the ligand, with their experimental values suggests that some of the $CyMe_4$-BTBP degradation products or adducts of $CyMe_4$-BTBP or TBP are probably able to extract the studied metals, too. In addition, the study of the influence of

This project has received funding from the EURATOM research and training programme 2014-2018 under grant agreement No 755171. The content of this deliverable reflects only the author's view. The European Commission is not responsible for any use that may be made of the information it contains.

nitric acid concentration shed some light on the nature of the degradation products – contrary to the original ligands, that extract by solvation mechanism, the degradation products extract by ion exchange mechanism. Also, these new radiolytically formed extractants don´t exhibit significant An/Ln selectivity.

- The study of extraction systems containing CyMe$_4$-BTBP or CyMe$_4$-BTPhen dissolved in BK-1 (bis(2,2,3,3-tetrafluoropropyl) carbonate) as a diluent revealed that from point of view of the extraction properties the BK-1-based solvents might seem promising. However, the radiation stability of CyMe$_4$-BTBP and CyMe$_4$-BTPhen in this diluent proved insufficient for practical application. The results of this study have been published in a paper[47].
- In a thermodynamic study, negative values of ΔH and ΔS were found for the extraction quantities[37].

HYDROPHILIC DIGLYCOLAMIDES

RADIOLYTIC AND HYDROLYTIC STABILITY OF HYDROPHILIC DIGLYCOLAMIDES

The radiolytic and hydrolytic stability of the hydrophilic diglycolamides shown in Figure 33 was studied[9].

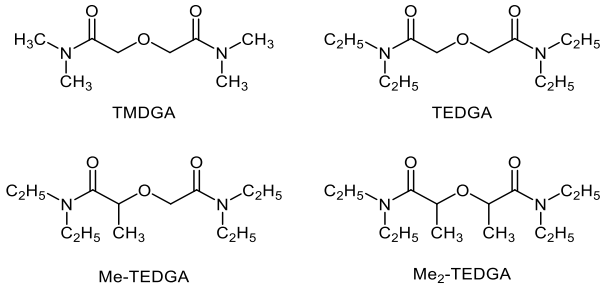

Figure 33. Chemical structures of TMDGA, TEDGA, Me-TEDGA, and Me$_2$-TEDGA.

The results were already published in a journal article; full details can be bound in the reference[9]. The summary on this paper is given below:

"The stability of different hydrophilic diglycolamides against acid degradation and radiolysis was studied. Tetraethyldiglycolamide (TEDGA) was found to undergo degradation in nitric acid at high reaction rates at elevated temperatures with a maximum of a ≈8% decrease per hour at 65°C in 4 mol L^{-1} HNO_3. The radiolysis was studied for tetramethyldiglycolamide (TMDGA), TEDGA, methyl-tetraethyldiglycolamide (Me-TEDGA), and dimethyl-tetraethyldiglycolamide (Me$_2$-TEDGA). The degradation rates decreased with increasing molecular weight, following the trend TMDGA > TEDGA > Me-TEDGA ≥ Me$_2$-TEDGA. Degradation products were identified by mass spectrometric techniques and were found to be comparable to those previously reported for the radiolysis of lipophilic diglycolamides in dodecane. Significant insight into the degradation mechanism in water was gained using pulse radiolysis experiments. The $^{\bullet}OH$ radical was identified as the most important reactive species and predominant mechanism of radical reaction is one of electron transfer rather than H-atom abstraction."

This project has received funding from the EURATOM research and training programme 2014-2018 under grant agreement No 755171. The content of this deliverable reflects only the author's view. The European Commission is not responsible for any use that may be made of the information it contains.

RADIOLYTIC STABILITY OF HYDROPHILIC DIGLYCOLAMIDES IN CONCENTRATED AQUEOUS NITRATE SOLUTION

The radiolytic stability of the hydrophilic diglycolamides in concentrated aqueous nitrate solution was studied[32]. The study was already published, and the details can be found in reference[32]. The summary on the results is presented below.

The radiation chemistry of a series of hydrophilic diglycolamides (DGAs: TEDGA, Me-TEDGA, Me_2-TEDGA, and TPDGA) has been investigated under neutral *p*H, concentrated, aqueous nitrate solution conditions. A combination of steady-state gamma and time-resolved pulsed electron irradiation experiments, supported by advanced analytical techniques and multi-scale modelling calculations, have demonstrated that: (i) the investigated hydrophilic DGAs undergo first-order decay with an average dose constant of (-3.18 ± 0.23) x 10^{-6} Gy^{-1}; (ii) their degradation product distributions are similar to those under pure water conditions, except for the appearance of NO_x adducts; and (iii) radiolysis is driven by hydroxyl and nitrate radical oxidation chemistry moderated by secondary degradation product scavenging reactions. Overall, the radiolysis of hydrophilic DGAs in concentrated, aqueous nitrate solutions is significantly slower and less structurally sensitive than under pure water conditions, similar to their lipophilic analogues. Overall, acid hydrolysis, not radiolysis, is expected to limit their useful lifetime. These findings are promising for the deployment of hydrophilic DGAs as actinide aqueous phase stripping and hold-back agents, due to the presence of high concentrations of nitrate in envisioned large-scale process conditions.

CDTA

During the partitioning of trivalent actinides from High Active Raffinate (HAR) solutions, most processes have to deal with an undesirable co-extraction of some of the fission products (FPs). For that reasons, different hydrophilic complexing agents of the group of polyaminocarboxylic acids were studied in the last decade for their ability to complex FPs and therefore preventing their extraction into an organic solvent[48]. From that group of complexing agents, CDTA (trans-1,2-cyclohexanediaminetetraacetic acid, Figure 34) seems to be the one most efficient agent to retain the problematic FPs (*e.g.* Pd, Zr, Mo) in the aqueous phase during the partitioning of trivalent actinides[48].

For instance, CDTA (Figure 34) is used as a masking agent to keep FPs in the aqueous phase meanwhile Ln's are extracted into the organic phase, *e.g.* TODGA (*N,N,N´,N´*-tetraoctyl diglycolamide) such in *i*-SANEX process or TODGA + DMDOHEMA (*N,N'*-dimethyl-*N,N'*-dioctylhexyloxyethyl malonamide, Figure 34) in EURO-GANEX process. In fact, it has been used in several successful spiked and hot EURO-GANEX process tests[31, 49-51] and in a spiked *i*-SANEX process test[53-54]. In this work CDTA stability and the effect of its degradation over the extraction performance have been studied against gamma radiation for the EURO-GANEX process conditions.

This project has received funding from the EURATOM research and training programme 2014-2018 under grant agreement No 755171. The content of this deliverable reflects only the author's view. The European Commission is not responsible for any use that may be made of the information it contains.

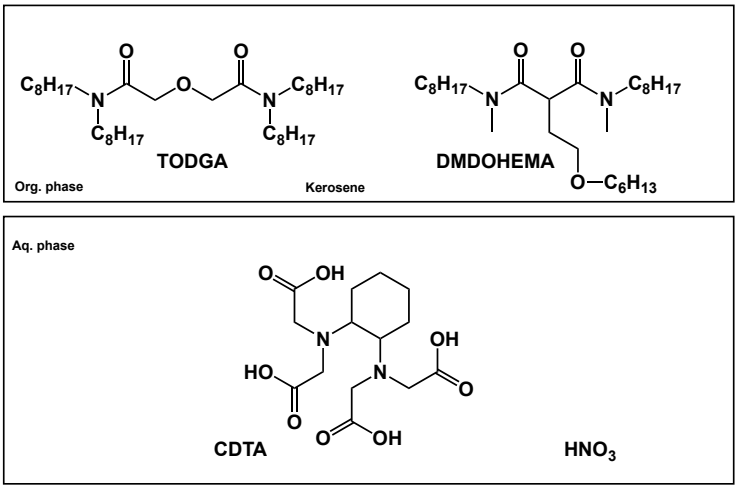

Figure 34: Structures of molecules involved in the co-extraction of Ln and An in EURO-GANEX process.

STABILITY OF CDTA vs. GAMMA IRRADIATION

In the first studies, it was decided to irradiate CDTA solutions up to 1000 kGy to compare with previous studies of diglycolamides (DGAs). A solution of CDTA (0.055 mol/L in 4 mol/L HNO_3) has been submitted to gamma radiation (1000 kGy, 4.1 kGy/h) at Náyade facility for comparison with DGAs data. The analysis performed by HPLC-MS and shown in Figure 35 demonstrates that the molecule was completely degraded after that high dose.

Therefore, as it is not expected CDTA aqueous solution will be recycled, it was decided to carry out two new irradiations at lower doses such 200 and 500 kGy, which have been used for EURO-GANEX stability studies [see Deliverable D5.2 Impacts of solvent degradation and recycle on the EURO-GANEX process], containing:

a) 0.055 mol/L CDTA in 4 mol/L HNO_3.

b) 0.055 mol/L CDTA in 4 mol/L HNO_3 + 10%$_{vol}$ of simulated HAR solution.

In a first visual inspection of samples after gamma radiation, it was found a white precipitate only in samples containing during the irradiation a 10%$_{vol}$ of a simulated HAR solution, particularly appreciable in sample irradiated up to 500 kGy (Figure 36).

After that, the behaviour of those CDTA degraded solvents as part of Euro-GANEX process was assessed. For that, organic solvents (0.2 ml/L TODGA + 0.5 mol/L DMDOHEMA in OK) have been contacted with the corresponding fresh and irradiated CDTA solutions. For ICP-MS and gamma spectrometry, it was added a 10%$_{vol}$ of simulated solution to those samples that need it, as well as all of them were spiked with 10 µL of a solution of ^{241}Am (100 kBq/mL) and ^{152}Eu (100 kBq/mL).

This project has received funding from the EURATOM research and training programme 2014-2018 under grant agreement No 755171. The content of this deliverable reflects only the author's view. The European Commission is not responsible for any use that may be made of the information it contains.

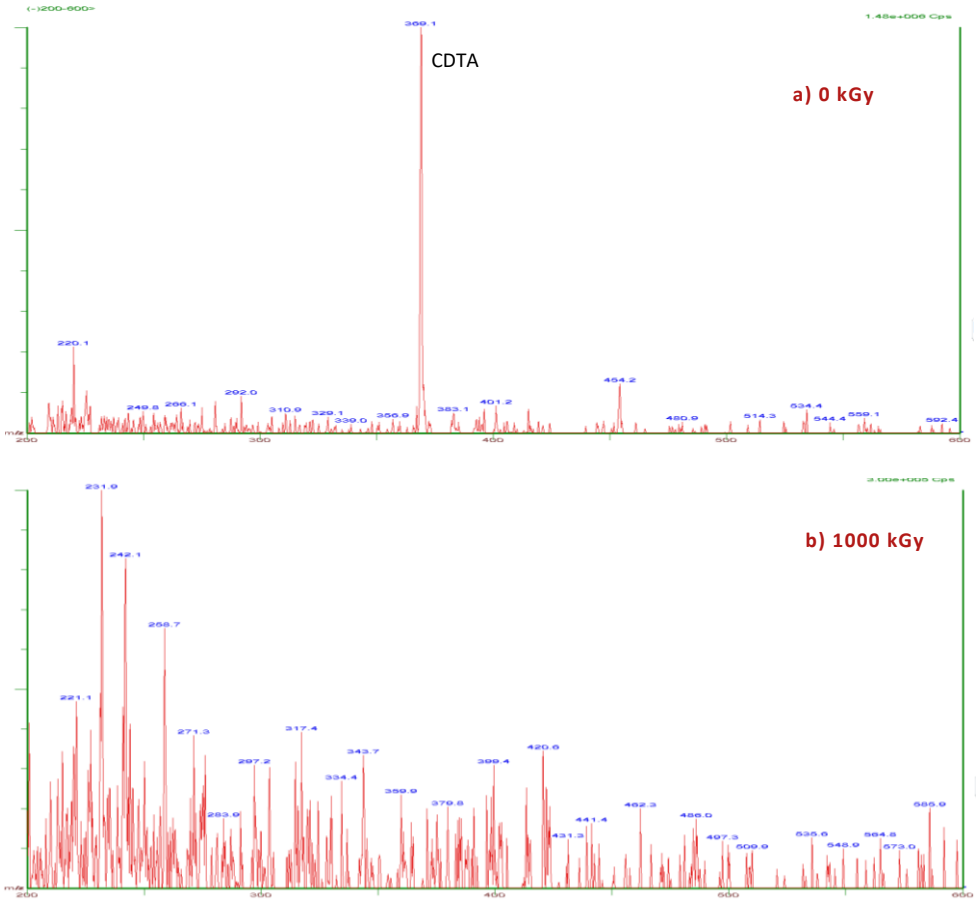

Figure 35: Mass spectra (ESI negative mode) of CDTA samples (0.055 mol/L CDTA in 4 mol/L HNO_3) at a) 0 kGy and b) 1000 kGy.

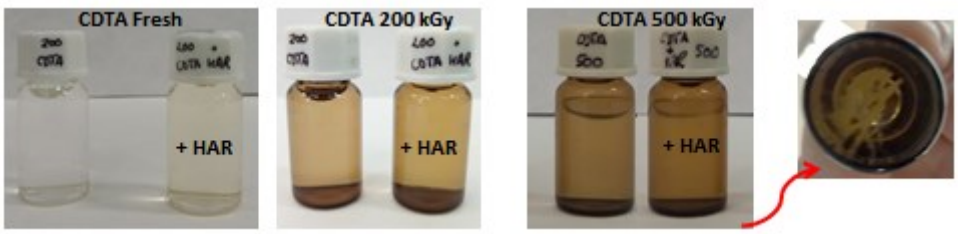

Figure 36: CDTA samples (0.055 mol/L CDTA in 4 mol/L HNO_3 and 0.055 mol/L CDTA in 4 mol/L HNO_3 + 10%$_{vol}$ of simulated HAR solution) fresh and after the irradiation (200 kGy and 500 kGy).

By gamma spectrometry, no effects over Ln and An extraction were found. However, by ICP-MS was found that the precipitate formed in samples irradiated in presence of HAR solution contains mainly Zr and Pd, metals that CDTA complexes, and it was formed also in those samples where HAR solution was added after irradiation. Therefore, CDTA DCs could form insolubilities of Zr and Pd in the aqueous phase after 200 kGy. The Ln and FP extraction using the EURO-GANEX solvent and fresh, aged and irradiated CDTA solution is shown in Figure 37. On the one hand, results demonstrate that the most FPS affected by CDTA degradation are Zr and Pd. In the case of Zr the *D* values obtained are higher than 1 in all irradiated cases. By contrast, D_{Pd} is less affected because the *D* values are still lower than 1. On the other hand, it can be seen that Ln extraction is not affected in any of the studied cases, maintaining excellent *D* values (D>100) for all Ln.

This project has received funding from the EURATOM research and training programme 2014-2018 under grant agreement No 755171. The content of this deliverable reflects only the author's view. The European Commission is not responsible for any use that may be made of the information it contains.

4 mol/L HNO_3			
Lanthanides		Fission products	
	mg/L		mg/L
Ce	60.5	Ba	29.5
Eu	3.8	Cd	2.2
Gd	3.3	Cr	9.6
La	2.56	Cu	2.9
Nd	5.43	Mo	70.5
Pr	2.38	Pd	18.3
Sm	1.49	Rb	6.9
Y	9.2	Rh	8.2
…	…	Sn	8
…	…	Sr	17.7
…	…	Zr	84.3

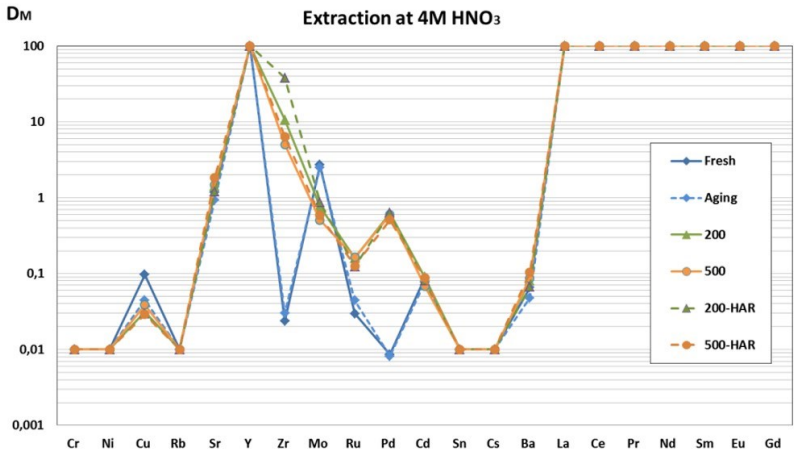

Figure 37: Ln and FP extraction by Euro-GANEX solvent (0.2 ml/L TODGA +0.5 mol/L DMDOHEMA in OK) from fresh, aged and irradiated CDTA solvent (0.055 mol/L in 4 mol/L HNO_3 + 10%$_{vol}$ HAR). In 200 and 500 kGy irradiated samples a 10%$_{vol}$ of a simulate HAR solution was added after irradiation. Samples 200-HAR and 500-HAR were irradiated in presence of the mixture of metal. D_{Zr} and D_{Pd} were calculated considering only the concentration of metal in solution.

Hence, to know if these insolubilities can give place to a mal-operation, new irradiation experiments considering a real concentration of HAR solution and real estimated doses for a CDTA solvent are needed. For that reason, a new series of irradiation experiments taking into account the real concentration of metals in the feed (100%$_{vol}$ HAR solution) and a more realistic estimated doses (0-50 kGy) were performed. Besides, parallels experiments were carried out for EDTA because this compound presents similar properties to CDTA as masking agent and it has no a cyclohexyl group in its structure (Figure 38)[48], which could be the responsible of the formation of non-water soluble degradation compounds.

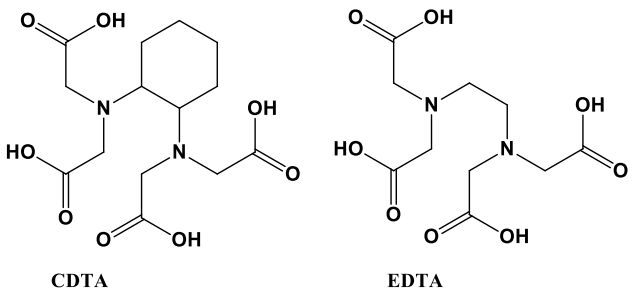

Figure 38: CDTA and EDTA structures.

In both cases, when CDTA and EDTA were added to a non-diluted HAR solution in 4 mol/L HNO_3, a no clear solution was obtained. After thermal treatment, CDTA was completely dissolved but not EDTA. Therefore, EDTA samples had to be filtered to continue with the experiments. Both solutions were irradiated (up to 50 kGy, 3.49 kGy/h, ^{60}Co sources) and Figure 39 show samples of CDTA and EDTA before and after each irradiation step (5, 10, 20 and 50 kGy). No visual precipitates were found after any of irradiated samples.

This project has received funding from the EURATOM research and training programme 2014-2018 under grant agreement No 755171. The content of this deliverable reflects only the author's view. The European Commission is not responsible for any use that may be made of the information it contains.

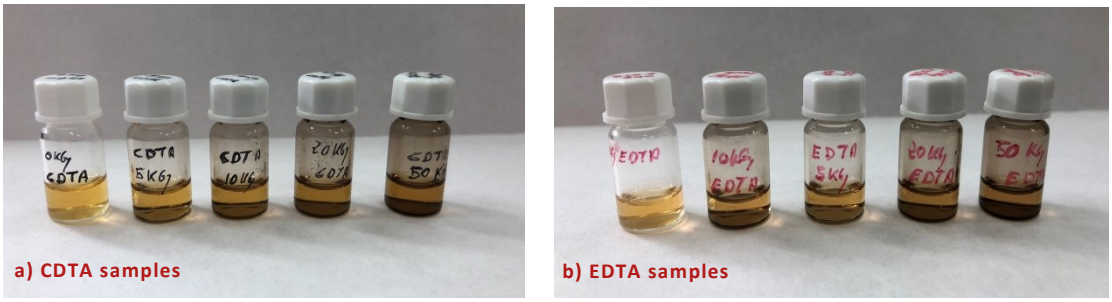

Figure 39: a) 0.055 mol/L CDTA in 4 mol/L HNO_3 samples (after 0, 5, 10, 20 and 50 kGy); b) EDTA in 4 mol/L HNO_3 samples (after 0, 5, 10, 20 and 50 kGy).

The extraction behaviour of those degraded aqueous phases as part of Euro-GANEX process has been studied. For that, organic solvents (0.2 ml/L TODGA + 0.5 mol/L DMDOHEMA in OK) have been contacted with the corresponding spiked with 10 µL of a solution of ^{241}Am (100 kBq/mL) and ^{152}Eu (100 kBq/mL). Although no precipitates were observed just after irradiation, a small third phase formation was noted for most of the samples (Figure 40A).

Figure 40B shows D_{Eu} and D_{Am} values by Euro-GANEX solvent from irradiated aqueous phases containing CDTA or EDTA. Despite the third phase formation, Ln and An mass balance for D_{Eu} and D_{Am} calculation were good. D_{Eu} and D_{Am} from CDTA samples were almost invariable, therefore, it can be said that CDTA degradation is neither affecting to Ln and Am extraction under these more realistic conditions. However, degradation of EDTA produces a decrease of D_{Eu} and D_{Am} values just after 10 kGy. The insolubilities problems and the decrease of Ln and An extraction by Euro-GANEX solvent due to EDTA degradation exclude EDTA from being an alternative to CDTA as masking agent of FP.

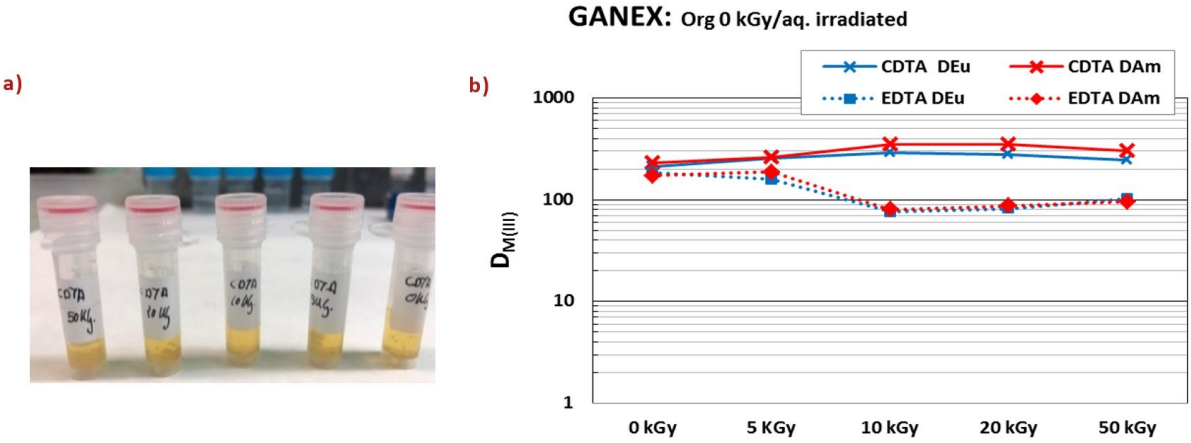

Figure 40. Ln and An extraction by Euro-GANEX solvent (0.2 mol/L TODGA +0.5 mol/L DMDOHEMA in OK) from aged and irradiated CDTA or EDTA solutions (0.055 mol/L in 4 mol/L HNO_3 HAR): a) Small third phase formation observed; b) *D*Eu and *D*Am values calculated.

Regarding FP, ICP-MS measurement was carried out only for CDTA samples and mass balance have corroborated that third phases observed after extraction experiments contain mainly Zr and Pd. Figure 41 shows Ln and FP distribution ratios obtained as function of dose by Euro-GANEX solvent from aged and irradiated CDTA solutions. Only changes can be observed for Zr and Pd extraction, particularly for Pd, while Ln are excellent extracted into the organic phase (D>100). Therefore, dose estimation and more realistic

This project has received funding from the EURATOM research and training programme 2014-2018 under grant agreement No 755171. The content of this deliverable reflects only the author's view. The European Commission is not responsible for any use that may be made of the information it contains.

experiments, including online-monitoring of FP extraction, should be considered for future irradiation loop experiments.

4 mol/L HNO_3			
Lanthanides		Fission products	
	mg/L		mg/L
Ce	605	Ba	295
Eu	38	Cd	22
Gd	33	Cr	96
La	256	Cu	29
Nd	543	Mo	705
Pr	238	Pd	183
Sm	149	Rb	69
Y	92	Rh	82
…	…	Sn	8
…	…	Sr	177
…	…	Zr	843

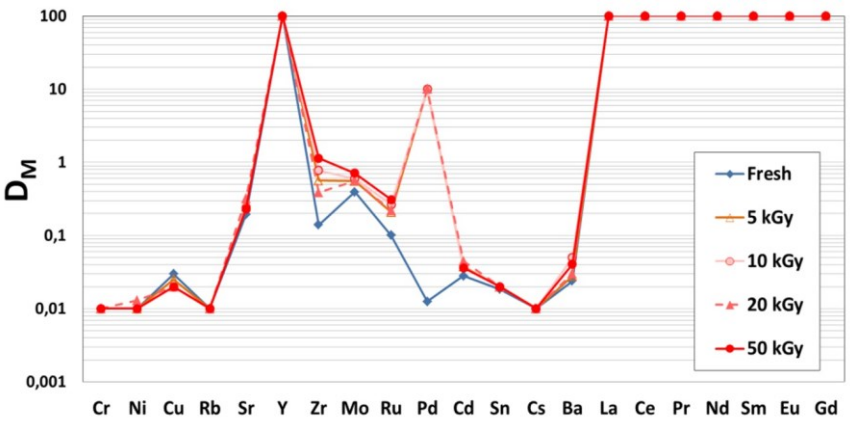

Figure 41: Ln and FP extraction by Euro-GANEX solvent (0.2 mol/L TODGA + 0.5 mol/L DMDOHEMA in OK) from aged and irradiated CDTA solutions (0.055 mol/L in 4 mol/L HNO_3 HAR). D_{Zr} and D_{Pd} were calculated considering only the concentration of metal in solution.

CONCLUSIONS

Different irradiation experiments containing 0.055 mol/L CDTA in 4 mol/L HNO_3 were performed. First, after 1000 kGy CDTA was completely destroyed, and then, next irradiation experiment was performed to lower doses, 200 and 500 kGy. A white precipitate only in samples containing during the irradiation a 10%$_{vol}$ of a simulated HAR solution was found, particularly appreciable in sample irradiated up to 500 kGy. This precipitate was mainly due to Zr and Pd, metals that CDTA complexes, and it was formed in samples irradiated in presence of HAR solution but also in those samples where HAR solution was added after irradiation. Therefore, CDTA DCs could form insolubilities of Zr and Pd in the aqueous phase after 200 kGy.

As aqueous solutions will not be recycled, further irradiations at lower doses (up to 50 kGy) were performed, containing either EDTA or CDTA, with the aim to compare both agents. EDTA samples showed solubility problems and moreover, the EDTA degradation produces a decrease of D_{Eu} and D_{Am} values just after 10 kGy. Therefore, for both reasons, this compound was excluded from being an alternative to CDTA as a masking agent of FP.

Regarding CDTA efficiency to complex problematic FPs, all studies performed point out that unirradiated CDTA efficiently complexes Pd and Zr, preventing their extraction into an organic solvent. However, when irradiated even at low doses (5-50 kGy), the D_{Pd} and D_{Zr} are affected producing an undesirable extraction by the Euro-GANEX solvent. These outcomes should be considered in the next experiments where CDTA will be present.

PTD

The stability towards radiolysis of PTD-based (Figure 42) stripping solvent has been extensively investigated in the past SACSESS project and the current GENIORS project. According to these radiolytic studies, several new species, named degradation products (DPs), were observed in the irradiated solutions. HPLC-ESI-MS analyses combined with mass tandem spectrometry experiments enabled to hypothesize the DPs reported in, further confirmed by radiolytic studies performed by CEA in gamma and alpha irradiated solutions. As shown in Figure

This project has received funding from the EURATOM research and training programme 2014-2018 under grant agreement No 755171. The content of this deliverable reflects only the author's view. The European Commission is not responsible for any use that may be made of the information it contains.

42, the ligand degradation has been considered mainly caused by indirect reaction with radiolytic species of the diluent (water and nitric acid). Consequently, to the most probable reaction of hydrogen atom abstraction from the C-H bond in alpha position with respect to the triazolyl ring or to the alcoholic group, the proposed degradation paths entail the addition of radical species coming from diluent radiolysis. On the other hand, the branch loss could follow hydrogen atom abstraction from the alpha position adjacent to the triazolyl ring.

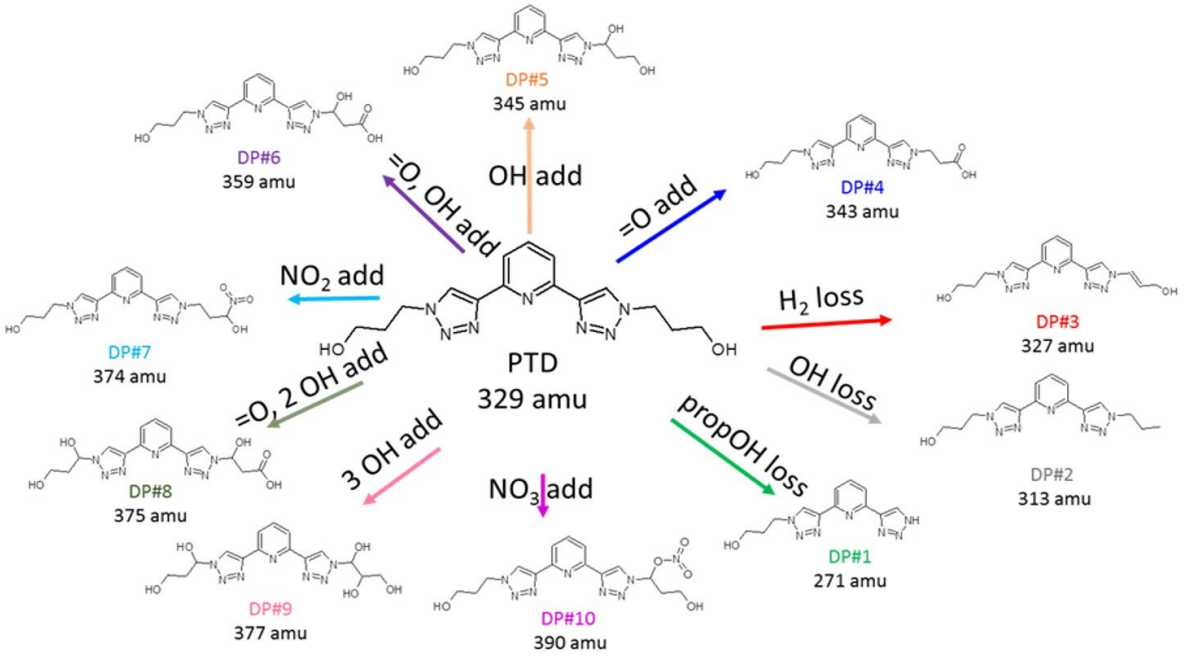

Figure 42: Hypothesized structures of identified PTD DPs.

Concerning the impact of radiolytic degradation, and thus of the presence of the observed DPs, on the extracting performances of the system, solvent extraction tests on PTD solutions irradiated under different conditions enabled to assess that the PTD-based stripping solvent keeps unaltered its capacity to achieve An stripping when irradiated up to a total absorbed dose of 200 kGy. At higher dose (500 kGy), the Am(III) complexation with PTD improves, but that of Eu(III) to a greater extent, leading to a severe reduction of Eu/Am selectivity.

Concerning the impact of radiolytic degradation, and thus of the presence of the observed DPs, on the extracting performances of the system, solvent extraction tests on PTD solutions irradiated under different conditions enabled to assess that the PTD-based stripping solvent keeps unaltered its capacity to achieve An stripping when irradiated up to a total absorbed dose of 200 kGy. At higher dose (500 kGy), the Am(III) stripping by PTD improves, but that of Eu(III) to a greater extent, leading to a severe reduction of Eu/Am selectivity.

It is worth noting that the proposed DPs structures are compatible with the liquid-liquid extraction results, since it is evident that both complexing ability and solubility of DPs should be similar to those of PTD. A detailed description of these activities is reported in Deliverable 2.2 *Stability studies of stripping agents*. In order to complete such stability studies, POLIMI has continued to work on the identification of the new degradation products (DPs) observed in the irradiated solutions and the impact of their presence on the extracting performances of the irradiated stripping phases.

This project has received funding from the EURATOM research and training programme 2014-2018 under grant agreement No 755171. The content of this deliverable reflects only the author's view. The European Commission is not responsible for any use that may be made of the information it contains.

IDENTIFICATION/CONFIRMATION OF SOME PTD DEGRADATION PRODUCTS

Due to the low concentration of each DPs in the irradiated solutions, direct isolation from irradiated PTD by means of preparative HPLC was not feasible. Therefore, POLIMI and UNIPR jointly decided to try to synthesize some of them. In particular, taking into consideration the complexities in the synthesis of such DPs, it has been decided to first try the synthesis of those compounds that could seem more abundant or the result of a single modification and thus could be the precursors of other DPs. Once synthesized, the compounds will be used as reference in the HPLC-MS analyses to confirm the identity of the new species observed in the irradiated solutions.

In this perspective, UNIPR succeeded in synthesizing two of the hypothesized degradation products, DP#1 and DP#4, whose molecular structures are reported in Figure 43.

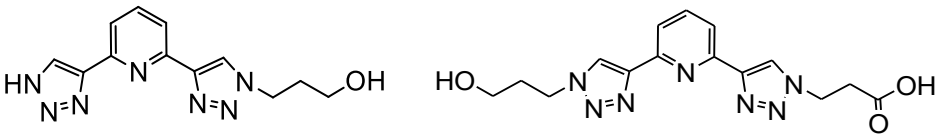

Figure 43: Molecular structures of DP#1 (*left*) and DP#4 (*right*).

UNIPR provided also two PTD derivatives, reported in Figure 44, that were not directly observed as DPs in irradiated PTD solutions, but they have been obtained in the different synthetic routes adopted and they worth to be tested since it could not be excluded their presence in the irradiated solutions. Further details about the compound synthesis could be found in UNIPR HYPARs.

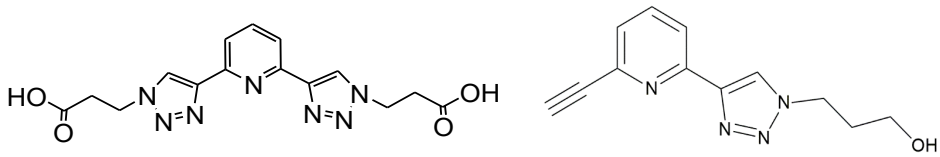

Figure 44: Molecular structures of the novel PTD derivatives: PTD derivative #1 (*left*) and mono-PTD (*right*).

The products were dissolved in 0.44 M HNO_3 at an initial concentration of 0.08 M. Such a high concentration has been tested in view of the extraction tests. DP#1 and MonoPTD compounds resulted soluble, while DP#4 and PTD derivative #1 resulted to be insoluble even at lower concentrations (Figure 45). The behaviour of the latter ones was quite surprising given their structure, however an explanation has not yet been found.

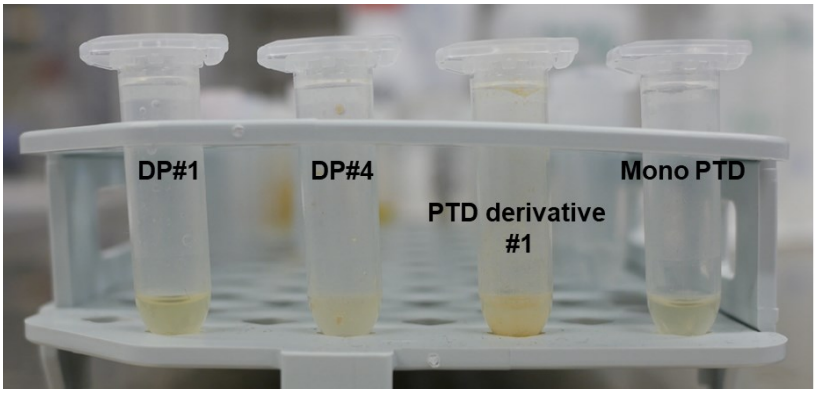

Figure 45: Sample solutions prepared for extraction tests.

This project has received funding from the EURATOM research and training programme 2014-2018 under grant agreement No 755171. The content of this deliverable reflects only the author's view. The European Commission is not responsible for any use that may be made of the information it contains.

The two stripping phases so-obtained were analyzed by HPLC-DAD coupled with ESI-MS, under the standardized HPLC-MS protocol previously optimized for PTD irradiated solutions. First, a fresh PTD solution, suitably diluted in methanol, was analyzed to check the elution time confirming the analysis repeatability. Then, each of the abovementioned stripping solution in 0.44M HNO_3 was diluted in methanol and injected in the HPLC system. Figure 46 reports the HPLC-MS profiles obtained for a fresh PTD solution, the DP#1 solution and the DP#4 solution.

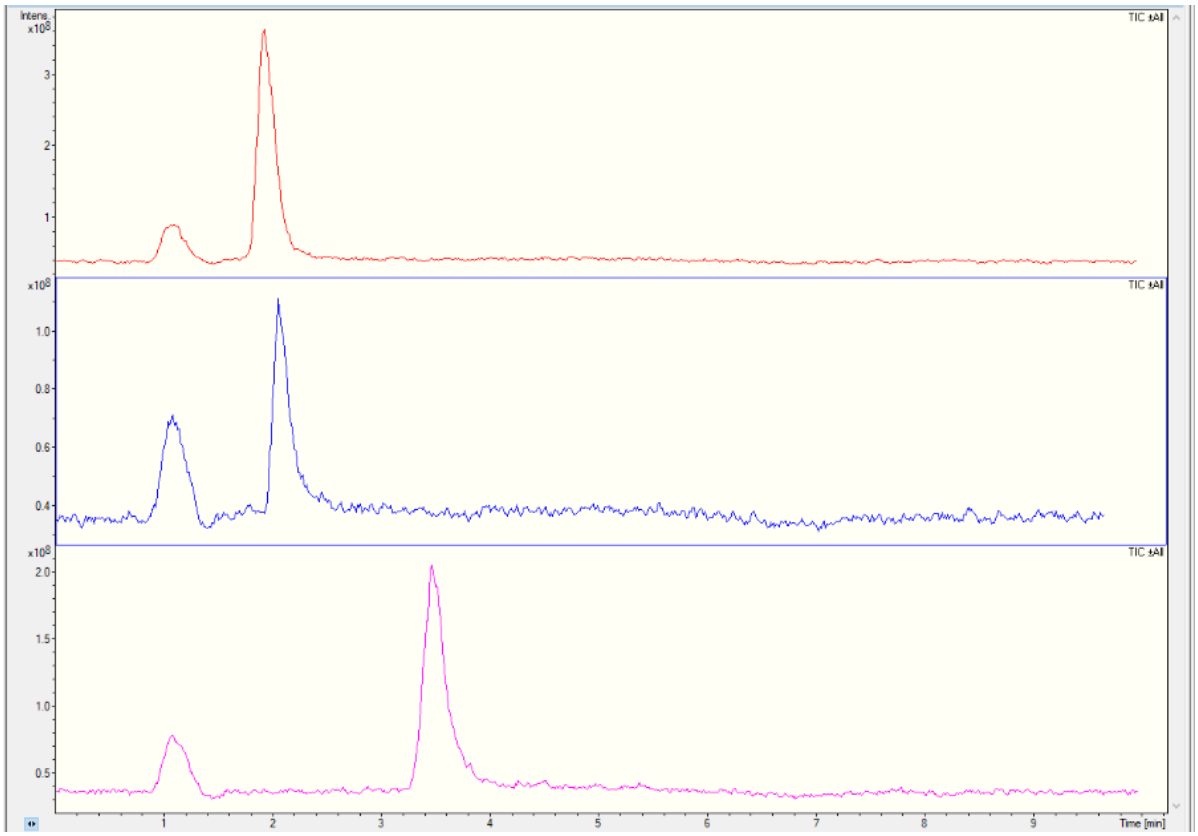

Figure 46: Full-view of HPLC-MS spectra of fresh PTD solution (*top*), DP#1 solution (*middle*) and DP#4 solution (*bottom*). All the initial solutions were prepared at a concentration of 0.08M in 0.44M HNO_3.

By studying PTD solutions irradiated up to 500 kGy, HPLC-MS experiments and mass tandem spectrometry enabled to observe DP#1 (271.12 g/mol) and DP#4 (343.14 g/mol) mainly as sodium adducts (*m/z* = 294 and *m/z* = 366, respectively) at an elution time of about 1.6 minutes and to hypothesize their structures.

As shown in Figure 46, DP#1 elution time obtained with the reference DP#1 solution corresponds to that observed for the hypothesized DP#1 in the PTD solutions irradiated at 200 and 500 kGy, thus confirming its identity.

By applying the same protocol, mono-PTD compound was eluted at 3.3 minutes. In the light of this result, HPLC-MS analyses of PTD solutions irradiated at 200 and 500 kGy were reconsidered, but no evidence of its presence in the irradiated PTD solutions could be found by means of its extracted ion current.

Concerning the compounds resulted insoluble in diluted nitric acid, some attempts were made to analyze them, by dissolving them in methanol and acetonitrile. Unfortunately, PTD derivative #1 was not enough

This project has received funding from the EURATOM research and training programme 2014-2018 under grant agreement No 755171. The content of this deliverable reflects only the author's view. The European Commission is not responsible for any use that may be made of the information it contains.

soluble in the considered experimental conditions and no useful data could be collected. On the contrary, HPLC-MS analyses on DP#4 enabled to collect some worthy indications. Indeed, DP#4 has been dissolved in acetonitrile, suitably diluted in the same solvent and injected in HPLC system, obtaining that DP#4 was eluted from the column at 6.4 minutes. The registered elution time is not coherent with the elution time observed in the irradiated PTD solution for the hypothesized DP, however, taking into consideration the complex composition of the irradiated PTD solutions, *i.e.* complex mixtures of several compounds that have somewhat a very similar structure, with respect to the simple DP#4 solution and the slightly different experimental conditions imposed by solubility issues, it could not be excluded that DP#4 is the hypothesised compound. Therefore, the compound was isolated as *m/z* = 366 (sodium adduct), fragmented and detected by ESI-MS^2 and the ESI-MS^2 spectrum compared with that of the hypothesized DP in the irradiated PTD solution. The comparison highlighted fragmentation patterns that seem to show some similarities but also some differences, that prevent to definitively confirm the DP#4 identification. Indeed, it has to be taken into consideration that DP#4 could have three possible structural isomers (Figure 47) and that they could be concurrently present in the irradiated PTD solutions, resulting in a more complex fragmentation path with respect to those obtained from the DP#4 reference solution.

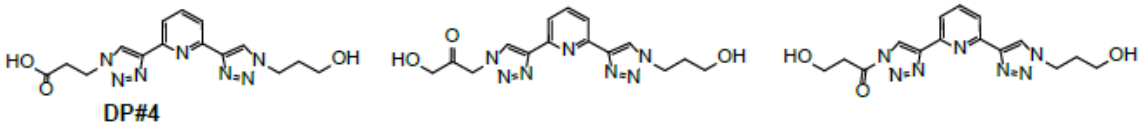

Figure 47: Possible structural isomers of DP#4

EXTRACTING PROPERTIES OF DEGRADATION PRODUCTS

After the confirmation of the hypothesized structure of DP#1 by HPLC-MS, it is paramount to better understand the impact of such DP on the extracting properties of the PTD-based stripping solvent under irradiation during the process. Besides DP#1, due to solubility limitation, only monoPTD could be tested in liquid-liquid extraction experiments under the same experimental conditions of PTD.

First, a TODGA-based organic phase was loaded with ^{241}Am and ^{152}Eu from a 3M HNO_3 solution and scrubbed with a 0.5M HNO_3 solution. Then, aqueous stripping solutions were prepared by separately dissolving each compound at a concentration of 0.08M in 0.44M HNO_3. The stripping phases were contacted with the loaded organic phase according to the proven experimental protocol. The results are presented in Table 36.

Table 36: Results of stripping tests, compared with the references (stripping in 0.44M HNO_3 and with PTD stripping phase). Aq. Phase: 0.08M ligand in 0.44M HNO_3: Org. Phase: 0.2M TODGA in kerosene with 5%v 1-octanol, previously loaded with ^{241}Am and ^{152}Eu.

Stripping agent	D_{Am}	D_{Eu}	$SF_{Am/Eu}$
No agent – 0.44M HNO_3	15.08 ± 1.51	95.13 ± 9.51	6.31
Reference PTD	0.30 ± 0.03	35.12 ± 3.51	117.07
DP#1	2.28 ± 0.20	78.19 ± 7.82	34.42
MonoPTD	15.30 ± 1.50	107.03 ± 10.50	6.99

As shown in Table 36, MonoPTD, that has lost the complexing core, does not exhibit any valuable stripping capacity with in diluted nitric acid. In contrast, DP#1 that results from the radiation-induced loss of the lateral chain and preserves the complexing core, still retains an affinity for Am cations even if it exhibits an overall worsening of the complexing properties of the original PTD structure.

This project has received funding from the EURATOM research and training programme 2014-2018 under grant agreement No 755171. The content of this deliverable reflects only the author's view. The European Commission is not responsible for any use that may be made of the information it contains.

From the previous stability studies, it has been observed that several new species are formed in solution after irradiation and their percentage increases with increasing the absorbed dose. Coherently, increasing the dose, the overall performances of the PTD-based stripping phase are determined by the overall contribution of all the species.

Taking into consideration the information gained concerning DP#1, whose identity has been confirmed by HPLC-MS analysis, it can be only inferred that at 200 kGy its worse stripping performances did not affect the overall PTD-based stripping phase performances, while at 500 kGy it could contribute to the improved Eu extraction and not to that of Am.

CONCLUSIONS

A systematic investigation on the DPs formed in PTD solutions irradiated by alpha and gamma radiation has been hampered by the difficulties arisen from their synthesis and the unexpected solubility issues. Furthermore, the complexity of the irradiated solutions has made difficult the spectra interpretation and the comparison with the reference DPs solutions.

However, the work done demonstrated that the approach followed is promising in fully explaining the radiolytic degradation of PTD-based stripping solvent and also in discovering new modified PTD stripping agents with better properties than PTD ligand.

SO_3-Ph-BTP, SO_3-Ph-BTBP and SO_3-Ph-BTPhen

Below, the most recent data are presented from the study of the separation of trivalent actinides from lanthanides by i-SANEX processes combining An-selective hydrophilic masking agents (*e.g.* SO_3-Ph-BTP or SO_3-Ph-BTBP Figure 48) in the aqueous phase with the TODGA extractant in the organic phase, to allow for An(III)/Ln(III) separation. Two different i-SANEX systems were studied – 0.018 M SO_3-Ph-BTP or SO_3-Ph-BTBP in 0.35 M HNO_3 in the aqueous phase and 0.2 M TODGA in 5% 1-octanol/95% kerosene as the organic phase. The effect of temperature on the kinetics of extraction was studied as well as thermodynamic parameters of such systems. Further, kinetics models of Eu(III) extraction are discussed. Latter study embraces distribution ratios and separation factors dependency on the temperature and the absorbed dose from accelerated electrons. Moreover, irradiated extraction systems were subjected to analysis via HPLC-ESI-MS to obtain analytic concentration of masking agents.

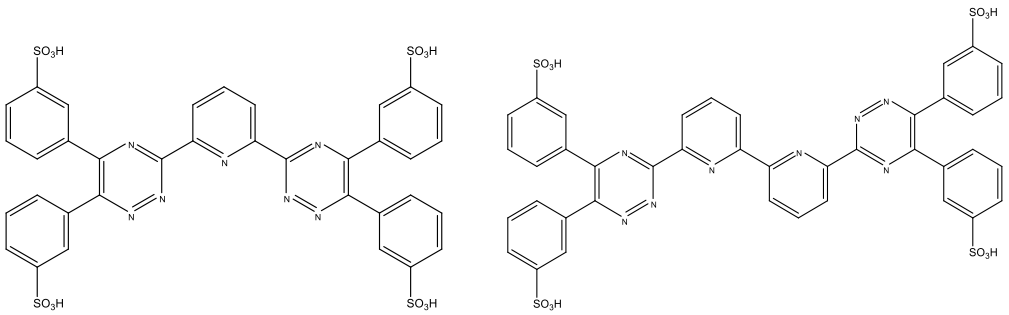

Figure 48. Chemical structures of SO_3-Ph-BTP (left) and SO_3-Ph-BTBP (right).

This project has received funding from the EURATOM research and training programme 2014-2018 under grant agreement No 755171. The content of this deliverable reflects only the author's view. The European Commission is not responsible for any use that may be made of the information it contains.

SO_3-Ph-BTP / TODGA IN 5% 1-OCTANOL/95% KEROSENE

NON-IRRADIATED SYSTEMS

KINETICS AT 250 RPM

The system comprising 0.018 M SO_3-Ph-BTP in 0.35 M HNO_3 as the aqueous and 0.2 M TODGA in 5% 1-octanol/95% kerosene as the organic phase was selected for this study. Kinetics of the extraction was followed at different temperatures. The data obtained for 4 different temperatures are shown in Table 37. It can be seen that at higher temperatures the equilibrium for Am(III) and Eu(III) extraction was achieved faster. The equilibrium was also achieved faster for Am(III) than for Eu(III). Both the *D*-values and $SF_{Eu/Am}$ were found to decrease with the increasing temperature. The kinetics of this system was slightly slower than the similar one (18 mM SO_3-Ph-BTP in 0.29 M HNO_3) reported in the literature, where the thermodynamic equilibrium was achieved within 10 minutes[55].

Table 37: The dependence of D_{Am}, D_{Eu} and $SF_{Eu/Am}$ values on temperature for the i-SANEX system with 0.018 M SO_3-Ph-BTP in 0.35 M HNO_3 / 0.2 M TODGA in 5% 1-octanoctol/95% kerosene.

t [min]	D_{Am}	D_{Eu}	$SF_{Eu/Am}$	D_{Am}	D_{Eu}	$SF_{Eu/Am}$
	T = 15 ºC			*T* = 25 ºC		
2	0.013 ± 0.001	0.90 ± 0.01	68.7 ± 5.7	0.005 ± 0.001	0.76 ± 0.01	168 ± 28
4	0.009 ± 0.001	2.50 ± 0.03	277 ± 22	0.007 ± 0.001	2.51 ± 0.03	355 ± 50
6	0.014 ± 0.001	3.93 ± 0.07	274 ± 16	0.008 ± 0.001	2.93 ± 0.04	366 ± 52
10	0.021 ± 0.001	8.04 ± 0.13	378 ± 26	0.008 ± 0.001	3.99 ± 0.05	514 ± 80
30	0.024 ± 0.001	17.3 ± 0.4	732 ± 41	0.009 ± 0.001	4.94 ± 0.06	566 ± 63
60	0.024 ± 0.001	18.0 ± 0.4	764 ± 42	0.008 ± 0.001	5.11 ± 0.07	607 ± 78
	T = 35 ºC			*T* = 45 ºC		
2	0.003 ± 0.001	0.72 ± 0.01	216 ± 67	< 0.003	0.47 ± 0.01	> 144
4	0.004 ± 0.001	1.16 ± 0.01	286 ± 55	< 0.003	0.43 ± 0.01	> 137
6	0.004 ± 0.001	1.23 ± 0.01	287 ± 62	< 0.003	0.42 ± 0.01	> 142
10	0.004 ± 0.001	1.29 ± 0.01	310 ± 85	< 0.003	0.47 ± 0.01	> 155
30	0.004 ± 0.001	1.38 ± 0.02	311 ± 77	< 0.003	0.51 ± 0.01	> 170
60	0.004 ± 0.001	1.34 ± 0.01	372 ± 110	< 0.003	0.45 ± 0.01	> 193

THERMODYNAMIC STUDY

The equilibrium values of distribution coefficients and Eu/Am separation factors for SO_3-Ph-BTP at different temperatures are shown in Table 38. From the obtained values, thermodynamics characteristics were calculated and are shown in Table 39.

This project has received funding from the EURATOM research and training programme 2014-2018 under grant agreement No 755171. The content of this deliverable reflects only the author's view. The European Commission is not responsible for any use that may be made of the information it contains.

Table 38: The equilibrium values of D_{Am}, D_{Eu} and $SF_{Eu/Am}$ for the i-SANEX system with 0.018 M SO_3-Ph-BTP in 0.35 M HNO_3 / 0.2 M TODGA in 5% 1-octanol/95% kerosene.

T [ºC]	D_{Am}	D_{Eu}	$SF_{Eu/Am}$
15	0.024 ± 0.001	18.0 ± 0.4	764 ± 42
25	0.008 ± 0.001	5.11 ± 0.06	607 ± 77
35	0.0036*	1.34 ± 0.01	> 372
45	0.0024*	0.46 ± 0.01	> 193

** These values are close to the detection limit.*

Table 39: The thermodynamic quantities of Am(III) and Eu(III) extraction for the i-SANEX system with 0.018 M SO_3-Ph-BTP in 0.35 M HNO_3 / 0.2 M TODGA in 5% 1-octanol/95% kerosene.

Ion	ΔS [J/mol.K]	ΔH [kJ/mol]	ΔG [kJ/mol]
Am^{3+}	-272 ± 8	-69.3 ± 2.5	11.8 ± 1.0
Eu^{3+}	-303 ± 6	-94.2 ± 1.9	-3.9 ± 0.2

THE OVERALL MASS-TRANSFER COEFFICIENTS

To elucidate the rate-controlling process of Eu(III) extraction, six kinetic models were tested. The model based on mass transfer (DM) as the rate-controlling process was found to best describe the kinetic data and the values of the overall mass-transfer coefficients were calculated (Table 40). The DM model is based on the so-called two-film theory of interphase diffusion. The methodology is described in[39]. The kinetics at 45 °C was too fast, therefore, it is not evaluated. Next, activation energy E_a was calculated as 95.9 kJ/mol and frequency factor A as 3.8 * 10^{15} min^{-1}. The value of frequency factor is in an agreement with data published in[40].

Table 40: Different kinetic models and their overall mass-transfer coefficients, *k*, and the corresponding goodness-of-fit criteria, *WSOS/DF*, values for Eu(III) extraction from 0.018 M SO_3-Ph-BTP in 0.35 M HNO_3 into 0.2 M TODGA in 5% 1-octanol/95% kerosene.

Model	15 °C (TBP)		25 °C (TBP)		35 °C (TBP)	
	k [1/min]	*WSOS/DF*	*k* [1/min]	*WSOS/DF*	*k* [1/min]	*WSOS/DF*
DM	0.02	1.71	0.06	2.26	0.20	0.07
FD	0.26	1.73	0.25	1.89	0.28	0.07
ID	0.12	39.1	0.04	2.22	0.11	0.33
CR	1.24	39.2	0.40	0.46	0.55	0.07
GD	0.00	9.61	0.01	1.24	0.06	0.17
RLD	0.07	47.2	0.01	2.22	0.07	0.32

IRRADIATED SYSTEMS

The extraction systems were irradiated by pulse linear electron accelerator LINAC 4-1200 (Tesla v.t. Mikroel). The mean electron energy was 4.5 MeV, pulse width 3 μs and repeating frequency 500 Hz. The total doses were up to 300 kGy. Ampules were shaked and termostated during the irradiation.

This project has received funding from the EURATOM research and training programme 2014-2018 under grant agreement No 755171. The content of this deliverable reflects only the author's view. The European Commission is not responsible for any use that may be made of the information it contains.

IRRADIATION OF THE NEAT AQUEOUS PHASE

Even after the irradiation, the trends in *D*-Values (Table 41) agreed with non-irradiated behaviour of samples. The main difference was that at the doses of 200 and 300 kGy some of D-values were for SO_3-Ph-BTP higher than values for a blank (without a masking agent). It can be possibly explained by the formation of degradation products of masking agent that are soluble in organic phase similar to other degradation products[56,57] and that act as additional extractants. When comparing the results at different temperatures, the slowest increase in *D*-values was at 15 °C. This is in good agreement with the fact that the rate of the complexant degradation decreases with decreasing temperature (cf. Table 43 below). When discussing the values of $SF_{Eu/Am}$, at a dose of 300 kGy the $SF_{Eu/Am}$ increase with the increasing temperature (opposite than for non-irradiated samples). However, they are much lower than in the non-irradiated systems and not far from their values in the respective blanks. The next parameter, that influences the properties during the irradiation, is the radiation chemistry of HNO_3 solutions. With increasing doses, the concentration of NO_3^- decreases and it influences the masking and extraction properties[20].

Table 41: The dependence of D_{Am} , D_{Eu} and $SF_{Eu/Am}$ values on absorbed dose at different temperatures for the i-SANEX system with 0.018 M SO_3-Ph-BTP in 0.35 M HNO_3 / 0.2 M TODGA in 5% 1-octanol/95% kerosene (neat aqueous phase irradiated).

***Dose* [kGy]**	D_{Am}	D_{Eu}	$SF_{Eu/Am}$	D_{Am}	D_{Eu}	$SF_{Eu/Am}$
	T = 15 ºC			*T* = 25 ºC		
0	0.024 ± 0.001	18.0 ± 0.4	764 ± 42	0.008 ± 0.001	5.11 ± 0.07	607 ± 78
50	0.076 ± 0.004	31.3 ± 2.9	413 ± 43	0.042 ± 0.005	12.2 ± 0.4	290 ± 36
100	0.34 ± 0.01	35.9 ± 2.8	105 ± 9	0.18 ± 0.01	25.1 ± 1.1	144 ± 11
150	1.45 ± 0.03	61.8 ± 4.1	42.8 ± 2.9	0.58 ± 0.01	45.7 ± 2.8	78.6 ± 5.2
200	2.99 ± 0.09	46.6 ± 5.1	15.6 ± 1.8	2.20 ± 0.05	61.1 ± 4.1	27.7 ± 1.9
300	13.1 ± 0.5	76.5 ± 5.9	5.88 ± 0.48	7.68 ± 0.22	89.6 ± 8.3	11.7 ± 1.2
Blank	16.4 ± 0.7	91.2 ± 16.9	5.57 ± 1.06	7.32 ± 0.23	56.2 ± 5.6	7.68 ± 0.79
	T = 35 ºC			*T* = 45 ºC		
0	0.004 ± 0.001	1.34 ± 0.01	372 ± 110	< 0.003	0.46 ± 0.01	193 ± 54
50	0.014 ± 0.002	6.45 ± 0.08	416 ± 64	0.007 ± 0.002	2.10 ± 0.04	324 ± 93
100	0.067 ± 0.004	10.0 ± 0.4	151 ± 10	0.041 ± 0.003	4.00 ± 0.11	98.5 ± 7.3
150	0.28 ± 0.01	12.3 ± 0.6	44.5 ± 2.4	0.17 ± 0.01	10.5 ± 0.5	62.7 ± 3.3
200	0.78 ± 0.02	31.9 ± 2.4	41.1 ± 3.2	0.51 ± 0.01	19.6 ± 1.1	38.2 ± 2.2
300	3.33 ± 0.08	40.7 ± 11.8	12.2 ± 3.6	2.00 ± 0.04	30.1 ± 2.3	15.1 ± 1.2
Blank	2.70 ± 0.06	21.2 ± 1.3	7.88 ± 0.50	1.12 ± 0.02	6.41 ± 0.19	5.73 ± 0.20

IRRADIATION OF THE AQUEOUS PHASE IN CONTACT WITH SOLVENT

The solvent consisted of 0.2 M TODGA in 5% 1-octanol/95% kerosene. The results for SO_3-Ph-BTP irradiated in contact with solvent are shown in Table 42. When compared with Table 41, it is obvious that radiation degradation is slower in this case. Even the selectivity remains higher even at a dose of 300 kGy. For example, at 25°C and 300 kGy, $SF_{Eu/Am}$ is still 8.2× times higher than in blank (it was only 1.5× times higher in the case of the irradiation of neat aqueous phase). These results are in good agreement with the data published in[20].

This project has received funding from the EURATOM research and training programme 2014-2018 under grant agreement No 755171. The content of this deliverable reflects only the author's view. The European Commission is not responsible for any use that may be made of the information it contains.

Table 42: The dependence of D_{Am}, D_{Eu} and $SF_{Eu/Am}$ values on absorbed dose at different temperatures for the i-SANEX system with 0.018 M SO_3-Ph-BTP in 0.35 M HNO_3 / 0.2 M TODGA in 5% 1-octanol/95% kerosene (both phases in contact irradiated).

Dose [kGy]	D_{Am}	D_{Eu}	$SF_{Eu/Am}$	D_{Am}	D_{Eu}	$SF_{Eu/Am}$
	T = 15 ºC			*T* = 25 ºC		
0	0.024 ± 0.001	18.0 ± 0.4	764 ± 42	0.008 ± 0.001	5.11 ± 0.07	607 ± 78
50	0.060 ± 0.004	17.5 ± 1.4	301 ± 32	0.018 ± 0.002	6.05 ± 0.15	330 ± 31
100	0.064 ± 0.004	16.1 ± 0.8	253 ± 21	0.018 ± 0.002	5.24 ± 0.11	296 ± 39
150	0.09 ± 0.006	16.3 ± 0.9	190 ± 16	0.022 ± 0.002	5.42 ± 0.17	263 ± 37
200	0.18 ± 0.01	18.7 ± 1.1	103 ± 7	0.026 ± 0.003	4.61 ± 0.15	177 ± 20
300	0.51 ± 0.01	9.21 ± 0.43	18.0 ± 1.0	0.074 ± 0.004	4.69 ± 0.15	63.3 ± 3.6
Blank	16.4 ± 0.7	91.2 ± 16.9	5.57 ± 1.06	7.32 ± 0.23	56.2 ± 5.6	7.68 ± 0.79
	T = 35 ºC			*T* = 45 ºC		
0	0.004 ± 0.001	1.34 ± 0.01	372 ± 110	< 0.003	0.46 ± 0.01	193 ± 54
50	0.010 ± 0.001	2.74 ± 0.11	270 ± 41	0.005 ± 0.001	1.03 ± 0.02	224 ± 19
100	0.041 ± 0.004	5.04 ± 0.16	125 ± 13	0.010 ± 0.002	1.44 ± 0.03	139 ± 10
150	0.026 ± 0.003	3.19 ± 0.08	123 ± 14	0.021 ± 0.002	1.79 ± 0.05	83.8 ± 8.1
200	0.022 ± 0.003	2.62 ± 0.08	119 ± 15	0.026 ± 0.002	1.25 ± 0.03	48.2 ± 3.8
300	0.052 ± 0.003	1.85 ± 0.05	36.1 ± 2.6	0.013 ± 0.002	0.36 ± 0.01	27.9 ± 3.8
Blank	2.7 ± 0.06	21.2 ± 1.3	7.88 ± 0.50	1.12 ± 0.02	6.41 ± 0.19	5.73 ± 0.20

RESIDUAL CONCENTRATIONS OF MASKING AGENTS

Another part of activity in cooperation between IIC CAS and CTU was devoted to development of a LC-MS method that would allow for determination of residual concentration of masking agent and its degradation products that arose upon irradiation. Sample was supplied CTU and analysis was performed in IIC CAS. HPLC method with MS detection was developed and tested with use of standard (10 mM, 1 mL water solution) before irradiation. The sample was analyzed in more details by NMR and tandem LC-MS by newly developed method that employed sufficiently volatile buffer allowing for on-line MS detection during the chromatographic run. Several HPLC analyses under different conditions were performed. Example of the chromatogram before its irradiation is depicted in Figure 49, together with its mass spectra of SO_3-Ph-BTP. After successful development of the separation method, the calibration plot was measured and constructed. The linear dynamic range was monitored over the entire measured area (0.1 – 10 mM) and the coefficient of determination was close to one (0.999).

Another goal was paid to two factors. i.e. to the effect of temperature (15° – 45°C) on decrease in concentration depending on different irradiation doses from 50 kGy to 500 kGy, and to the focus on the influence of contact with the second organic phase (0.2 M TODGA in 5% 1-octanol/95% kerosene) present or absent in the system. From the percentage values of the residual masking agent concentrations (Table 43), the following statements can be done: a) Degradation of SO_3-Ph-BTP increases with increasing temperature (the bigger difference starts after 150 kGy), and b) when the aqueous phase is irradiated in contact with solvent, the degradation of masking agent is suppressed.

This project has received funding from the EURATOM research and training programme 2014-2018 under grant agreement No 755171. The content of this deliverable reflects only the author's view. The European Commission is not responsible for any use that may be made of the information it contains.

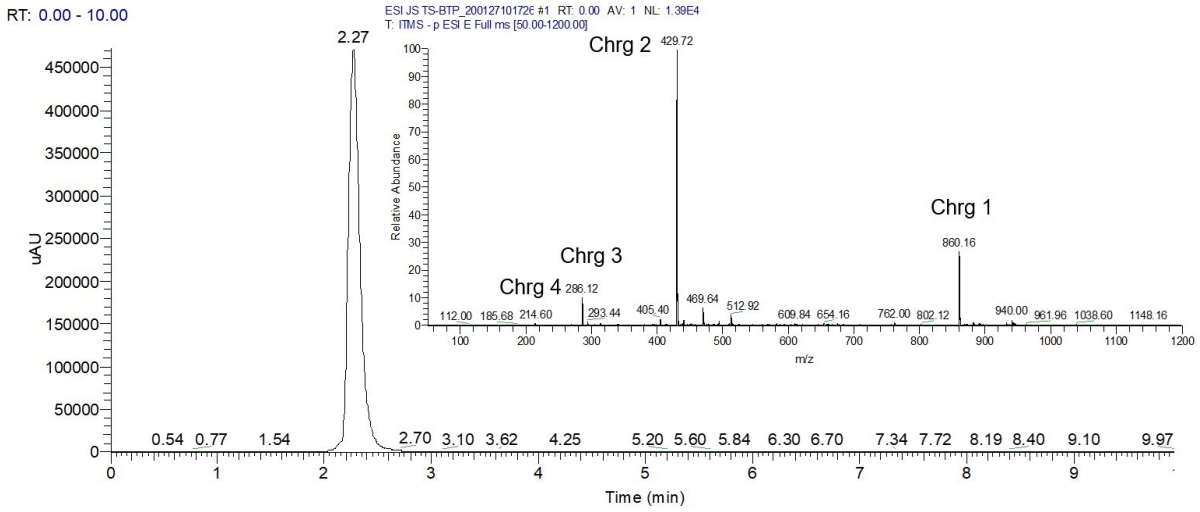

Figure 49: HPLC chromatogram with isocratic elution of masking agent; with PDA and MS detection; flow rate 0.2 mL min^{-1}; column: Gemini-NX C18 110 Å (3 µm, 150 x 2.00 mm *I.D.*); mobile phase: 10 mM AF pH 3.8 with 5% ACN.

Table 43: The dependence of residual concentrations of SO_3-Ph-BTP on absorbed dose at different temperatures for the i-SANEX system (0.018 M SO_3-Ph-BTP in 0.35 M HNO_3) irradiated in the presence / absence of the solvent (0.2 M TODGA in 5% 1-octanol/95% kerosene).

Dose [kGy]	Neat aqueous phase irradiated				Aqueous phase + solvent irradiated			
	Relative concentration of SO_3-Ph-BTP [%]							
	15 ºC	25 ºC	35 ºC	45 ºC	15 ºC	25 ºC	35 ºC	45 ºC
50	94.3	92.8	96.7	91.1	93.5	95.2	96.6	99.4
100	84.8	82.5	81.2	83.0	89.2	90.7	92.5	89.1
150	76.5	73.4	70.2	70.7	84.6	86.7	N/A	83.5
200	67.9	58.3	58.2	54.4	77.2	77.1	73.5	67.2
300	46.9	41.7	39.9	32.3	58.2	58.1	56.9	50.3

Let's discuss our results and results published in[56]. In the recent article[56], it was concluded that app. 50 % of SO_3-Ph-BTP was degraded already after a dose of 60 kGy (when neat aqueous phase was irradiated), at the dose of 300 kGy, only 10 % of the initial masking agent remained in solution. From the experimental data presented here (Table 43) follows that the residual concentrations are much higher. A possible reason for this discrepancy may be the indirect nature of the residual concentration determination used in[56] where it was not measured but calculated from the decrease of *D*-values. Hence, this indirect procedure does not seem to yield correct results.

The degradation of SO_3-Ph-BTP proceeds mainly by reactions with $OH^{\bullet}$ radicals created in the interaction of ionizing radiation with the aqueous phase. It can be hence suggested that in this system the organic phase acts as a scavenger of $OH^{\bullet}$ radicals. Decrease in $OH^{\bullet}$ concentration in aqueous phase by mixing with organic phase can then decrease the degradation of SO_3-Ph-BTP[57].

This project has received funding from the EURATOM research and training programme 2014-2018 under grant agreement No 755171. The content of this deliverable reflects only the author's view. The European Commission is not responsible for any use that may be made of the information it contains.

SO_3-Ph-BTBP / TODGA IN 5% 1-OCTANOL/95% KEROSENE

NON-IRRADIATED SYSTEMS

KINETICS AT 250 RPM

The system comprising 0.018 M SO_3-Ph-BTBP in 0.35 M HNO_3 as the aqueous and 0.2 M TODGA in 5% 1-octanol/95% kerosene as the organic phase was selected for this study. In the first step, the kinetics of Am(III) and Eu(III) extraction was measured at 25 °C (Table 44). Since the results were so similar with SO_3-Ph-BTP, no other temperatures were tested. Even the *SF*-values were very similar: $SF_{Eu/Am}$ (SO_3-Ph-BTBP) = 560 ± 97 and $SF_{Eu/Am}$ (SO_3-Ph-BTP) = 607 ± 78 after 60 minutes of shaking.

Table 44: The dependence of D_{Am} , D_{Eu} and $SF_{Eu/Am}$ values on time at 25 °C for the i-SANEX system with 0.018 M SO_3-Ph-BTBP in 0.35 M HNO_3 / 0.2 M TODGA in 5% 1-octanol/95% kerosene.

t [min]	D_{Am}	D_{Eu}	$SF_{Eu/Am}$
2	0.008 ± 0.002	1.25 ± 0.02	162 ± 34
4	0.008 ± 0.001	1.27 ± 0.01	158 ± 36
6	0.007 ± 0.001	1.86 ± 0.02	254 ± 61
10	0.006 ± 0.002	2.87 ± 0.03	472 ± 130
30	0.009 ± 0.002	4.69 ± 0.06	544 ± 119
60	0.009 ± 0.001	4.93 ± 0.07	560 ± 97

THERMODYNAMIC STUDIES

The equilibrium values of metal extraction at different temperatures are shown in Table 45. From the obtained values, thermodynamics characteristics were calculated and are shown in Table 46. The trends were very similar to the system with SO_3-Ph-BTP.

Table 45: The equilibrium values of D_{Am}, D_{Eu} and $SF_{Eu/Am}$ for the i-SANEX system with 0.018 M SO_3-Ph-BTBP in 0.35 M HNO_3 / 0.2 M TODGA in 5% 1-octanol/95% kerosene.

T [ºC]	D_{Am}	D_{Eu}	$SF_{Eu/Am}$
15	0.026 ± 0.002	17.6 ± 0.4	683 ± 59
25	0.009 ± 0.001	4.93 ± 0.07	560 ± 97
35	0.004 ± 0.001	1.11 ± 0.01	265 ± 46
45	0.003 ± 0.001	0.34 ± 0.01	111 ± 36

Table 46: The thermodynamic quantities of Am(III) and Eu(III) extraction for the i-SANEX system with 0.018 M SO_3-Ph-BTBP in 0.35 M HNO_3 / 0.2 M TODGA in 5% 1-octanol/95% kerosene.

Ion	ΔS [J/mol.K]	ΔH [kJ/mol]	ΔG [kJ/mol]
Am^{3+}	-222 ± 27	-54.9 ± 8.0	11.3 ± 3.2
Eu^{3+}	-329 ± 10	-102 ± 3	-3.9 ± 0.3

This project has received funding from the EURATOM research and training programme 2014-2018 under grant agreement No 755171. The content of this deliverable reflects only the author's view. The European Commission is not responsible for any use that may be made of the information it contains.

It is difficult to compare the obtained results with the data published in other papers, because the compositions of extraction systems differ (different concentrations of ligands, masking agents, acids or diluents used). Most of the published results deal with TODGA only, without the presence of any masking agent in the aqueous phase[57-61].

THE OVERALL MASS-TRANSFER COEFFICIENTS

To elucidate the rate-controlling process of Eu(III) extraction at 25 °C, six kinetic models were tested. A model based on mass transfer (DM) as the rate-controlling process was found to best describe the kinetic data and the values of the overall mass-transfer coefficients were calculated (Table 47). The DM model is based on the so-called two-film theory of interphase diffusion. The methodology is described in[39].

Table 47: Different kinetic models and their overall mass-transfer coefficients, *k*, and the corresponding goodness-of-fit criteria, *WSOS/DF*, values for Eu(III) extraction from 0.018 M SO_3-Ph-BTBP in 0.35 M HNO_3 into 0.2 M TODGA in 5% 1-octanol/95% kerosene.

Model	25 °C (BTBP)	
	k [1/min]	*WSOS/DF*
DM	0.05	1.76
FD	0.27	3.71
ID	0.10	13.5
CR	0.78	12.3
GD	0.01	0.67
RLD	0.02	13.5

IRRADIATED SYSTEMS

The extraction systems were irradiated by pulse linear electron accelerator LINAC 4-1200 (Tesla v.t. Mikroel). The mean electron energy was 4.5 MeV, pulse width 3 μs and repeating frequency 500 Hz. The total doses were up to 300 kGy. Ampules were shaken and termostated during the irradiation.

IRRADIATION OF NEAT AQUEOUS PHASE

For the irradiated systems containing SO_3-Ph-BTBP, D-values increase with increasing absorbed dose for all temperatures (Table 48). In this case, the *D*-values did not exceed the values of blanks even after 300 kGy. However, $SF_{Eu/Am}$ values are much smaller for irradiated samples. In general, the system with SO_3-Ph-BTBP is more stable than that with SO_3-Ph-BTP. It should be noted here that at 15 °C irradiation up to the dose of 50 kGy has a negligible effect on D-values. At any temperature, the $SF_{Eu/Am}$ values remain higher than 100 up to the absorbed dose of 150 kGy.

IRRADIATION OF THE AQUEOUS PHASE IN CONTACT WITH SOLVENT

The system with SO_3-Ph-BTBP showed, again, that the decrease in *D*(Am) is slower when the aqueous phase is irradiated in the presence of the organic (compare data in Table 48 and Table 49).

This project has received funding from the EURATOM research and training programme 2014-2018 under grant agreement No 755171. The content of this deliverable reflects only the author's view. The European Commission is not responsible for any use that may be made of the information it contains.

Table 48: The dependence of D_{Am}, D_{Eu} and $SF_{Eu/Am}$ values on absorbed dose at different temperatures for the i-SANEX system with 0.018 M SO_3-Ph-BTBP IN 0.35 M HNO_3 / 0.2 M TODGA in 5% 1-octanol/95% kerosene (neat aqueous phase irradiated).

***Dose* [kGy]**	D_{Am}	D_{Eu}	$SF_{Eu/Am}$	D_{Am}	D_{Eu}	$SF_{Eu/Am}$
	T = 15 ºC			*T* = 25 ºC		
0	0.026 ± 0.002	17.6 ± 0.4	683 ± 59	0.009 ± 0.001	4.91 ± 0.07	574 ± 141
50	0.024 ± 0.003	16.3 ± 0.8	717 ± 113	0.013 ± 0.003	5.75 ± 0.14	439 ± 88
100	0.065 ± 0.004	16.5 ± 0.9	254 ± 21	0.040 ± 0.003	7.49 ± 0.27	187 ± 16
150	0.18 ± 0.01	24.3 ± 1.6	140 ± 10	0.068 ± 0.004	11.4 ± 0.5	168 ± 12
200	0.38 ± 0.01	24.3 ± 1.7	63.4 ± 4.7	0.18 ± 0.01	15.2 ± 0.7	84.0 ± 4.9
300	1.45 ± 0.04	35.5 ± 3.3	24.1 ± 2.3	0.73 ± 0.02	22.3 ± 1.7	30.8 ± 2.5
Blank	16.4 ± 0.7	91.2 ± 16.9	5.57 ± 1.06	7.32 ± 0.23	56.2 ± 4.5	7.68 ± 0.79
	T = 35 ºC			*T* = 45 ºC		
0	0.004 ± 0.001	1.11 ± 0.01	265 ± 45	0.003 ± 0.001	0.34 ± 0.01	111 ± 36
50	0.006 ± 0.002	1.52 ± 0.04	227 ± 35	0.010 ± 0.002	0.74 ± 0.02	71.7 ± 14.2
100	0.024 ± 0.002	–	–	–	–	–
150	0.037 ± 0.003	4.57 ± 0.14	122 ± 10	0.024 ± 0.002	2.42 ± 0.07	103 ± 9
200	0.12 ± 0.01	8.89 ± 0.89	73.3 ± 7.7	0.053 ± 0.003	3.08 ± 0.06	58.0 ± 3.8
300	0.51 ± 0.01	11.5 ± 0.5	22.4 ± 1.2	0.23 ± 0.01	6.02 ± 0.20	26.8 ± 1.2
Blank	2.7 ± 0.1	21.2 ± 1.3	7.88 ± 0.5	1.12 ± 0.02	6.59 ± 0.20	5.89 ± 0.22

This project has received funding from the EURATOM research and training programme 2014-2018 under grant agreement No 755171. The content of this deliverable reflects only the author's view. The European Commission is not responsible for any use that may be made of the information it contains.

Table 49: The dependence of D_{Am}, D_{Eu} and $SF_{Eu/Am}$ values on absorbed dose at different temperatures for the i-SANEX system with 0.018 M SO_3-Ph-BTBP in 0.35 M HNO_3 / 0.2 M TODGA in 5% 1-octanol/95% kerosene (both phases in contact irradiated).

Dose [kGy]	D_{Am}	D_{Eu}	$SF_{Eu/Am}$	D_{Am}	D_{Eu}	$SF_{Eu/Am}$
	T = 15 ºC			*T* = 25 ºC		
0	0.026 ± 0.002	17.6 ± 0.4	683 ± 59	0.009 ± 0.001	4.91 ± 0.07	574 ± 141
50	0.020 ± 0.002	11.1 ± 0.5	552 ± 70	0.009 ± 0.002	2.71 ± 0.08	316 ± 67
100	0.028 ± 0.003	10.9 ± 0.5	397 ± 53	0.016 ± 0.002	2.97 ± 0.08	186 ± 29
150	0.028 ± 0.003	9.77 ± 0.45	364 ± 44	0.013 ± 0.003	2.39 ± 0.04	186 ± 40
200	0.043 ± 0.004	7.5 ± 0.31	173 ± 17	0.025 ± 0.002	4.62 ± 0.15	188 ± 19
300	0.057 ± 0.004	6.02 ± 0.25	106 ± 8	0.014 ± 0.002	1.19 ± 0.02	90.3 ± 15.5
Blank	16.4 ± 0.7	91.2 ± 16.9	5.57 ± 1.06	7.32 ± 0.23	56.2 ± 5.6	7.68 ± 0.79
	T = 35 ºC			*T* = 45 ºC		
0	0.004 ± 0.001	1.11 ± 0.01	265 ± 45	0.003 ± 0.001	0.34 ± 0.01	111 ± 36
50	0.005 ± 0.001	1.20 ± 0.02	234 ± 44	0.004 ± 0.001	0.46 ± 0.01	115 ± 20
100	0.056 ± 0.002	1.01 ± 0.02	17.9 ± 0.8	0.004 ± 0.001	0.37 ± 0.01	95.9 ± 19.1
150	0.009 ± 0.002	1.03 ± 0.03	121 ± 24	0.007 ± 0.001	0.37 ± 0.01	53.9 ± 11.1
200	0.019 ± 0.002	0.94 ± 0.02	50.7 ± 6.2	0.011 ± 0.001	0.22 ± 0.01	19.8 ± 2.6
300	0.033 ± 0.002	0.77 ± 0.02	23 ± 1.7	0.002 ± 0.001	0.097 ± 0.005	44.8 ± 11.5
Blank	2.7 ± 0.06	21.2 ± 1.3	7.88 ± 0.5	1.12 ± 0.02	6.59 ± 0.2	5.89 ± 0.22

RESIDUAL CONCENTRATIONS OF MASKING AGENTS

As mentioned earlier the development of the method procedure in all steps for determination of SO_3-Ph-BTBP are identical. Sample of the same concentration and volume was supplied by CTU. Example of the chromatogram before its irradiation is depicted in Figure 50 together with its mass spectra and structure of masking agent; linear dynamic range over the entire measured area (0.1 – 10 mM) was monitored and the coefficient of determination was close to one (0.999).

The effect of temperature (15° – 45°C) on decrease in concentration depending on different irradiation doses from 50 kGy to 500 kGy was performed similarly with focus on the influence of contact with the second organic phase (0.2 M TODGA in 5% 1-octanol/95% kerosene) present or absent in the system. The general trends for values of the SO_3-Ph-BTBP residual concentrations (Table 50) are similar to SO_3-Ph-BTP. The main differences are the following: a) the values of the residual concentrations are higher; b) the effect of the presence of organic phase is smaller than for SO_3-Ph-BTP. It seems that the mechanism of SO_3-Ph-BTBP is different and less independent on presence of OH radicals.

As discussed above for the case of the system with SO_3-Ph-BTP, the degradation of SO_3-Ph-BTBP proceeds mainly by reactions with $OH^{\bullet}$ radicals created by ionizing radiation in the aqueous phase. It can be hence suggested that the organic phase acts here as a scavenger of $OH^{\bullet}$ radicals. Decrease in $OH^{\bullet}$ concentration in aqueous phase by mixing with organic phase can then decrease the degradation of SO_3-Ph-BTBP[57].

This project has received funding from the EURATOM research and training programme 2014-2018 under grant agreement No 755171. The content of this deliverable reflects only the author's view. The European Commission is not responsible for any use that may be made of the information it contains.

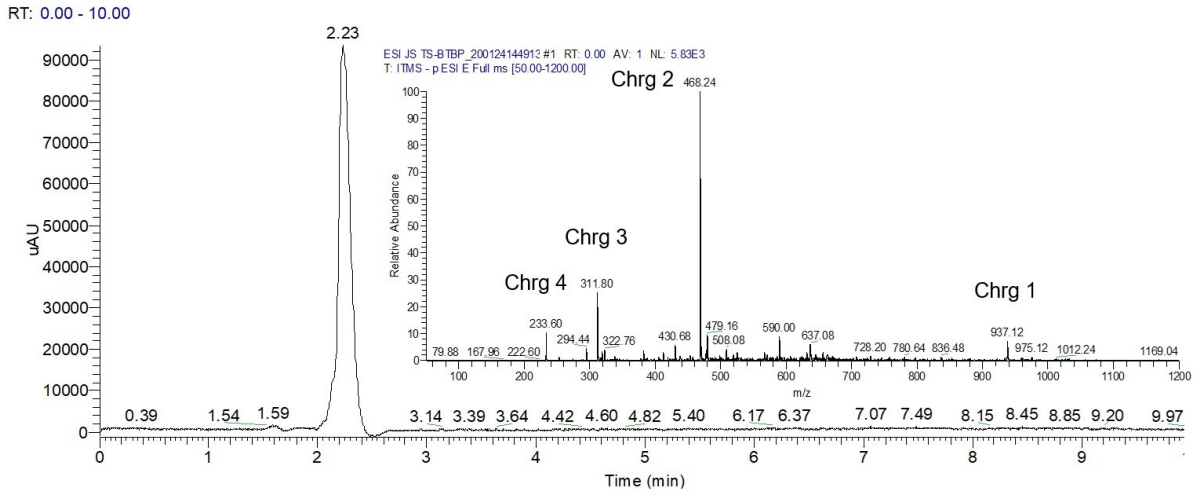

Figure 50: HPLC chromatogram with isocratic elution of masking agent; with PDA and MS detection; flow rate 0.2 mL min^{-1}; column: Gemini-NX C18 110 Å (3 µm, 150 x 2.00 mm *I.D.*); mobile phase: 10 mM AF pH 3.8 with 5% ACN.

Table 50: The dependence of residual concentrations of SO_3-Ph-BTBP on absorbed dose at different temperatures for the irradiation of aqueous phase (0.018 M SO_3-Ph-BTBP in 0.35 M HNO_3) in the presence / absence of the solvent (0.2 M TODGA in 5% octan-1 ol/95% kerosene).

Dose [kGy]	Neat aqueous phase irradiated				Aqueous phase + solvent irradiated			
	Relative concentration of SO_3-Ph-BTP [%]							
	15 ºC	25 ºC	35 ºC	45 ºC	15 ºC	25 ºC	35 ºC	45 ºC
50	93.3	92.1	92.1	92.0	89.9	97.7	93.8	92.2
100	88.4	87.9	91.4	0*	85.4	94.4	90.9	87.1
150	86.3	81.9	83.1	82.1	77.9	85.1	83.1	81.7
200	79.4	76.4	76.6	75.1	72.2	77.3	72.2	76.5
300	59.6	61.9	58.1	54.4	56.2	59.2	54.3	53.3

SO_3-Ph-BTPhen / TODGA IN 5% 1-OCTANOL/95% KEROSENE

The i-SANEX extraction system with the tetrasulfonated BTPhen ligand (SO_3-Ph-BTPhen) in aqueous phase was tested for its behaviour under irradiation (doses up to 300 kGy by gamma). The aqueous phases were irradiated with/without the organic phase. The general trend observed was, that up to 200/250 kGy, the *D* values for Am(III) and Eu(III) remained similar, but for higher doses the values of distribution ratios changed dramatically. Moreover, the effect of HNO_3 concentration was tested as well (0.25, 0.50 and 0.75 M HNO_3). The influence of irradiation on ability of the SO_3-Ph-BTPhen complexing / masking agent to suppress Am(III) and Cm(III) extraction into TODGA solution was also studied. The trend in $SF_{Cm/Am}$ values was similar to the trend of values of $SF_{Eu/Am}$, *i.e.* a gradual decrease of the separation factors with increasing dose was observed. These results are presented in more detail in a draft paper[37].

This project has received funding from the EURATOM research and training programme 2014-2018 under grant agreement No 755171. The content of this deliverable reflects only the author's view. The European Commission is not responsible for any use that may be made of the information it contains.

CONCLUSIONS

Properties and radiation stability of three systems with hydrophilic masking agents (SO_3-Ph-BTP, SO_3-Ph-BTBP or SO_3-Ph-BTPhen) were studied throughout the project. The results obtained and the conclusions drawn can be summarized as follows:

- The i-SANEX extraction system with the tetrasulfonated BTPhen ligand (SO_3-Ph-BTPhen) in aqueous phase was tested for its behaviour under irradiation (doses up to 300 kGy by gamma). The general trend observed was, that up to 200/250 kGy, the D values for Am(III) and Eu(III) remained similar, but for higher doses the values of distribution ratios changed dramatically. The influence of irradiation on ability of the SO_3-Ph-BTPhen complexing / masking agent to suppress Am(III) and Cm(III) extraction into TODGA solution was studied as well. The trend in $SF_{Cm/Am}$ values was similar to the trend of values of $SF_{Eu/Am}$[37].
- Characterization of two different i-SANEX systems with tetrasulfonated BTP/BTBP (0.018 M SO_3-Ph-BTP or SO_3-Ph-BTBP in 0.35 M HNO_3 / 0.2 M TODGA in 5% 1-octanol/95% kerosene) at different temperatures was performed in the last part of the GENIORS project. The effect of temperature on the kinetics of extraction was evaluated as well as thermodynamic parameters of these systems. The obtained values were similar as trends observed before and were used for comparison with samples irradiated by accelerated electrons. The overall mass transfer coefficients for Eu(III) extraction from the SO_3-Ph-BTP-containing solution increase with increasing temperature. After the irradiation of SO_3-Ph-BTP-containing aqueous phase without contact with organic phase to high absorbed doses, the D_{Am} and D_{Eu} exceed the values of blank - some degradation products/adducts formed probably act as efficient non-selective extractants of the mentioned metals. When the aqueous phase was in contact with organic phase during the irradiation, the system was more stable against radiolysis and D_{Am} values increased more slowly. Residual concentrations of SO_3-Ph-BTP were higher in the case when the aqueous phase was irradiated in contact with the organic phase. The system with SO_3-Ph-BTBP behaved in a very similar way as the SO_3-Ph-BTP one, however, it was much more radiation-stable than the SO_3-Ph-BTP system.

AHA AND SO_3-Ph-BTP

Following an homogeneous recycling strategy, the EURO-GANEX process is one of the most successful options developed for the second cycle of GANEX process [34,31,54]. During the first cycle (GANEX-1) U(VI) is selectively extracted leaving TRU, trivalent lanthanides (Ln(III)) and the other fission products (FPs) in the aqueous phase[62]. Then, the EURO-GANEX solvent consisting in a mixture of the DGA TODGA and the malonamide DMDOHEMA (*N*,*N*'-dimethyl-*N*,*N*'-dioctylhexyloxyethyl malonamide), co-extracts An and Ln from GANEX-1 raffinate; to avoid the extraction of some FPs such as Zr(IV) and Pd(II), the masking agent CDTA (trans-1,2-cyclohexanediaminetetraacetic acid) is used. After that, all TRU are stripped using the combination of the water soluble SO_3-Ph-BTP and AHA (acetohydroxamic acid) (Figure 51)[50]. The role of DMDOHEMA in EURO-GANEX solvent is to increase the Pu loading capacity of the organic phase[50] and of AHA to strip Pu(IV), Np(VI), and Np(VI) into aqueous phase[63,64].

This project has received funding from the EURATOM research and training programme 2014-2018 under grant agreement No 755171. The content of this deliverable reflects only the author's view. The European Commission is not responsible for any use that may be made of the information it contains.

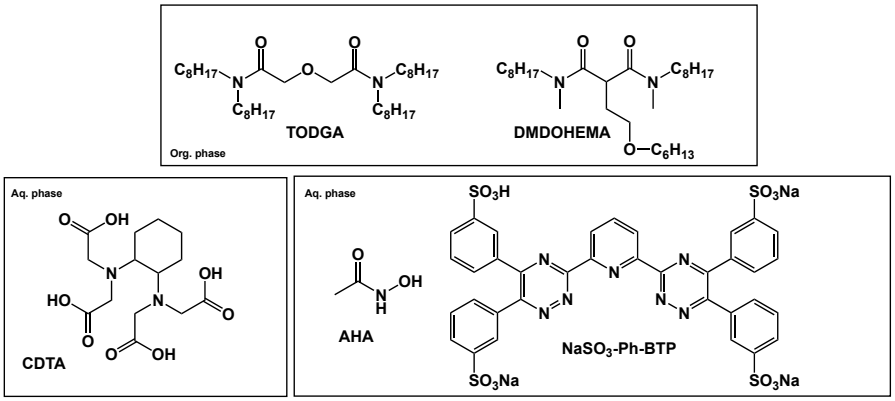

Figure 51: Structures of the molecules involved in the EURO-GANEX process: TODGA, DMDOHEMA, CDTA, $NaSO_3$-Ph-BTP and AHA.

Although it is not expected that the EURO-GANEX aqueous phases be recycled, its degradation might lead the transfer of degradation products into recycled organic phase and their accumulation therein.

The stability of CDTA aqueous phase and the effect of its degradation over the extraction performance have been studied against gamma radiation for the EURO-GANEX process conditions in a section before.

Regarding SO_3-Ph-BTP, the first chemical and radiolytic stability studies of SO_3-Ph-BTP were performed during SACSSES project focus on *i*-SANEX process[60,65]. During the current GENIORS project, more detailed stability studies have been carried out considering different conditions such as the interaction with different organic phase (focus on *i*-SANEX and Euro-GANEX processes) during the irradiation, and the irradiation way (static and dynamic irradiation). These results are partially published in 61 and summarised in the Deliverable 2.2 Stability studies of stripping agents[66]. From these results, it can be concluded that SO_3-Ph-BTP aqueous phases show a better resistance against γ-irradiation when the irradiation takes place in contact with the organic phases. This was evaluated by using an estimation of SO_3-Ph-BTP concentration by the correlation with D_{Am}. Additional studies have also been reported by *D*. Peterman *et. al.*[17] and G. P. Horne *et al.*[56]. However, they were performed under different experiment conditions. An extended study about process-relevant conditions to simulate effects of radiation over SO_3-Ph-BTP aqueous phases will be reported in Deliverable D5.2 (Impacts of solvent degradation and recycle on the EURO-GANEX process).

With respect to AHA, several studies have been carried out regarding to its hydrolysis. Acetic acid (AcOH) and hydroxylamine (HA) were identified as hydrolysis products. However, only two studies about the gamma radiolysis of AHA were found[67,68]. In both studies, authors analyse the AHA concentration as a function of time by an indirect method of measurement, the UV-visible spectrophotometric measurements of AHA-Fe(III) complex. Both studies determined that radiation stability of AHA in HNO_3 depends on the absorbed dose and HNO_3 concentration, but the effect of the latter is greater than that of the former.

Notwithstanding all studies done, there are none about the stability against gamma radiation including both molecules, SO_3-Ph-BTP and AHA. In this section, a stability study of AHA and SO_3-Ph-BTP with both of them irradiated together is presented. The studies were performed up to 50 kGy and under EURO-GANEX process conditions, considering factors such as AHA hydrolysis, the acidity of the media and AHA and SO_3-Ph-BTP radiolysis.

In order to investigate the effect of gamma radiation on the aqueous phase involved in the stripping step of EURO-GANEX, three different irradiation experiments have been designed and carried out (detailed in Table 51). For a better understanding of the system, first, the individual radiolysis of AHA and SO_3-Ph-BTP in HNO_3

This project has received funding from the EURATOM research and training programme 2014-2018 under grant agreement No 755171. The content of this deliverable reflects only the author's view. The European Commission is not responsible for any use that may be made of the information it contains.

under the same experimental conditions has been studied, 1 mol/L AHA in 0.5 mol/L HNO_3 in Exp.1 and 0.018 mol/L SO_3-Ph-BTP in 0.5 mol/L HNO_3 in Exp.2. Then, Exp. 1 and Exp. 2 have been compared with Exp. 3, which contains both molecules together.

After the irradiation, An(III) and Ln(III) extraction were measured and compared for all solvent compositions explored and the original performance of the system. For a real comparison of the D_M values obtained and the individual effects of AHA or BTP or AHA and BTP, extraction experiments were always performed using a fresh EURO-GANEX solvent, 0.2 mol/L TODGA + 0.5 mol/L DMDOHEMA in OK. The aqueous phase employed during the extraction experiment contains 0.018 mol/L SO_3-Ph-BTP + 1 mol/L AHA in 0.5 mol/L HNO_3 (EURO-GANEX stripping composition). For those first experiments in which AHA has been irradiated alone, fresh SO_3-Ph-BTP was dissolved in the irradiated AHA solution before the extraction test. In the second case, where SO_3-Ph-BTP has been irradiated alone, fresh AHA was dissolved in the irradiated SO_3-Ph-BTP solution before the extraction test. In the last trial, AHA and SO_3-Ph-BTP have been irradiated together. Therefore, the extraction test was carried out without any additional treatment. Table 51 also shows the composition of the organic and aqueous phase used for the extraction experiments.

All experiments containing AHA were carried out using the same methodology that control samples, *i.e.* the quantification and extraction experiments were carried out always after 2 hours, to keep constant the hydrolysis effect of AHA in all studied samples.

Table 51: Composition of the aq. phases that have been irradiated (up to 50 kGy) and the org. and aq. phases used for the extraction experiments.

Experiment		Sample Composition	
		Organic phase	Aqueous phase
Exp. 1	1.1) Irradiation	-	1 mol/L AHA in 0.5 mol/L HNO_3
	1.2) Extraction	0.2 mol/L TODGA + 0.5 mol/L DMDOHEMA in OK	1 mol/L AHA **IRR** + 0.018 mol/L SO_3-Ph-BTP **FRESH** in 0.5 mol/L HNO_3
Exp. 2	2.1) Irradiation	-	0.018 mol/L SO_3-Ph-BTP in 0.5 mol/L HNO_3
	2.1) Extraction	0.2 mol/L TODGA + 0.5 mol/L DMDOHEMA in OK	1 mol/L AHA **FRESH** + 0.018 mol/L SO_3-Ph-BTP **IRR** in 0.5 mol/L HNO_3
Exp. 3	3.1) Irradiation	-	1 mol/L AHA + 0.018 mol/L SO_3-Ph-BTP in 0.5 mol/L HNO_3
	3.2) Extraction	0.2 mol/L TODGA + 0.5 mol/L DMDOHEMA in OK	1 mol/L AHA **IRR** + 0.018 mol/L SO_3-Ph-BTP **IRR** in 0.5 mol/L HNO_3

The quantification of the mentioned molecules has been carried out by quantitative Raman spectroscopy (QRS). It should be noted that Raman technique has been chosen as a main tool due to two main reasons: (1) we had already demonstrated that Raman technique is a handy tool for the in-situ analysis of the AHA hydrolysis[69,70]; and (2) Raman spectroscopy can be used for quantifying not only AHA and its hydrolysis products but also the remaining concentration of SO_3-Ph-BTP after irradiation.

First, with the aim of analyzing liquid samples safely, a new Raman cell have been designed, which must meet certain requirements: to allow the measurements of a very small amount of sample, to be practical and easy to work with, and the radioactive samples must be confined to avoid the risk of contamination. Moreover, this cell must be refrigerated, since the laser power density provided during a Raman measurement can increase the sample temperature, which causes several changes in the Raman modes and, sometimes, the sample

This project has received funding from the EURATOM research and training programme 2014-2018 under grant agreement No 755171. The content of this deliverable reflects only the author's view. The European Commission is not responsible for any use that may be made of the information it contains.

alteration. Figure 52 shows the main components and details of the design[71]. This cell was manufactured and it was employed for the mentioned studies.

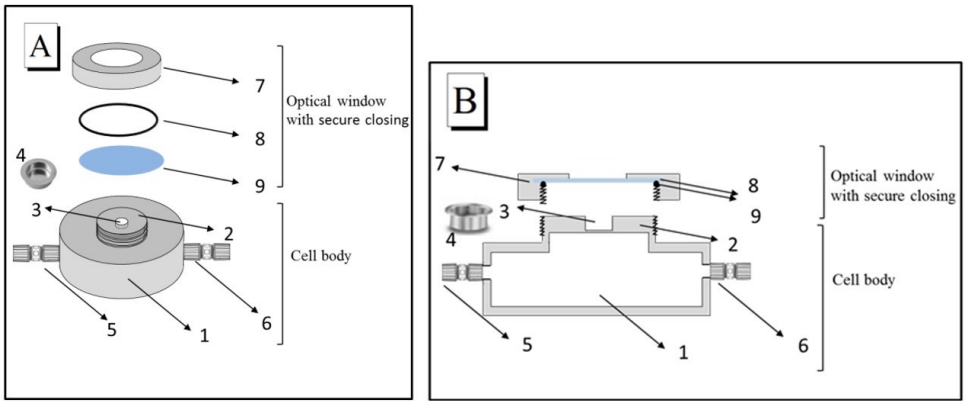

Figure 52: A and B schematic drawings of the Raman cell. Cell body: 1-Chamber base; 2- Elevated platform; 3-Slit; 4-Sample holder; 5-Water inlet; 6-Water outlet, and Optical window with secure closing: 7-Teflon PTFE screw cap; 8-O-ring; 9-Optical window.

STABILITY OF AHA VS. GAMMA IRRADIATION UNDER EURO-GANEX PROCESS CONDITIONS

In this experiment, 1 mol/L AHA in 0.5 mol/L HNO_3 was irradiated up to an integrated dose of 50 kGy and the QRS methodology to calculate the concentration decrease was employed. Raman spectra are shown in Figure 53 and based on our last works[69,70], the bands at ≈950 cm^{-1}, ≈881 cm^{-1} and ≈997 cm^{-1} were used to calculate AHA, AcOH, and HA concentrations, respectively.

Spectra of AHA irradiated samples do not present any new Raman bands at our measure conditions, apart from the Raman features corresponding to the hydrolysis of the samples, observed in our most recent studies[69,70]. In addition, the relative intensity of all bands corresponding to the AHA is equal. For this reason, using Raman spectroscopy at the studied conditions, different products to AHA, AcOH and HA are not observed.

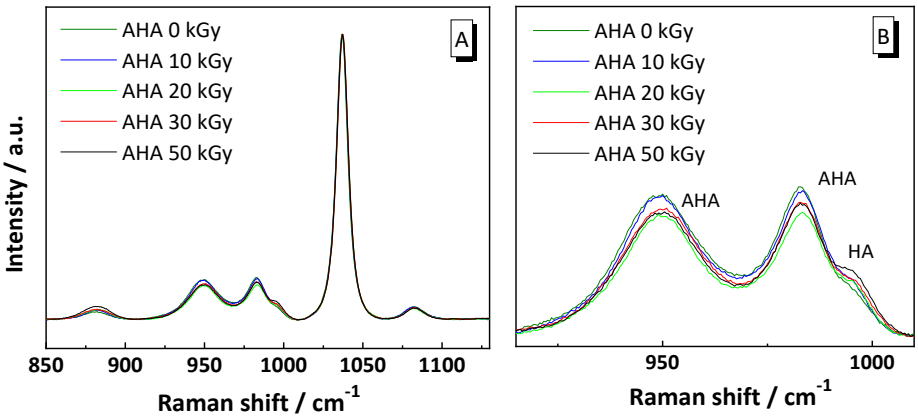

This project has received funding from the EURATOM research and training programme 2014-2018 under grant agreement No 755171. The content of this deliverable reflects only the author's view. The European Commission is not responsible for any use that may be made of the information it contains.

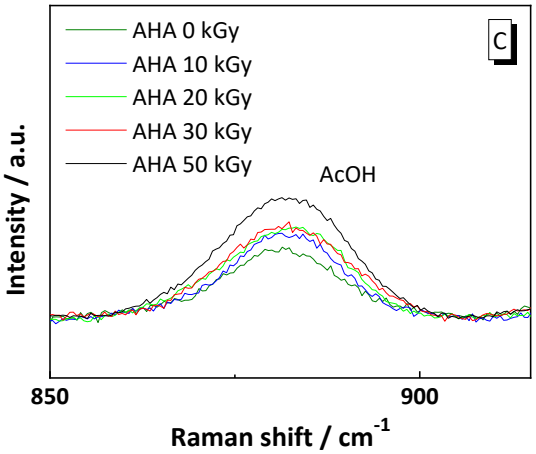

Figure 53: Experimental Raman spectra corresponding to irradiated samples up to 50 kGy of 1 mol/L AHA in 0.5 mol/L HNO_3. A) from 850 to 1150 cm^{-1}, B) from 910 to 1010 cm^{-1}, and C) from 850 to 910 cm^{-1}. These spectra were acquired by using a laser excitation source of 532 nm with a Horiba LabRam HR evolution spectrometer.

Following the methodology used in the aforementioned works, both the decrease in the concentration of the AHA and the increase in the concentration of AcOH and HA have been obtained using QRS, *i.e.* the Raman analysis of the relative integrated intensities of the mentioned bands give us a measure of the concentration.

First of all, control sample for the hydrolysis of AHA has been studied at two hours. As expected from known kinetics studies in the literature[70], the AHA concentration decreases from 1 mol/L to 0.87 ± 0.05 mol/L; AcOH and HA are formed by hydrolysis reaction from 0 mol/L to 0.11 ± 0.05 mol/L and 0.05 ± 0.07 mol/L, respectively; and proton concentration decreases from 0.50 mol/L to 0.41 ± 0.01 mol/L. This result was taken as our control sample to obtain the variation in the AHA, AcOH and HA concentrations (ΔConc) produced only by radiolysis as shown in Figure 54, where our results are also compared with the obtained by Wang et al[68].

The variation of AHA concentration is negative (-0.124 mol/L at 50 kGy) and it is in agreement with the obtained by Wang et al.[68] where the variation of the AHA concentration reported was -0.05 mol/L at 25 kGy, as can be observed in Figure 54. However, as a consequence of AHA degradation, AcOH and HA are formed and so, the variation of AcOH and HA concentrations are positive. On the one hand, the variation in AcOH concentration increases slightly with the dose reaching ~0.07 mol/L at 50 kGy, in agreement with Wang et al.[68] who showed a variation in the concentration of ~0.0375 mol/L at 25 kGy. Furthermore, it can be observed that the AcOH concentration is always higher than HA. This could be explained because AcOH is also a radiolysis product while HA is only a hydrolysis product and its concentration increase less significant, as is also detailed in Wang et al.[68].

Proton concentration variation before the extraction experiments was evaluated when samples were irradiated and the results are also shown in Table 52. As mentioned before, the control sample after 2 hours, a decrease from 0.50 mol/L to (0.41 ± 0.01) mol/L was observed due to the increase in HA concentration because of hydrolysis process, in agreement with our previous works. However, a slight decrease of $[H^+]$ with the absorbed dose was observed only for 50 kGy.

This project has received funding from the EURATOM research and training programme 2014-2018 under grant agreement No 755171. The content of this deliverable reflects only the author's view. The European Commission is not responsible for any use that may be made of the information it contains.

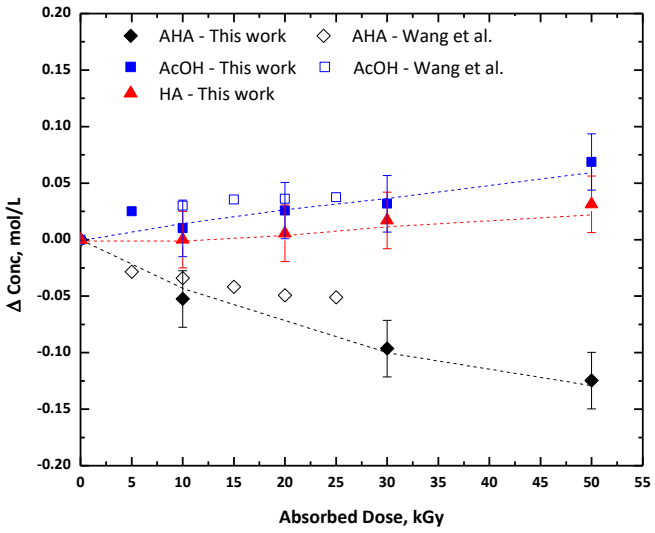

Figure 54. Variation in the concentrations obtained for AHA, acetic acid (AcOH), hydroxylamine (HA) in this work, and for AHA and AcOH obtained by Wang et al,[74] as a function of absorbed dose up to 50 kGy.

Table 52: Proton concentrations obtained in the AHA aqueous phase at 2 hours as a function of dose taking into account the hydrolysis and radiolysis.

Sample		Absorbed Dose, kGy	$[H^+]$, mol/L
1 mol/L AHA in 0.5 mol HNO_3	No hydrolysis effect (t = 0 hours)	0	0.50 ± 0.01
	Hydrolysis effect (t = 2 hours)	0	0.41 ± 0.01
	Radiolysis effect (t = 2 hours)	10	0.41 ± 0.01
		20	0.43 ± 0.01
		30	0.40 ± 0.01
		50	0.36 ± 0.01

The evaluation of D_{Am} and D_{Eu} for Exp. 1 at 2 hours hydrolysis is shown in Figure 55A. As can be expected, as the fresh organic EURO-GANEX solvent is used Eu is kept in the organic phase, although a slight decrease in the D_{Eu} is observed as a function of absorbed dose. This could be attributed to the decrease in proton concentration and the reduction of nitrate concentration in the media. As SO_3-Ph-BTP is also added fresh into the aqueous phase, Am is maintained there (D_{Am}<1). A slight decrease of D_{Am} is also observed as a function of absorbed dose, in agreement with the effects observed for D_{Eu}. Therefore, the individual irradiation of AHA has only a small effect on the extraction performance of the system producing a slight decrease in the both $D_{M(III)}$, but at these absorbed doses, the separation factor of Ln and An are good enough ($SF_{Eu(III)/Am(III)}$>290 at 50 kGy) to mantain effecient separation.

The same extraction experiments were carried out at 192 hours of hydrolysis, where due to the AHA hydrolysis and the consequential decrease of the proton concentration, $D_{Eu(III)}$ becomes much lower than 1 ($D_{Eu(III)}$ ≈0.1), producing an ineffective separation between Eu(III) and Am(III) as can be seen in Figure 55B. Under these long time conditions, hydrolysis is more significant than radiolysis, and this is fundamental when designing simulation strategies to assess the system (composition and extraction properties) involved in the EURO-GANEX process under these conditions.

This project has received funding from the EURATOM research and training programme 2014-2018 under grant agreement No 755171. The content of this deliverable reflects only the author's view. The European Commission is not responsible for any use that may be made of the information it contains.

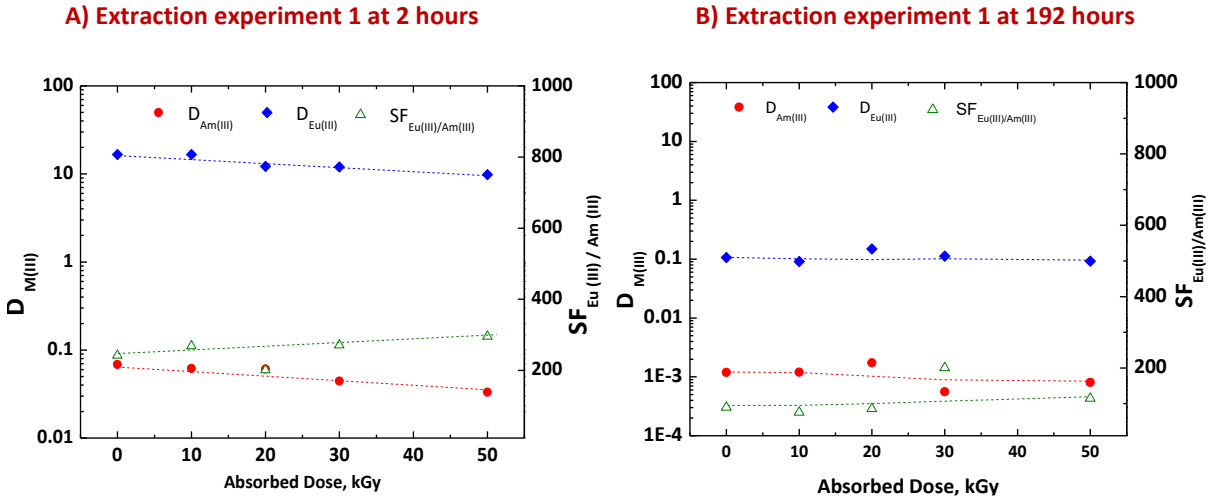

Figure 55: Distribution ratios of Am(III) and Eu(III) as a function of dose for the Exp. 1 containing a fresh organic phase of 0.2 mol/L TODGA and 0.5 mol/L DMDOHEMA in OK and an aqueous phase of fresh 0.018 mol/L SO_3-Ph-BTP and irradiated 1 mol/L AHA in 0.5 mol/L HNO_3 at A) 2 hours and B) 192 hours.

STABILITY OF SO_3-Ph-BTP VS. GAMMA IRRADIATION UNDER EURO-GANEX PROCESS CONDITIONS

Although it was possible to follow three of main mass signals obtained for di, tri and tetra charged compounds by mass spectroscopy (*m/z* = 214.3, 286.3 and 429.9, respectively, for samples treated with H_2SO_4/H_2O/MeOH), calibrations curves by HPLC-MS were not reproducible. Considering these problems found by HPLC-MS and the feasibility of Raman spectroscopy in different applications in the nuclear field such as online monitoring, a methodology to measure and quantify AHA and its hydrolysis compounds by Raman spectroscopy was developed[70,71]. This methodology allowed explaining the effect of AHA hydrolysis in the stability study of stripping step of EURO-GANEX process. Using the same Raman methodology developed for AHA, the analysis of SO_3-Ph-BTP degradation by Raman spectroscopy has been carried out.

Subsequently, qualitative Raman analysis was performed to SO_3-Ph-BTP. Figure 56 shows the Raman spectra of an aqueous solution of 0.018 mol/L SO_3-Ph-BTP dissolved in 0.5 mol/L HNO_3 and a solution of 0.5 mol/L HNO_3. Raman bands related to aqueous solution of HNO_3 appear, as expected, as a broad band at high frequencies (2800–3400 cm^{-1}) corresponds to the OH-bond stretching, ν_s(O-H) and a very intense band located at around 1037 cm^{-1} corresponding to the N-O stretching of the nitrate ion, $\nu_s(NO_3^-)$[72]. This figure also shows the characteristics bands of SO_3-Ph-BTP *i.e.* three narrow and intense bands at 996, 1509 and 1597 cm^{-1} and a few broad and low intensity bands at 2000- 3000 cm^{-1} which could be related to the SO_3 groups[73,74].

This project has received funding from the EURATOM research and training programme 2014-2018 under grant agreement No 755171. The content of this deliverable reflects only the author's view. The European Commission is not responsible for any use that may be made of the information it contains.

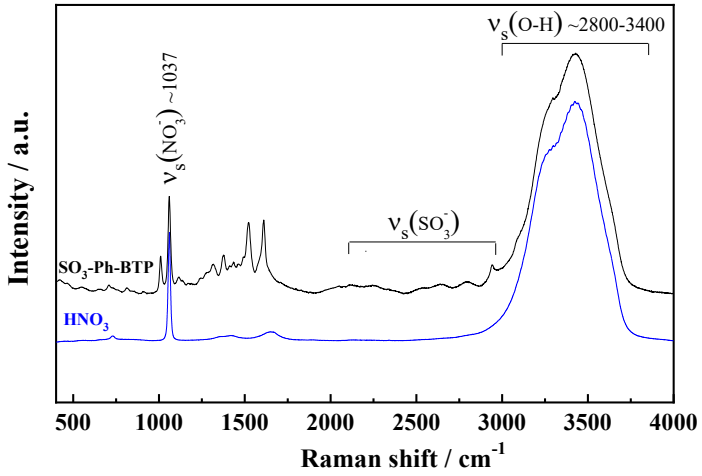

Figure 56: Raman spectra of 0.5 mol/L HNO_3 and 0.018 mol/L SO_3-Ph-BTP dissolved in 0.5 mol/L HNO_3.

After that, samples of SO_3-Ph BTP (0.018 mol/L in 0.5 mol/L HNO_3) were irradiated to doses of 10, 20, 30 and 50 kGy at dose rate of ≈40 kGy/h. The significant darkening of solutions was attributed to the radiolytic degradation of SO_3-Ph-BTP that takes place when the aqueous phase is irradiated individually, in line with other previous works[17,60] (Figure 57). Following the methodology established for AHA[69,70], samples were analyzed by Raman spectroscopy using 532 nm and 633 nm lasers with a Horiba LabRam HR evolution spectrometer, but an increase of baseline producing a low quality of spectra was observed. However, this phenomenon is minimized with the use of the laser of 785 nm, giving place to the desirable spectra. For that reason, a HeNe laser with a wavelength of 785 nm and a B&W Tek i-RamanTM spectrometer have been employed to determine the spectra of irradiated SO_3-Ph-BTP solutions.

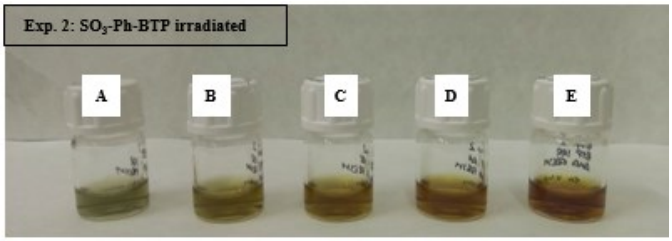

Figure 57: Photographs of samples of 18 mmol/L SO_3-Ph-BTP in 0.5 mol/L HNO_3 irradiated at different doses: (A) 0 kGy, (B) 10 kGy, (C) 20 kGy, (D) 30 kGy and (E) 50 kGy.

Figure 58 shows the spectra of irradiated SO_3-Ph-BTP samples obtained by Raman spectroscopy. The spectra do not present any new Raman bands additional to the SO_3-Ph-BTP bands at our measure conditions. Moreover, the relative intensity of the bands keeps constant. Therefore, we assume that the band analysed for the QRS (Quantitative Raman spectroscopy) corresponds to the SO_3-Ph-BTP, and no degradation compounds are observed.

With the mentioned conditions, calibration curves were obtained from Raman spectra of fresh SO_3-Ph-BTP aqueous solutions in concentration from 0 to 18 mmol/L. The band area was calculated from the fitting results (using a Voigt function) of the band at around ≈996 cm^{-1} for SO_3-Ph-BTP. A linear calibration equation $C = a \cdot A + b$ was obtained, where C is the molar concentration of each molecule and A is the ratio between the area of the corresponding band of SO_3-Ph-BTP (A_{996}) and the band corresponding to NO_3 (A_{1037}). The obtained experimental Raman spectra, fitted curves and the calibration curve are shown in Figure 59.

This project has received funding from the EURATOM research and training programme 2014-2018 under grant agreement No 755171. The content of this deliverable reflects only the author's view. The European Commission is not responsible for any use that may be made of the information it contains.

.

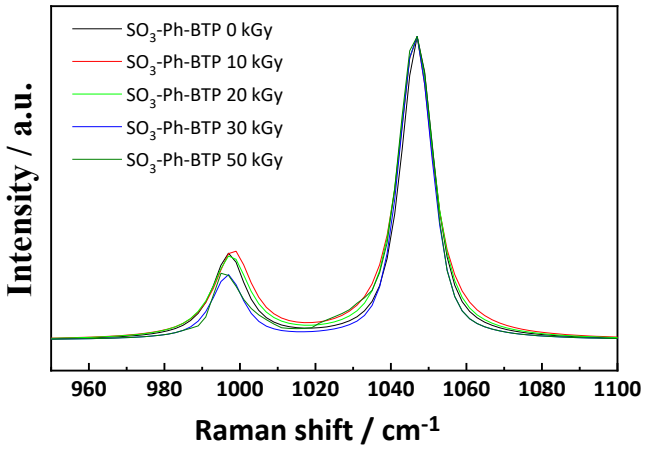

Figure 58: Raman spectra corresponding to irradiated samples up to 50 kGy of 18 mmol/L SO_3-Ph-BTP in 0.5 mol/L HNO_3.

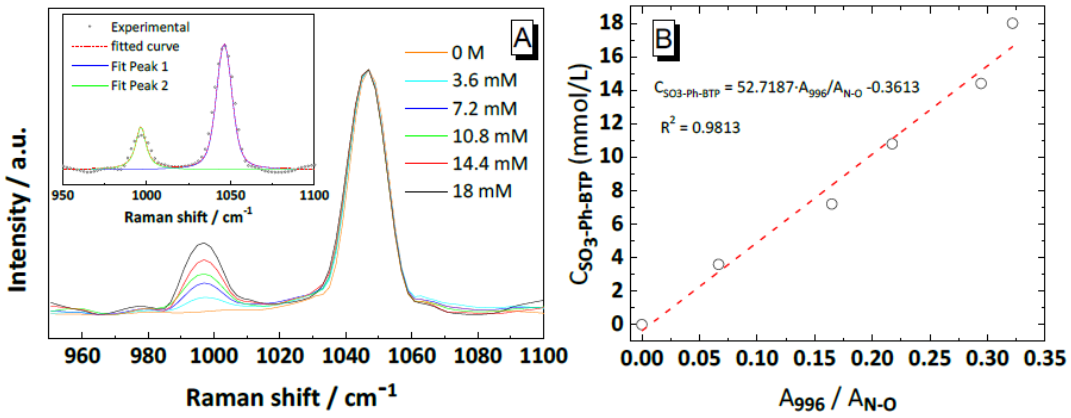

Figure 59: (A) Experimental Raman spectra, fitted curve and (B) calibration curve corresponding to different concentrations of SO_3-Ph-BTP in 0.5 mol/L HNO_3.

Figure 60A shows the comparison of the quantification of SO_3-Ph-BTP by Raman spectroscopy done after the irradiation, with the concentration estimated by an indirect method ($D_{Am(III)}$ dependency with the SO_3-Ph-BTP concentration) for EURO-GANEX system stability studies reported in HYPAR-5 WP5 CIEMAT[74]. A good linear correlation is found, supporting the validity of the methods to determine the SO_3-Ph-BTP concentration

The SO_3-Ph-BTP concentration decreases with the dose, i.e., approx. 50% is lost at a dose of 50 kGy in both cases (Figure 60B). The reduction in the SO_3-Ph-BTP concentration highlighted that this molecule is very susceptible to degradation under the studied radiation conditions, in agreement with our previous work about the individual irradiation of SO_3-Ph-BTP aqueous phase[17], despite the use of a much higher dose rate.

Proton concentration remained approximately constant (from 0.54 ± 0.01 mol/L to 0.53 ± 0.01 mol/L in 50 kGy) during the irradiation of SO_3-Ph-BTP up to 50 kGy, indicating that at these conditions the aqueous phase acidity is not considerably affected by the degradation of SO_3-Ph-BTP.

Figure 60C shows the $D_{Am(III)}$ and $D_{Eu(III)}$ extraction experiment carried out for Exp. 2. As happened in Exp. 1, the organic solvent shows an efficient Eu extraction along the irradiation experiment since the organic phase is not degraded; in fact, a slightly increase with the absorbed dose is observed that could be attributed to the

This project has received funding from the EURATOM research and training programme 2014-2018 under grant agreement No 755171. The content of this deliverable reflects only the author's view. The European Commission is not responsible for any use that may be made of the information it contains.

degradation of SO_3-Ph-BTP. Regarding $D_{Am(III)}$, a progressive increase was measured, reducing the separation factor between Am(III) and Eu(III), explained by the progressive destruction of SO_3-Ph-BTP as function of the dose. Even at 50 kGy $D_{Am(III)}$ is lower than 1, still maintaining a good $SF_{Eu(III)/Am(III)}$.

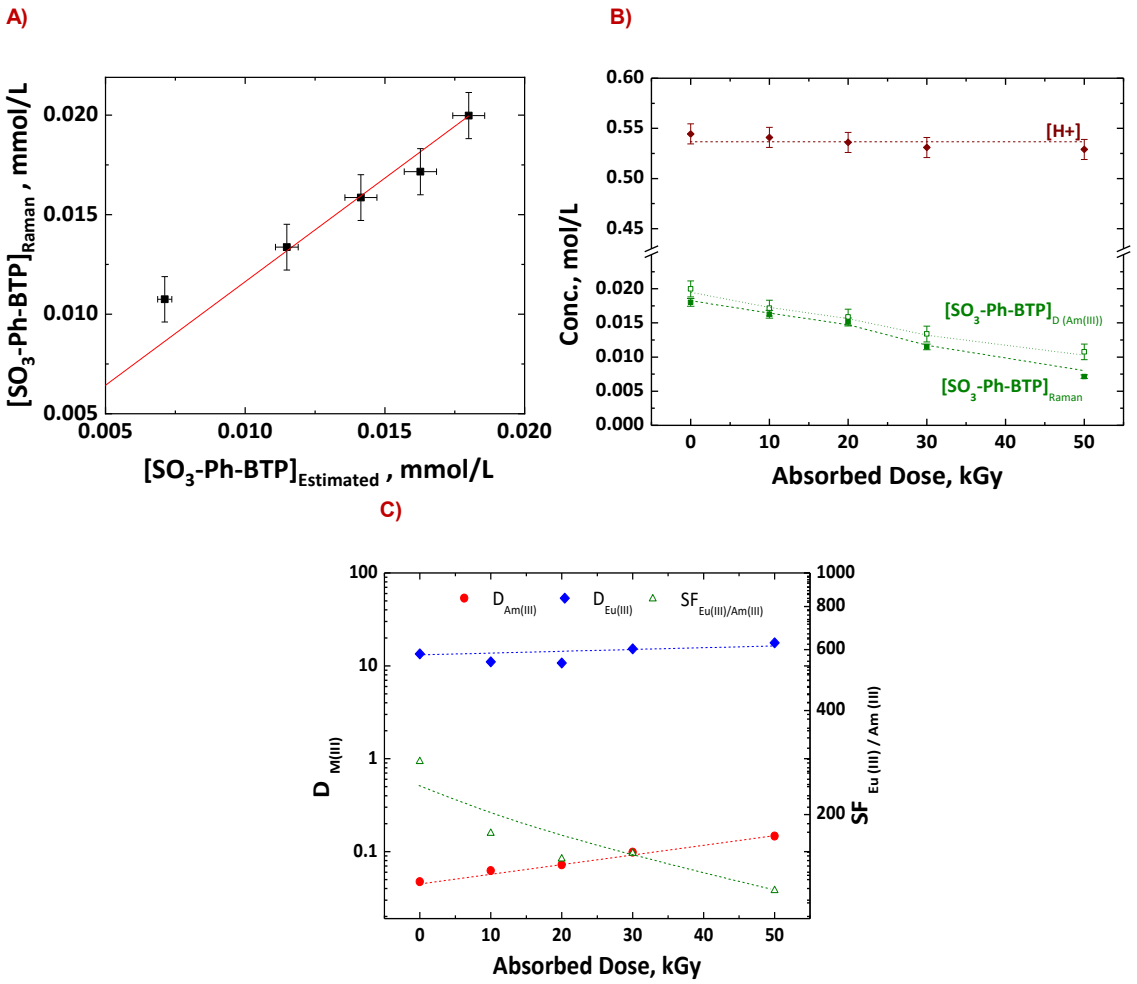

Figure 60: A) Comparison between SO_3-Ph-BTP concentrations obtained by Raman spectroscopy ($[SO_3\text{-Ph-BTP}]_{Raman}$) and using the relation with the $D_{Am(III)}$ ($[SO_3\text{-Ph-BTP}]_{D(Am(III))}$). B) Concentrations of SO_3-Ph-BTP obtained by Raman spectroscopy ($[SO_3\text{-Ph-BTP}]_{Raman}$) and using the relation with the $D_{Am(III)}$ ($[SO_3\text{-Ph-BTP}]_{D(Am(III))}$) and [H+] as a function of absorbed dose. C) Comparison between SO_3-Ph-BTP quantification by Raman spectroscopy ($[SO_3\text{-Ph-BTP}]_{Raman}$) and the concentration estimation using the relation with the $D_{Am(III)}$ ($[SO_3\text{-Ph-BTP}]_{D(Am(III))}$).

STABILITY OF AHA AND SO_3-PH-BTP VS. GAMMA IRRADIATION UNDER EURO-GANEX PROCESS CONDITIONS

In the Exp. 3 (see Table 51), solutions containing both AHA and SO_3-Ph-BTP were irradiated at the same absorbed doses. As can be observed in Figure 61A the irradiated solutions showed no visual colour changes, in contrast with the Exp. 2. As this system contains AHA, all experiments (Raman measurements for quantification and extraction experiments) were taken after 2 hours as we did for Exp.1 in order to minimise its hydrolysis effects. Raman spectra of irradiated samples obtained by this technique are shown in Figure 61B. Figure 61C shows the results of the AHA and SO_3-Ph-BTP quantification by QRS as well as the proton concentration as a

This project has received funding from the EURATOM research and training programme 2014-2018 under grant agreement No 755171. The content of this deliverable reflects only the author's view. The European Commission is not responsible for any use that may be made of the information it contains.

function of absorbed dose. Results obtained show that concentrations of both AHA and SO_3-Ph-BTP are practically invariable with absorbed dose, in contrast to what was observed for Exp.1 and Exp. 2.

It was not possible to calculate the concentration of AHA hydrolysis products (HA and AcOH) because of the spectra obtained by using a 785 nm laser with the B&W Tek i-RamanTM spectrometer have a lower detection limit than those obtained with the laser excitation source of 532 nm, Horiba LabRam HR evolution spectrometer. As consequence of the constant AHA concentration, neither an increase in proton concentration nor significant variations of $D_{M(III)}$ values are observed at 2 hours (Figure 62A).

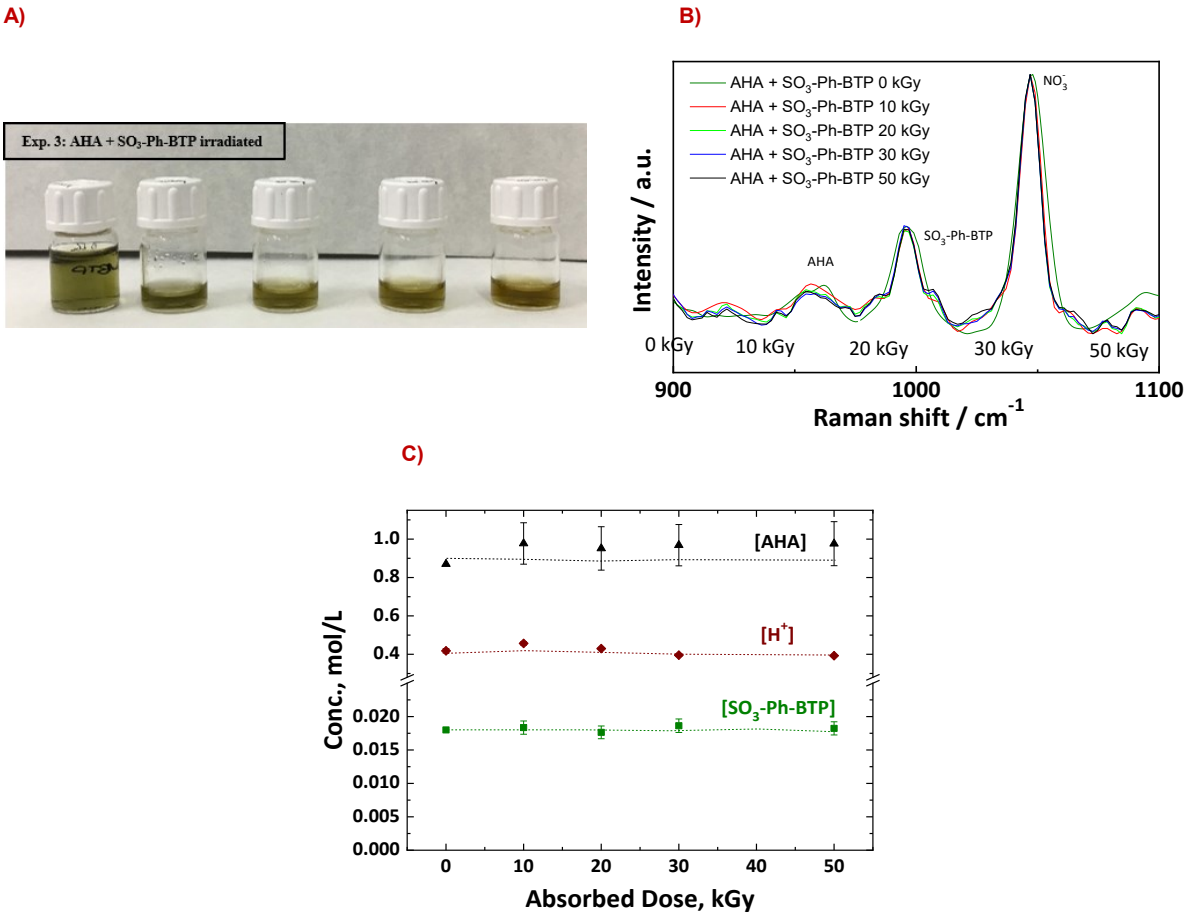

Figure 61. A) Photographs of irradiated samples of 1 mol/L AHA and 0.018 mol/L SO_3-Ph-BTP in HNO_3 0.5 mol/L at different doses, B) Experimental Raman spectra corresponding to 1 mol/L AHA + 0.018 mol/L SO_3-Ph-BTP in 0.5 mol/L HNO_3 and C) Concentrations obtained of AHA, SO_3-Ph-BTP and protons (H+) always at 2 hours of AHA hydrolysis, all figures as a function of absorbed dose for Exp.3.

The extraction efficiency was also measured for Exp.3 at 192 hours (Figure 62). The results are in agreement with those obtained in Exp. 1 and in our last works[71], reporting an ineffective separation of Am(III) and Eu(III) as a consequence of the increase of the pH due AHA hydrolysis. This result highlights the importance of the AHA hydrolysis at long times, being more significant than radiolysis effect. Therefore, stability studies should be carefully designed and monitored along the time if AHA is involved.

This project has received funding from the EURATOM research and training programme 2014-2018 under grant agreement No 755171. The content of this deliverable reflects only the author's view. The European Commission is not responsible for any use that may be made of the information it contains.

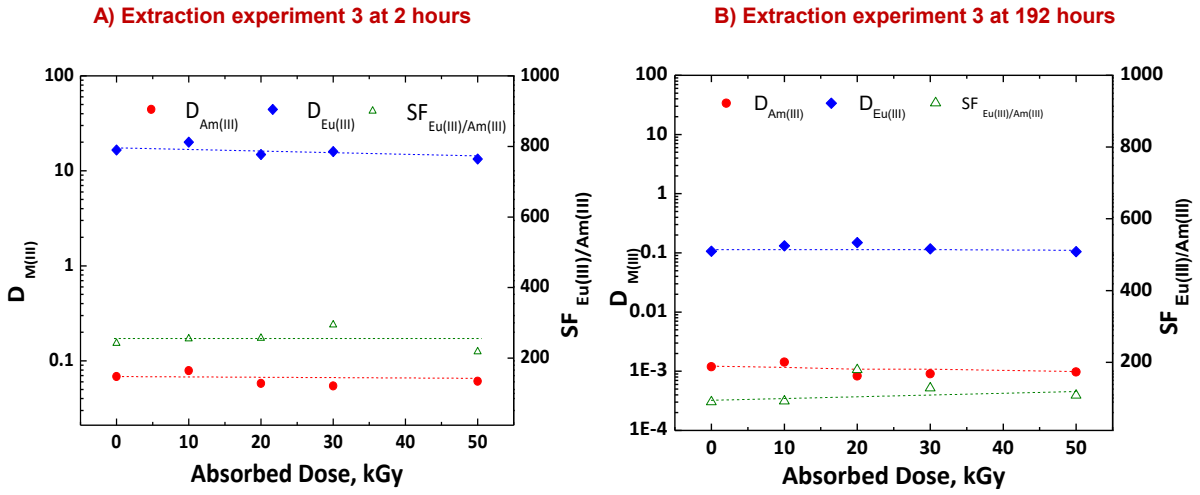

Figure 62: Distribution ratios of Am(III) and Eu(III) as a function of dose for the Exp. 3 containing a fresh organic phase of 0.2 mol/L TODGA and 0.5 mol/L DMDOHEMA in OK and an aqueous phase of fresh 0.018 mol/L SO_3-Ph-BTP and irradiated 1 mol/L AHA in 0.5 mol/L HNO_3 at A) 2 hours and B) 192 hours.

CONCLUSIONS

The resistance to γ-radiation of molecules involved in the aqueous phase of EURO-GANEX stripping step, AHA and SO_3-Ph-BTP, has been explored together. With the aim to complete the different stability studies already published and to obtain the right comparison of the effects of each compound on the media, they were first studied individually. These initial results indicated that SO_3-Ph-BTP is more susceptible to radiolysis effects than AHA. Additionally, it allowed studying the effects of pH variation due to AHA degradation. Even more important, the same methodology of quantification by Raman spectroscopy that had been reported previously for AHA has been established for SO_3-Ph-BTP, showing that this technique can be used as a reliable tool for monitoring the stability of these systems.

AHA and SO_3-Ph-BTP were irradiated together using the experimental conditions of the EURO-GANEX process and simulating the low expected doses for aqueous phases that will not be recycled (at a maximum of 50 kGy). This experimental configuration allowed investigating factors such as AHA hydrolysis, the acidity of the media and AHA and SO_3-Ph-BTP destruction due to radiation effects at the same time. The results obtained show an increased resistance of SO_3-Ph-BTP against radiation when it is irradiated in presence AHA and indicate a lower AHA degradation and a constant acidity of the media during the first two hours studied. The insignificant degradation is reflected by the excellent Eu(III)/Am(III) selectivity being maintained during the irradiation experiment. These studies point out a better behaviour against radiation of the full EURO-GANEX system (Org.+Aq.: TODGA-DMDOHEMA / AHA-SO_3-Ph-BTP) than expected from the stability of SO_3-Ph-BTP itself.

These results also manifest clearly that the effects of irradiation on solvent extraction systems depends upon experimental design and conditions employed. Although basic stability studies remain relevant for the fundamental understanding of degradation pathways, it is essential to design reliable simulating strategies to predict the long-term performance of extraction systems submitted to nuclear fuel radiation. These results provide important keys to take into account during the design of EURO-GANEX stability experiments and supply an easy monitoring tool. Moreover, these results show how Raman spectroscopy can be very useful as a direct technique for quantifying the concentrations of AHA and SO_3-Ph-BTP. This technique is highlighted as a technique which is faster, more versatile and simpler than the traditional indirect UV–Vis method, which needs a complex formation with Fe in the case of AHA.

This project has received funding from the EURATOM research and training programme 2014-2018 under grant agreement No 755171. The content of this deliverable reflects only the author's view. The European Commission is not responsible for any use that may be made of the information it contains.

REFERENCES

1. Zarzana, C. A.; Groenewold, G. S.; Mincher, B. J.; Mezyk, S. P.; Wilden, A.; Schmidt, H.; Modolo, G.; Wishart, J. F.; Cook, A. R. A Comparison of the γ-Radiolysis of TODGA and T(EH)DGA Using UHPLC-ESI-MS Analysis. *Solvent Extr. Ion Exch.* 2015, *33*, 5, 431-447.

2. Sugo, Y., Sasaki, Y. and Tachimori, S., Studies on hydrolysis and radiolysis of N,N,N ',N '-tetraoctyl-3-oxapentane-1,5-diamide, *Radiochimica Acta*, 2002, 90, 161-165.

3. Sugo, Y.; Taguchi, M.; Sasaki, Y.; Hirota, K.; Kimura, T. Radiolysis study of actinide complexing agent by irradiation with helium ion beam. *Radiation Physics and Chemistry* 2009, *78*, 12, 1140-1144.

4. Galán, H.; Núñez, A.; Espartero, A. G.; Sedano, R.; Durana, A.; de Mendoza, J. Radiolytic Stability of TODGA: Characterization of Degraded Samples under Different Experimental Conditions. *Proc. Chem.* 2012, *7*, 195-201.

5. Gujar, R. B.; Ansari, S. A.; Bhattacharyya, A.; Kanekar, A. S.; Pathak, P. N.; Mohapatra, P. K.; Manchanda, V. K. Radiolytic Stability of N,N,N′,N′-Tetraoctyl Diglycolamide (TODGA) in the Presence of Phase Modifiers Dissolved in n-Dodecane. *Solvent Extr. Ion Exch.* 2012, *30*, 3, 278-290.

6. Malmbeck, R.; Banik, N. L. Radiolytic Behaviour of a TODGA Based Solvent under Alpha Irradiation. *J. Radioanal. Nucl. Chem.* 2020, *326*, 3, 1609-1615.

7. Zsabka, P.; Van Hecke, K.; Wilden, A.; Modolo, G.; Hupert, M.; Jespers, V.; Voorspoels, S.; Verwerft, M.; Binnemans, K.; Cardinaels, T. Gamma radiolysis of TODGA and $CyMe_4BTPhen$ in the ionic liquid tri-*n*-octylmethylammonium nitrate. *Solvent Extr. Ion Exch.* 2020, *38*, 2, 212-235.

8. Horne, G. P.; Zarzana, C.; Rae, C.; Cook, A. R.; Mezyk, S. P.; Zalupski, P.; Wilden, A.; Mincher, B. J. Does Addition of 1-Octanol as a Phase Modifier Provide Radical Scavenging Radioprotection for *N,N,N′,N′*-tetraoctyldiglycolamide (TODGA)? *Phys. Chem. Chem. Phys.* 2020, *22*, 43, 24978-24985. DOI:10.1039/D0CP04310A.

9. Wilden, A., Mincher, B. J., Mezyk, S. P., Twight, L., Rosciolo-Johnson, K. M., Zarzana, C. A., Case, M. E., Hupert, M., Stärk, A. and Modolo, G., Radiolytic and hydrolytic degradation of the hydrophilic diglycolamides, *Solvent Extraction and Ion Exchange*, 2018, 36, 347-359.

10. Mincher, B. J., Modolo, G. and Mezyk, S. P., The effects of radiation chemistry on solvent extraction: 1. conditions in acidic solution and a review of TBP radiolysis, *Solvent Extraction and Ion Exchange*, 2009, 27, 1-25.

11. Mincher, B. J. and Curry, R. D., Considerations for choice of a kinetic fig. of merit in process radiation chemistry for waste treatment, *Applied Radiation and Isotopes*, 2000, 52, 189-193.

12. Sugo, Y., Izumi, Y., Yoshida, Y., Nishijima, S., Sasaki, Y., Kimura, T., Sekine, T. and Kudo, H., Influence of diluent on radiolysis of amides in organic solution, *Radiation Physics and Chemistry*, 2007, 76, 794-800.

13. Galan, H., Zarzana, C. A., Wilden, A., Nunez, A., Schmidt, H., Egberink, R. J. M., Leoncini, A., Cobos, J., Verboom, W., Modolo, G., Groenewold, G. S. and Mincher, B. J., Gamma-radiolytic stability of new methylated TODGA derivatives for minor actinide recycling, *Dalton Transactions*, 2015, 44, 18049-18056.

14. Sánchez-García, I., Galán, H., Perlado, J. M. and Cobos, J., Stability studies of GANEX system under different irradiation conditions, *EPJ Nuclear Sci. Technol.*, 2019, 5, 19.

This project has received funding from the EURATOM research and training programme 2014-2018 under grant agreement No 755171. The content of this deliverable reflects only the author's view. The European Commission is not responsible for any use that may be made of the information it contains.

15. Ansari, S. A., Pathak, P., Mohapatra, P. K. and Manchanda, V. K., Chemistry of Diglycolamides: Promising Extractants for Actinide Partitioning, *Chemical Reviews*, 2012, 112, 1751-1772.

16. Modolo, G., Asp, H., Schreinemachers, C. and Vijgen, H., Development of a TODGA based process for partitioning of actinides from a PUREX raffinate part I: Batch extraction optimization studies and stability tests, *Solvent Extraction and Ion Exchange*, 2007, 25, 703-721.

17. Peterman, D., Geist, A., Mincher, B., Modolo, G., Galan, M. H., Olson, L. and McDowell, R., Performance of an i-SANEX System Based on a Water-Soluble BTP under Continuous Irradiation in a gamma-Radiolysis Test Loop, *Industrial & Engineering Chemistry Research*, 2016, 55, 10427-10435.

18. Hubscher-Bruder, V., Mogilireddy, V., Michel, S., Leoncini, A., Huskens, J., Verboom, W., Galan, H., Nunez, A., Cobos, J., Modolo, G., Wilden, A., Schmidt, H., Charbonnel, M. C., Guilbaud, P. and Boubals, N., Behaviour of the extractant Me-TODGA upon gamma irradiation: quantification of degradation compounds and individual influences on complexation and extraction, *New Journal of Chemistry*, 2017, 41, 13700-13711.

19. Koubsky, T. and Kalvoda, L., Application of ab-initio molecular electronic structure calculations of radiolytic and hydrolytic stabilities of prospective extractants, *Journal of Radioanalytical and Nuclear Chemistry*, 2015, 304, 227-235.

20. Koubsky, T., Fojtikova, J. and Kalvoda, L., Radical degradation stability of ether linkage in N,N,N ',N '-tetraoctyldiglycolamide and related organic extractants: A density functional study, *Progress in nuclear energy*, 2017, 94, 208-215.

21. Frisch, M. J. T., G. W.; Schlegel, H. B.; Scuseria, G. E.; Robb, M. A.; Cheeseman, J. R.; Scalmani, G.; Barone, V.; Petersson, G. A.; Nakatsuji, H.; et al., Gaussian 16, Revision C.01. , *Gaussian, Inc.: Wallingford CT 2016.*

22. McLean, A. D. C., G. S., Contracted Gaussian-Basis Sets for Molecular Calculations., *J. Chem. Phys.*, 1980, 72, 5639-5648.

23. Krishnan, R. B., J. S.; Seeger, R.; Pople, J. A., Self-Consistent Molecular Orbital Methods. XX. A Basis Set for Correlated Wave Functions., *J. Chem. Phys.*, 1980, 72, 650-654.

24. Barone, V. C., M., Quantum Calculation of Molecular Energies and Energy Gradients in Solution by a Conductor Solvent Model., *J. Phys. Chem. A*, 1998, 102, 1995-2001.

25. Cossi, M. R., N.; Scalmani, G.; Barone, V., Energies, Structures, and Electronic Properties of Molecules in Solution with the C-PCM Solvation Model., *J. Comput. Chem.*, 2003, 24, 669-681.

26. Berthon, L. P., A.; Saint-Louis, G.; Guilbaud, P., How Phase Modifiers Disrupt Third-Phase Formation in Solvent Extraction Solutions. , *Solvent Extraction and Ion Exchange*, 2020 accepted.

27. Campbell, E. L., Holfeltz, V. E., Hall, G. B., Nash, K. L., Lumetta, G. J. and Levitskaia, T. G., Nitric Acid and Water Extraction by T2EHDGA in n-Dodecane, *Solvent Extraction and Ion Exchange*, 2017, 35, 586-603.

28. Singh, M. B., Patil, S. R., Lohi, A. A. and Gaikar, V. G., Insight into nitric acid extraction and aggregation of N, N, N', N'-Tetraoctyl diglycolamide (TODGA) in organic solutions by molecular dynamics simulation, *Separation Science and Technology*, 2018, 53, 1361-1371.

29. Nave, S., Modolo, G., Madic, C. and Testard, F., Aggregation properties of N,N,N',N'-tetraoctyl-3-oxapentanediamide (TODGA) in n-dodecane, *Solvent Extraction and Ion Exchange*, 2004, 22, 527-551.

This project has received funding from the EURATOM research and training programme 2014-2018 under grant agreement No 755171. The content of this deliverable reflects only the author's view. The European Commission is not responsible for any use that may be made of the information it contains.

30. Prathibha, T., Venkatesan, K. A. and Antony, M. P., Comparison in the aggregation behaviour of amide extractant systems by dynamic light scattering and ATR-FTIR spectroscopy, *Colloids and Surfaces a-Physicochemical and Engineering Aspects*, 2018, 538, 651-660.

31. Malmbeck, R.; Magnusson, D.; Bourg, S.; Carrott, M.; Geist, A.; Hérès, X.; Miguirditchian, M.; Modolo, G.; Müllich, U.; Sorel, C.; Taylor, R.; Wilden, A. Homogenous Recycling of Transuranium Elements from Irradiated Fast Reactor Fuel by the EURO-GANEX Solvent Extraction Process. *Radiochim. Acta* 2019, *107*, 9-11, 917-929.

32. Wilden, A.; Kowalski, P. M.; Klaß, L.; Kraus, B.; Kreft, F.; Modolo, G.; Li, Y.; Rothe, J.; Dardenne, K.; Geist, A.; Leoncini, A.; Huskens, J.; Verboom, W. Unprecedented Inversion of Selectivity and Extraordinary Difference in the Complexation of Trivalent *f*-Elements by Diastereomers of a Methylated Diglycolamide. *Chem. Eur. J.* 2019, *25*, 21, 5507-5513.

33. Horne, G. P.; Wilden, A.; Mezyk, S. P.; Twight, L.; Hupert, M.; Stärk, A.; Verboom, W.; Mincher, B. J.; Modolo, G. Gamma Radiolysis of Hydrophilic Diglycolamide Ligands in Concentrated Aqueous Nitrate Solution. *Dalton Trans.* 2019, *48*, 17005–17013.

34. Hallerod J., Ekberg C., Authen T., Bertolo L., Lin M., Grűner B., Švehla J., Wagner C., Geist A., Panak P., Aneheim E. On the Basic Extraction Properties of a Phenyl Trifluoromethyl Sulfone-Based GANEX System Containing $CyMe_4$-BTBP and TBP, *Solvent Extraction-Ion Exchange,* 2018, 36(4), pp. 360-372.

35. Wilden, A.; Hallerod, J.; Schneider, D.; Kreft, F.; Modolo, G.; Ekberg, C., Batch Tests for Optimisation of Solvent Composition and Process Flexibility of the CHALMEX FS-13 Process. *Solvent Extraction and Ion Exchange* 2021, *39* (1), 1-17.

36. Authen, T. L.; Wilden, A.; Schneider, D.; Kreft, F.; Modolo, G.; Foreman, M. R. S.; Ekberg, C., Batch flowsheet test for a GANEX-type process: the CHALMEX FS-13 process. *Solvent Extraction and Ion Exchange*, 2021

37. P. Distler, M. Mindova, J. Sebesta, J. John, B. Gruner, D. Bavol, R.J.M. Egberink, W. Verboom, V.A. Babain "Stability of Different BTBP and BTPhen Extracting or Masking Compounds Against Gamma Radiation" (to be submitted).

38. HALLEROD, J.: Phenyl Trifluoromethyl Sulfone as Diluent in a Grouped ActiNide EXtraction Process. Gothenburg, Sweden, 2015. Thesis for the degree of Licentiate of Engineering. Chalmers University of Technology.

39. DISTLER, P.; STAMBERG, K.; JOHN, J.; HARWOOD, L. M.; LEWIS, F. W.: Modelling of the Am(III) - Cm(III) kinetic separation effect observed during metal ion extraction by bis-(1,2,4)-triazine ligands. Separation Science and Technology, 2018, 53(2), pp. 277–285.

40. DISTLER, P.; STAMBERG, K.; JOHN, J.; HARWOOD, L. M.; LEWIS, F. W.: Thermodynamic Parameters of Am(III), Cm(III) and Eu(III) Extraction by CyMe4-BTPhen in Cyclohexanone from HNO3 Solutions. The Journal of Chemical Thermodynamics, 2020, 141, p. 105955.

41. LÖFSTRÖM-ENGDAHL, E.; ANEHEIM, E.; EKBERG, Ch.; FOREMAN, M.; HALLERÖD, J.; SKARNEMARK, G.: Extraction thermodynamics of Am(III) and Eu(III) using CyMe4-BTBP in various organic diluents. 2014, 76, pp. 64-69.

42. LEWIS, F. W.; HARWOOD, L. M.; HUDSON, M. J.; et al.: BTBPs versus BTPhens: Some Reasons for Their Differences in Properties Concerning the Partitioning of Minor Actinides and the Advantages of BTPhens. 2013, 52(9), pp. 4993-5005.

43. SCHMIDT, H.; WILDEN, A.; MODOLO, G.; ŠVEHLA, J.; GRÜNER, B.; EKBERG, Ch.: Gamma radiolytic stability of CyMe4-BTBP and the effect of nitric acid. Nukleonika, 2015, 60(4), pp. 879-884.

This project has received funding from the EURATOM research and training programme 2014-2018 under grant agreement No 755171. The content of this deliverable reflects only the author's view. The European Commission is not responsible for any use that may be made of the information it contains.

44. MINDOVÁ, M.: Study of the influence of ionising radiation on the behaviour of the systems for Ln(III)/An(III) separation based on lipophilic extractants (in Czech), Praha 2019. Research project report. Czech Technical University in Prague.

45. KONDÉ, J.; DISTLER, P.; JOHN, J.; ŠVEHLA, J.; GRÜNER, B.; BĚLČICKÁ, Z.: Radiation Influencing of the Extraction Properties of the CyMe4-BTBP and CyMe4-BTPhen Solvents with FS-13. Procedia Chemistry, 2016, 21, pp. 174-181.

46. Schmidt, H.; Wilden, A.; Modolo, G.; Bosbach, D.; Santiago-Schübel, B.; Hupert, M.; Mincher, B. J.; Mezyk, S. P.; Švehla, J.; Grüner, B.; Ekberg, C. Gamma and pulsed electron radiolysis studies of $CyMe_4BTBP$ and $CyMe_4BTPhen$: identification of radiolysis products and effects on the hydrometallurgical separation of trivalent actinides and lanthanides. *Phys. Chem. Chem. Phys.* 2021, *Submitted*.

47. Distler, M. Mindová, J. John, V.A. Babain, M.Yu. Alyapyshev, L.I. Tkachenko, E.V. Kenf, L.M. Harwoodd and A. Afsard "Fluorinated Carbonates as New Diluents for Extraction and Separation of f- Block Elements", Solvent Extraction and Ion Exchange. 2020, 38(2), 180-193.

48. Sypula, M., Wilden, A., Schreinemachers, C., Malmbeck, R., Geist, A., Taylor, R., & Modolo, G.: Use of polyaminocarboxylic acids as hydrophilic masking agents for fission products in actinide partitioning processes. Solvent Extraction and Ion Exchange, 2012, 30(7), 748-764.

49. Malmbeck, R., et al. Proceedings of Internat. Conf. ISEC 2014, Würzburg, Germany, 7–11 September, 2014

50. Carrott, M., Bell, K., Brown, J., Geist, A., Gregson, C., Hères, X., Maher, C., Malmbeck, R., Mason, C. & Modolo, G.: Development of a new flowsheet for co-separating the transuranic actinides: the "EURO-GANEX" process. Solvent Extraction and Ion Exchange, 32, 2014, 447-467.

51. Carrott, M., Geist, A., Heres, X., Lange, S., Malmbeck, R., Miguirditchian, M., Modolo, G., Wilden, A., & Taylor, R.: Distribution of plutonium, americium and interfering fission products between nitric acid and a mixed organic phase of TODGA and DMDOHEMA in kerosene, and implications for the design of the "EURO-GANEX" process. Hydrometallurgy, 2015, 152, 139-148.

52. Modolo, G., Wilden, A., Kaufholz, P., Bosbach, D., & Geist, A.: Development and demonstration of innovative partitioning processes (i-SANEX and 1-cycle SANEX) for actinide partitioning. Progress in nuclear energy, 2014, 72, 107-114.

53. Wilden, A., Modolo, G., Kaufholz, P., Sadowski, F., Lange, S., Sypula, M., Magnusson, D., Müllich, U., Geist, A., & Bosbach, D. Laboratory-scale counter-current centrifugal contactor demonstration of an innovative-SANEX process using a water soluble BTP. Solvent extraction and ion exchange, 2015, 33(2), 91-108.

54. Miguirditchian, M., Roussel, H., Chareyre, L., Baron, P., Espinoux, D., Calor, J., Viallesoubranne, C., Lorrain, B. & Masson, M.: HA demonstration in the Atalante facility of the Ganex 2nd cycle for the grouped TRU extraction. In Proceedings GLOBAL Conference 2009.

55. GEIST, A.; MÜLLICH, U.; MAGNUSSON, D.; KADEN, P.; MODOLO, G.; WILDEN, A.; ZEVACO, T: Actinide(III)/lanthanide(III) Separation Via Selective Aqueous Complexation of Actinides(III) Using a Hydrophilic 2.6-Bis(1.2.4-Triazin-3-Yl)-Pyridine in Nitric Acid. Solvent Extraction and Ion Exchange, 2012, 30(5), pp. 433-444.

56. HORNE, G.; MEZYK, S.; MOULTON, N.; PELLER, J.; GEIST, A.: Time-Resolved and Steady-State Irradiation of Hydrophilic Sulfonated Bis-triazinyl-(bi)pyridines – Modelling Radiolytic Degradation. Dalton Transactions, 2019, 48, pp. 4547-4554.

This project has received funding from the EURATOM research and training programme 2014-2018 under grant agreement No 755171. The content of this deliverable reflects only the author's view. The European Commission is not responsible for any use that may be made of the information it contains.

57. DISTLER. P.: Study of properties of extractants prospective for lanthanoids and actinoids separation (in Czech). Praha, 2013. Master thesis. Czech Technical University in Prague.

58. ANSARI, S.; PATHAK, P.; HUSAIN, M.; PRASAD, A.K.; PARMAR, V.; MANCHANDA, V.: Extraction of actinides using N. N. N'. N'-tetraoctyl diglycolamide (TODGA): A thermodynamic study. Radiochimica Acta, 2006, 94, pp. 307-312.

59. ZHIPENG, H.; HUANG, D.; SONG-DONG, H.; XIAOYANG, Z.; LIRONG, L.; YING, S.; LIANJUN, CH.; ZHILI, L.: Extraction of trivalent americium and europium with TODGA homologs from HNO3 solution. Journal of Radioanalytical and Nuclear Chemistry, 2017, 313 (2) , pp. 309-318.

60. GALÁN, H.; MUNZEL, D.; NÚÑEZ, A.; MÜLLICH, U.; COBOS, J.; GEIST, A.: Stability and recyclability of SO_3-Ph-BTP for i-SANEX process development. In Proc. Internat. Solvent Extr. Conf. (ISEC 2014). Würzburg. Germany. 7-11 September 2014; pp. 137-143.

61. Sánchez-García I., Galán H., Perlado J.M., Cobos J.: Development of experimental irradiation strategies to evaluate the robustness of TODGA and water-soluble BTP extraction systems for advanced nuclear fuel recycling. Radiation Physics and Chemistry, Volume 177, December 2020, 109094.

62. Miguirditchian, M., Sorel, C., Camès, B., Bisel, I., Baron, P., Espinoux, D., Calor, J., Viallesoubranne, C., Lorrain, B. & Masson, M.: HA demonstration in the Atalante facility of the Ganex 1st cycle for the selective extraction of Uranium from HLW. In Proceedings of GLOBAL Conference 2009, 1032-1035.

63. Taylor, R., May, I., Wallwork, A., Denniss, I., Hill, N., Galkin, B. Y., Zilberman, B. Y. & Fedorov, Y. S.: The applications of formo-and aceto-hydroxamic acids in nuclear fuel reprocessing. Journal of alloys and compounds, 1998, 271, 534-537.

64. Carrott, M., Fox, O., Maher, C., Mason, C., Taylor, R. J., Sinkov, S. I. & Choppin, G. R.: Solvent extraction behavior of plutonium (IV) ions in the presence of simple hydroxamic acids. Solvent Extraction and Ion Exchange, 2007, 25, 723-745.

65. Macerata, E., et. al.: "Process safety studies on hydro-BTP and Pytritetraol." D11.5. of SACSESS Project CONTRACT Nº FP7-CP-2012-323282.

66. Casnati, A., et al.: "Stability studies of stripping agents". D2.2 of GENIORS project.

67. Karraker, D.: Radiation chemistry of acetohydroxamic acid in the urex process. Savannah River Site (United States) ,2002.

68. Wang, J. H., Li, C., Li, Q., Wu, M. H., Zheng, W. F., & He, H: γ-Ray radiolysis of acetohydroxamic acid in HNO 3 and its radiolytic product. Nuclear Science and Techniques, 2018, 29(2), 1-8.

69. Sánchez-García, I., Bonales, L. J., Galán, H., Perlado, J. M., & Cobos, J.: Advanced direct method to quantify the kinetics of acetohydroxamic acid (AHA) by Raman spectroscopy. Spectrochimica Acta Part A: Molecular and Biomolecular Spectroscopy, 2020, 229, 117877.

70. Sánchez-García, I., Bonales, L. J., Galán, H., Perlado, J. M., & Cobos, J.: Spectroscopic study of acetohydroxamic acid (AHA) hydrolysis in the presence of europium. Implications in the extraction system studies for lanthanide and actinide separation. New Journal of Chemistry, 2019, 43(39), 15714-15722.

71. Bonales L. J., Sánchez-García, I., Galán, H., & Cobos, J.: "Quantitative Raman spectroscopy (QRS) for nuclear fuel reprocessing applications. A direct method to analyse acetohydroxamic acid (AHA)." 2020, LAMBERT Academic Publising. LAP. In press. ISBN: 978-3-659-91071-5

72. Waterland, M. R., et al. The Journal of Chemical Physics 2001, 114.14, 6249-6258.

This project has received funding from the EURATOM research and training programme 2014-2018 under grant agreement No 755171. The content of this deliverable reflects only the author's view. The European Commission is not responsible for any use that may be made of the information it contains.

73. Coates, John. Encyclopedia of analytical chemistry: applications, theory and instrumentation 2006.

74. H. Galán, et. al. 5th half yearly partner activity report of GENIORS project (HYPAR-5_CIEMAT). Grant agreement nº 730227, reporting period: 01/06/2018 – 30/11/2018.

This project has received funding from the EURATOM research and training programme 2014-2018 under grant agreement No 755171. The content of this deliverable reflects only the author's view. The European Commission is not responsible for any use that may be made of the information it contains.